2001

Bioanalytical applications of fluorescence line-narrowing and non-line-narrowing spectroscopy interfaced with capillary electrophoresis and high-performance liquid chromatography

Kenneth Paul Roberts
Iowa State University

INFORMATION TO USERS

This manuscript has been reproduced from the microfilm master. UMI films the text directly from the original or copy submitted. Thus, some thesis and dissertation copies are in typewriter face, while others may be from any type of computer printer.

The quality of this reproduction is dependent upon the quality of the copy submitted. Broken or indistinct print, colored or poor quality illustrations and photographs, print bleedthrough, substandard margins, and improper alignment can adversely affect reproduction.

In the unlikely event that the author did not send UMI a complete manuscript and there are missing pages, these will be noted. Also, if unauthorized copyright material had to be removed, a note will indicate the deletion.

Oversize materials (e.g., maps, drawings, charts) are reproduced by sectioning the original, beginning at the upper left-hand corner and continuing from left to right in equal sections with small overlaps.

Photographs included in the original manuscript have been reproduced xerographically in this copy. Higher quality 6" x 9" black and white photographic prints are available for any photographs or illustrations appearing in this copy for an additional charge. Contact UMI directly to order.

Bell & Howell Information and Learning
300 North Zeeb Road, Ann Arbor, MI 48106-1346 USA
800-521-0600

UMI®

Bioanalytical applications of fluorescence line-narrowing and non-line-narrowing spectroscopy interfaced with capillary electrophoresis and high-performance liquid chromatography

by

Kenneth Paul Roberts

A dissertation submitted to the graduate faculty

in partial fulfillment of the requirements for the degree of

DOCTOR OF PHILOSOPHY

Major: Analytical Chemistry

Major Professor: Gerald J. Small

Iowa State University

Ames, Iowa

2001

Graduate College

Iowa State University

This is to certify that the Doctoral dissertation of

Kenneth Paul Roberts

has met the dissertation requirements of Iowa State University

Signature was redacted for privacy.

Major Professor

Signature was redacted for privacy.

For the Major Program

Signature was redacted for privacy.

For the Graduate College

to my family—those past on, those here today, those yet to come

TABLE OF CONTENTS

ACKNOWLEDGEMENTS

I would like to thank my research advisor, Professor Gerald J. Small for his encouragement, support, guidance, and commitment to my education and scientific achievements. I would also like to express my sincere appreciation for the assistance of Dr. Ryszard Jankowiak, with whom I worked closely on my thesis (and non-thesis) projects, for the many discussions, and his willingness to listen to my ideas and encourage innovation. In addition, I am greatly indebted to Dr. John Hayes and Dr. Tonu Reinot for the generosity in offering their vast experience and comprehensive understanding of theoretical and experimental optical spectroscopy. I would also like to thank Dr. James Fritz for his charitable discussions regarding analytical separations, showing me that you're never too old (or too young) to be creative, competitive, and original—thank you.

I would like to give a special thanks to previous and present members of Dr. Small's research group; Dr. Nebojsa Milanovich, Dr. Hsing-Mei Wu, Dr. Cheng-Huang Lin, Dr. Margus Rätsep, Dr. Mohammad Toutounji, Richard (Rich) Walsh, Satoshi Matsuzaki, Nenad Grubor, Nhan Dang, and Dr. Walter Zazubovich. These are all people that have helped me through my graduate experience in more ways than they will ever know—thank you.

Lastly, I am forever grateful for the support and love of my family. This doctorate was attained by those wonderful people that fill me with love and inspiration. I called upon you many times for strength and resolve (in thought and prayer), and you were always there. For this, I will be eternally humble and will never forget that I would have not been able to accomplish this goal without you—thank you.

CHAPTER 1. INTRODUCTION

1.1. Overview

Capillary electrophoresis (CE) and high-performance liquid chromatography (HPLC) are widely used analytical separation techniques with many applications in chemical, biochemical, and biomedical sciences [1-4]. Conventional analyte identification in these techniques is based on retention/migration times of standards; requiring a high degree of reproducibility, availability of reliable standards, and absence of coelution. From this, several new "information-rich" detection methods (also known as hyphenated techniques)[1] are being explored that would be capable of providing unambiguous on-line identification of separating analytes in CE and HPLC [5]. As further discussed in Section 1.2 of this chapter, a number of such on-line detection methods have shown considerable success, including Raman [6-12], nuclear magnetic resonance (NMR) [13-19], mass spectrometry (MS) [20-25], and fluorescence line-narrowing spectroscopy (FLNS) [26-32]. In this thesis, the feasibility and potential of combining the highly sensitive and selective laser-based detection method of FLNS with analytical separation techniques are discussed and presented. A summary of previously demonstrated FLNS detection interfaced with chromatography and electrophoresis is given, and recent results from on-line FLNS detection in CE (CE-FLNS), and the new combination of HPLC-FLNS, are shown. It is believed that the continued development of on-line FLNS detection with modern separation techniques (e.g., CE and HPLC) will further expand this detection approach in environmental and bioanalytical sciences.

FLNS has proven to be a powerful, high-resolution detection method that can be used for identification and characterization of structurally similar molecular analytes. Its physical principles and attributes are only briefly mentioned here, and more thoroughly discussed in Chapter 2 of this thesis, and in several books [33-39] and reviews [40-44]. FLNS is a low temperature (typically 4.2 K) technique in which a tunable laser is used to selectively excite a narrow region within the inhomogeneously broadened absorption band of an analyte imbedded in an amorphous host [33]. Since only excited analytes fluoresce, the inhomogeneous broadening contribution to the fluorescence vibronic bands is largely eliminated at low temperature, i.e., the fluorescence spectrum is line-narrowed. Typically, the inhomogeneous broadening is in the range of 100-300 cm^{-1}. The line-narrowed widths of vibronic transitions are usually lifetime limited ($\approx$5 cm^{-1}) due to vibrational relaxation [41,43].

FLNS has been used for identification and spectroscopic characterization of a large number of organic [33,43,45] and inorganic [46] molecules as well as a wide variety of biomolecules including photosynthetic pigments [47-52], antenna protein-pigment complexes [53], hemoglobin [54], and antibody-PAH complexes [55]. FLNS has also been applied to nucleosides/nucleotides, oligonucleotides, macromolecular DNA, and proteins adducted to metabolites of polycyclic aromatic hydrocarbons (PAHs) [28-32,41,43,56]. In particular, FLNS has proven to be the most powerful optical spectroscopic technique for the detection and characterization of PAH-DNA adducts formed *in vitro* [43,56,57] and *in vivo* [58-62], where one is limited to picomole or sub-picomole quantities of bound metabolite. For example, one adduct in 10^8 base pairs for 100 μg of macromolecular DNA [56] can be detected, while at the nucleoside level 0.1

femtomole of a moderately strong fluorophore such as benzo[*a*]pyrene-6-N7-guanine can be detected with a spectral resolution of ~ 5 cm^{-1} [43,56]. The distinction between adduction of a given metabolite to different bases and to different nucleophilic centers of a given base such as guanine (Gua) and adenine (Ade) has been demonstrated [57,62]. Moreover, FLNS has been used to differentiate between external, base-stacked, and intercalated conformations of PAH-DNA adducts and stereoisomeric PAH-DNA adducts [59,60,63-66]. The success of FLNS is the result of a combination of high sensitivity, high selectivity, and versatility. It is with these attributes that we believe FLNS will be a valuable contributor as an information-rich detection method in chromatography and electrophoresis.

1.2. Information-rich Detection in Chromatography and Electrophoresis

There is a multitude of detection techniques available for electrophoresis and chromatography and a detailed comparison is beyond the scope of this thesis (for reviews see Refs. 5,67,68). The most common detection modes include optical absorption, fluorescence, and radioactivity, where analyte identification is based on retention times (or migration distances) that are determined using standards. Such identification requires the absence of co-elution from other separating species, a high degree of reproducibility, and the availability of reliable standards. To circumvent these problems a number of information-rich detection schemes have been developed to provide a higher level of confidence in the identification process. They include absorption and fluorescence spectroscopy at room temperature [5], MS [20-25], NMR [13-19], electrochemical (EC) detection [69,70], circular dichroism (CD) [71], Fourier transform-infrared (FTIR)

spectroscopy [72,73], Raman spectroscopy [6-12], and FLNS [26-32]. A direct comparison of their attributes is difficult due to the inherent differences between the identification processes; nonetheless, a brief summary of each technique is given below.

On-line wavelength-resolved absorbance detection is the most frequently applied method for monitoring separations due to its low cost and universal applicability. Although this method offers a spectral signature of the separated components, the spectra of liquid solutions are often broad and quite structureless at room temperature. Moreover, the sensitivity of this approach is low due to shot-noise and the typically short optical path. In contrast to absorbance, wavelength-resolved fluorescence emission/excitation detection provides higher sensitivity; this is especially true for laser-induced fluorescence (LIF), which can have picomolar detection limits [74,75]. Unfortunately, as in the case of absorption room temperature fluorescence spectra are often featureless, preventing identification of closely related analytes.

NMR detection in chromatography and electrophoresis can provide unequivocal structural and conformational information on separated species. However, due to field inhomogenities from limited residence times and technical difficulties of probe/coil design, the sensitivity of this technique is severely compromised for on-line analysis [76,77] with detection limits of about 0.1-1 M [5]. In addition, the current spectral resolution of on-line NMR detection is rather low, excluding the possibility to differentiate between stereoisomers [5,78]. Furthermore, the need for solvent suppression methodologies or deuterated solvents imposes additional constraints for practical applications of on-line NMR analysis.

FTIR spectroscopy can also provide spectral information from which analyte identity may be obtained in both off- and on-line [72,73]. However, since most solvents used in separation procedures absorb strongly in the mid-IR region, flow cells with a small pathlength have to be used, severely decreasing the limit of detection (LOD), which is in the sub-millimolar range for on-line CE-FTIR analysis. It has been shown that the LOD for liquid chromatography (LC) can be improved by using a novel semi-on-line approach, where the LC effluent is deposited on a zinc selenide substrate followed by evaporation of the mobile phase prior to analysis [79].

Raman spectroscopy has also been used to provide on-line detection for LC [8,9] and CE [6,7]. The main advantage of Raman detection over room temperature absorption and fluorescence spectroscopies is that Raman spectra are highly structured. Various forms of Raman spectroscopy have been employed for on-line detection [6-12]. As in the case of FTIR, on-line analysis by Raman spectroscopy suffers from inadequate sensitivity and limit of detection due to solvent interference. Sub-micromolar detection limits have been reported for CE-Raman [10].

In on-line electrochemical (EC) detection, specifically amperometric detection, compounds are selectively oxidized or reduced at the electrode surface within a potential window that is governed by the choice of electrode and mobile phase. In potentiometric detection, selectivity is attained with an ion-selective electrode. Both EC techniques are capable of selectively detecting components in complex biological fluids [80,81]. Detection limits for electroactive analytes in CE/LC with EC detection are typically in the low nanomolar range [67,82].

Fluorescence-detected circular dichroism (FDCD) is another information-rich detection method being used for on-line detection in electrophoresis and chromatography [71]. It is applicable to chiral molecules whose CD signature varies with molecular conformation, thereby providing the analyst with important structural information. Since many biomolecules are chiral, this type of detection has found applications to bioanalytical sciences [71,83]. As an example of sensitivity, CE-FDCD detection allows for optical activity measurements of riboflavin in picoliter volumes with a detection limit in the subfemtomole range [71].

Detection by MS in CE and chromatography provides a high degree of structural information and, thus, is becoming widely used. Both off- and on-line MS detection modes have been successfully employed [20-25]. With MS detection, separated analytes are identified based on mass-to-charge ratios of parent ions or fragment ions produced from collision-induced dissociation. MS has very good sensitivity and excellent selectivity [5,67]. However, in the case of structurally similar molecules (e.g., geometric isomers), the highly discretionary, multi-pass process used often results in a severe decrease in throughput. Nonetheless, MS has a LOD in the femtomole range, which is often adequate for many applications.

Finally, FLNS has been coupled both off- and on-line with chromatography and electrophoresis [26-32,84-89] as will be discussed and presented in the remainder of this thesis. FLNS is very sensitive and highly selective in both frequency and time domains and can provide structural/conformational information that lead to unambiguous analyte identification. Low attomole LOD for on-line FLNS has been demonstrated [30], and it is important to note that the applicability of FLNS can be expanded to non-fluorescent

compounds derivatized with a fluorescent marker, which adopts specific interactions with the analyte of interest [90].

1.3. Dissertation Organization

Chapter 1 begins by providing a general overview of FLNS detection. In addition, Section 1.2 gives a brief synopsis of other common forms of information-rich detection currently being developed. Chapter 2 describes the pertinent principles and concepts of fluorescence line-narrowing spectroscopy for its analytical application to detection in chromatography and electrophoresis. A general description of solid-state spectral broadening is given in Section 2.1 and traditional "off-line" detection with FLN and its experimental instrumentation used by this laboratory are given in Section 2.2. The remaining section of Chapter 2 discusses and presents previous reports of FLN detection with polyacrylamide gel electrophoresis and thin-layer chromatography. Chapter 3 provides a brief description of the principles of capillary electrophoresis (CE) (Section 3.1) and the instrumentation for the formerly developed on-line CE-FLNS system (Section 3.2). Preliminary tests previously published on the CE-FLNS are shown and discussed in Section 3.2.2. Chapter 4 presents published results by the candidate on applications of CE-FLN and non-line-narrowing (NLN) fluorescence spectroscopy to the identification of eight diastereomeric deoxyadenosine adducts of dibenzo[*a,l*]pyrene (the most potent chemical carcinogen). Likewise, Chapter 5 presents published results by the candidate of CE-FLNS for the first ever identification of depurinating benzo[*a*]pyrene-6-N7-guanine adduct in humans. In Chapter 6 the prospect, design, and application of on-line HPLC-FLNS for four structurally similar molecules, along with a real-world

application to chemical carcinogenesis, are presented. A general conclusion is presented in Chapter 7. In Appendix A, a previously published paper on FLN/NLN spectral and conformational off-line analysis of deoxyadenosine adducts derived from *syn*- and *anti*-dibenzo[*a,l*]pyrene diolepoxides are presented. In Appendix B, the preliminary results of DNA adduction from the anti-estrogen drug tamoxifen are reported with NLN fluorescence studies of intact DNA. Finally, Appendix C shows preliminary CE-NLN fluorescence results for a photosynthetic protein complex, CP43.

[1]Introductory portions of this thesis were adapted, in part, from Jankowiak, R., Roberts, K.P., and Small, G.J., *Electrophoresis* 2000, *21*, 1251.

References

1. Brown, R. S., Luong, J. H. T., Szolar, O. H. J., Halasz, A., Hawari, J., *Anal. Chem.* 1996, *68*, 287.

2. Kientz, C. E., Hulst, A. G., De Jong, A. L., Wils, E. R. J., *Anal. Chem.* 1996, *68*, 675.

3. Lee, T. T., Yeung, E. S., *J. Chrom.* 1992, *595*, 319.

4. Lurie, I. S., in: Adamovics, J.A., (Ed.), *Analysis of Addictive and Misused Drugs*, New York: Marcel Dekker, 1995, pp. 151.

5. Kok, S.J., Velthorst, N.H., Gooijer, C., and Brinkman, U.A.Th., *Electrophoresis* 1998, *19*, 2753.

6. Walker, P.A. and Morris, M.D., *J. Chromatogr. A.* 1998, *805*, 269.

7. Walker, P.A., Kowalchyk, W.K., and Morris, M.D., *Anal. Chem.*, 1995, *67*, 4255.

8. Kennedy, B.J., Milofsky, R., Carron, K.T., *Anal. Chem.* 1997, *69*, 4708.

9. Cooper, S.D., Robson, M.M., Batchelder, D.N., Bartle, K.D., *Chromatographia* 1997, *44*, 257.

10. Chen, C.-H., Morris, M., *J. Chromatogr.* 1991, *540*, 355.

11. Kowalchyk, W.K., Walker, P.A., Morris, M.D., *Appl. Spectrosc.* 1995, *49*, 1183.

12. Somsen, G.W., ter Riet, G.J.H.P., Gooijer, C., Velthorst, N.H., Brinkman, U.A.Th., *J. Planar Chrom.* 1997, *10*, 10.

13. Olson, D.L., Lacey, M.E., Sweedler, J.V., *Anal. Chem.* 1998, *70*, 645.

14. Webb, A.G., *Progr. Nucl. Magn. Reson. Spectr.* 1997, *31*, 1.

15. Olson, D.L., Peck, T.L., Webb, A.G., Margin, R.L., Sweedler, J.V., *Science* 1995, *270*, 1967.

16. Albert, K., *J. Chromatogr. A* 1995, *703*, 123.

17. Korhammer, S.A., Bernreuther, A., *Fresenius J. Anal. Chem.* 1996, *354*, 131.

18. Albert, K., *Analusis* 1996, *24/4*, M17.

19. Olson, D.L., Lacey, M.E., Sweedler, J.V, *Anal. Chem.* 1998, *70*, 257A.

20. Cai, J.Y., Henion, J., *J. Chromatogr. A* 1995, *703*, 667.

21. Banks, J.F., *Electrophoresis* 1997, *18*, 2255.

22. Ding, J., Vouros, P., *Am. Lab.* 1998, *30*, 15.

23. Severs, J.C., Smith, R.D., in: Landers, J. (Ed.), *Handbook of Capillary Electrophoresis, Second Ed.*, CRC Press, New York 1996, pp. 791-826.

24. Kelly, J.F., Ramaley, L., Thibault, P., *Anal. Chem.* 1997, *69*, 51.

25. Unger, M., Stöckigt, D., *J. Chromatogr. A* 1996, *752*, 271.

26. Jankowiak, R., Zamzow, D., Ding, W., Small, G.J., *Anal. Chem.* 1996, *68*, 2549.

27. Zamzow, D., Small, G.J., Jankowiak, R., *Mol.Cryst. Liq. Cryst.* 1996, *291*, 155.

28. Zamzow, D., Lin, C.-H., Small, G.J., Jankowiak, R., *J. Chromatogr. A* 1997, *781*,73.

29. Roberts, K.P., Lin, C.-H., Jankowiak, R., Small, G.J., *J. Chromatogr. A* 1999, *853*, 159.

30. Roberts, K.P., Lin, C.-H., Singhal, M., Casale, G.P., Small, G.J., Jankowiak, R., *Electrophoresis* 2000, *21*, 799.

31. Duhachek, S. D., Kenseth, J. R., Casale, G. P., Small, G. J., Porter, M. D., Jankowiak, R., *Anal. Chem.* 2000, *72*, 3709.

32. Roberts, K. P., Jankowiak, R., and Small, G. J., *Anal. Chem.*, 2001, *Anal. Chem.* 2001, 73, 951.

33. Personov, R.I., in: Agranovich, V.M., Hochstrasser, R.M. (Eds.), *Spectroscopy and Excitation Dynamics of Condesned Molecular Systems*, North-Holland, Amsterdam, Vol. 4, 1983, pp. 555-619.

34. Osadko, I.S., in: Dusek, K. (Ed.), *Advances in Polymer Science*, Springer-Verlag, Berlin, Heidelberg, Vol. 114, 1994, pp. 123-186.

35. Kohler, B.E., in: Moore, C.B. (Ed.), *Chemical and Biochemical Applications of Lasers*, Academic Press, New York, 1979, pp. 31-51.

36. Hofstraat, J.W., Gooijer, C., Velthorst, N.H., in: Schulman, S.G., (Ed.), *Molecular Luminescence Spectroscopy: Methods and Applications, Part 2*, John Wiley and Sons, New York, 1988, pp. 383-459.

37. Selzer, P.M., Yen, W.M., Selzer, P.M., (Eds.), *Topics in Applied Physics*, Springer-Verlag, New York, Heidelberg, Berlin, Vol. 49, 1986, p. 113.

38. Weber, M.J., in: Yen, W.M., Selzer, P.M., (Eds.), *Topics in Applied Physics*, Springer-Verlag, New York, Heidelberg, Berlin, Vol. 49, 1986, pp. 1189-240.

39. Fidy, J., Vanderkooi, J.M., in: Douglas, R.H., Moan, J., Rontó, Gy., (Eds.), *Light in Biology and Medicine*, Plenum Press, New York, Vol. 2, 1991, pp. 367-374.

40. Weber, J.M., *J. Lum.* 1987, *36*, 179.

41. Jankowiak, R., Small, G.J., *Anal. Chem.* 1989, *61*, 1023A.

42. Price, B.P., Wright, J.C., *Anal. Chem.* 1990, *62*, 1989.

43. Jankowiak, R., Small, G.J., *Chem. Res. Toxicol.* 1991, *4*, 256.

44. Riesen, H., *Comments Inorg. Chem.* 1993, *14*, 323.

45. Nakhimovski, L., Lamotte, M., Joussot-Dubien, J., *Handbook of Low Temperature Electronic Spectra of Polycyclic Aromatic Hydrocarbons*, Elsevier, Amsterdam-New York-Oxford-Tokyo, 1989.

46. Riseberg, L.A., *Phys. Rev.* 1973, *A7*, 67.

47. Renge, I., Mauring, K., Sarv, P., Avarmaa, J., *Chem. Phys.* 1986, *90*, 6611.

48. Fünfschilling, J., Williams, D.F., *Photochem. Photobiol.* 1977, *26*, 109.

49. Avarma, R., Rebane, K.K., *Spectrochim. Acta* 1985, *41A*, 1365.

50. Hala, J., Pelant, I., Ambroz, M., Pancoska, P., Vacek, K., *Photochem. Photobiol.* 1985, *41*, 643.

51. Rebane, K.K., Avarmaa, *Chem. Phys.* 1982, *68*, 191.

52. Fünfschilling, J., Zschokke-Gränacher, I., *Chem. Phys. Lett.* 1982, *91*, 122.

53. Avarmaa, R., Renge, I., Mauring, K., *FEBS Lett.* 1984, *167*, 186.

54. Jankowiak, R., Day, B.W., Lu, P., Doxtader, M.M., Skipper, P.L., Tannenbaum, S.R., Small, G.J., *J. Am. Chem. Soc.* 1990, *112*, 5866.

55. Singh, K., Skipper, P.L., Tannenbaum, S.R., Dasari, R.R., *Photochem. Photobiol.* 1993, *58*, 637.

56. Jankowiak, R., Small, G.J., in: *The Handbook of Environmental Chemistry: PAHs and Related Compounds* Neilson, A.H., Ed., Springer-Verlag, Berlin-Heidelberg-New York, 1998, *Chap 11*.

57. Li, K.-M., Todorovic, R., Rogan, E.G., Cavalieri, E.L., Ariese, F., Jankowiak, R., Small, G.J., *Biochemistry*, 1995, *34*, 8043.

58. Marsch, G.A., Jankowiak, R., Small, G.J., Hughes, N.C., Phillips, D.H., *Chem. Res. Toxicol.*, 1992, *5*, 765.

59. Suh, M., Ariese, F., Small, G.J., Jankowiak, R., Hewer, A., Phillips, D.H., *Carcinogenesis* 1995, *16*, 2561.

60. Jankowiak, R., Ariese, F., Hewer, A., Luch, A., Zamzow, D., Hughes, N.C., Phillips, D.H., Seidel, A., Platt, K.-L., Oesch, F., Small, G.J., *Chem. Res. Toxicol.*, 1998, *11*, 674.

61. Devanesan, P. D., RamaKrishna, N. V. S., Padmavathi, N. S., Higginbotham, S., Rogan, E. G., Cavalieri, E. L., Marsch, G. A., Jankowiak, R. and Small, G. J., *Chem. Res. Toxicol.*, 1993, *6*, 364.

62. Rogan, E. G., Devanesan, P. D., RamaKrishna, N. V. S., Higginbotham, S., Padmavathi, N. S., Chapman, K., Cavalieri, E. L., Jeong, H., Jankowiak, R., and Small, G. J., *Chem. Res. Toxicol.* 1993, *6*, 356.

63. Suh, M., Ariese, F., Small, G.J., Jankowiak, R., Liu, T.-M., and Geacintov, N.E., *Biophys. Chem.* 1995, *56*, 281.

64. Ariese, F., Small, G.J., Jankowiak, R., *Carcinogenesis*, 1996, *17*, 829.

65. Jankowiak, R., Ariese, F., Zamzow, D., Luch, A., Kroth, H., Seidel, A., Small, G.J., *Chem. Res. Toxicol.* 1997, *10*, 677.

66. Jankowiak, R., Lin, C.-H., Zamzow, D., Roberts, K.P., Li, K.-M., Small, G.J., *Chem. Res. Toxicol.* 1999, *12*, 768.

67. Holland, L.A., Chetwyn, N.P., Perkins, M.D., Lunte, S.M., *Pharm. Res.* 1997, *14*, 372.

68. Huber, L., George, S.A., *Diode Array Detection in HPLC*, Marcel Kekker, New York 1993.

69. Wallington, R.A., Ewing, A.G., *Anal. Chem.* 1987, *59*, 1762.

70. Hoekstra, J.C., Johnson, D.C., *Anal. Chem.* 1998, *70*, 83.

71. Christensen, P.L., Yeung, E.S., *Anal. Chem.* 1989, *61*, 1344.

72. Somsen, G.W., van Stee, L.P.P., Gooijer, C., Brinkman, U.A.Th., Velthorst, N.H., Visser, T., *Anal. Chim. Acta* 1994, *290*, 269.

73. Somsen, G.W., Hooijschuur, E.W.J., Gooijer, C., Brinkman, U.A.Th., Velthorst, N.H., *Anal. Chem.* 1996, *68*, 746.

74. Kok, S.J., Kristenson, E.M., Gooijer, C., Velthorst, N.H., Brinkman, U.A.Th., *J. Chromatogr. A* 1997, *771*, 331.

75. Pentoney, S.L., Sweedler, J.V. in: Landers, J. (Ed.), *Handbook of Capillary Electrophoresis*, Marcel Dekker, New York 1997, pp. 379-423.

76. Sweedler, J.V., Olson, D., Lacey, M., Webb, A.G., *Proceedings of the 19th International Symposium on Capillary Chromatography and Electrophoresis, Wintergreen*, May 18-22, 1997, pp. 52-53.

77. Wu, N., Peck, T.L., Webb, A.G., Magin, R.L., Sweedler, J.V., *Anal. Chem.* 1994, *66*, 3849.

78. Wu, N., Peck, T.L., Webb, A.G., Magin, R.L., Sweedler, J.V., *J. Am. Chem. Soc.* 1994, *116*, 7929.

79. Somsen, G.W., van de Nesse, R.J., Gooijer, C., Brinkman, U.A.Th., Velthorst, N.H., Visser, T., Kootstra, P.R., de Jong, A.P.J.M., *J. Chromatogr.* 1991, *552*, 635.

80. Zhou, W.H., Liu, J., Wang, E., *J. Chromatogr. A* 1995, *715*, 355.

81. Ye, J., Baldwin, R.P., *Anal. Chem.* 1994, *66*, 2669.

82. Zhou, J., Lunte, S.M., *Electrophoresis*, 1995, *16*, 498.

83. Synovec, R.E., Yeung, E.S., *J. Chromatogr.* 1986, *368*, 85.

84. Kok, S.J., Bakker, I., Gooijer, C., Brinkman, U.A.Th., Velthorst, N.H., *Anal. Chim. Acta*, 1999, *389*, 77.

85. Cooper, R.S., Jankowiak, R., Hayes, J.M., Pei-qui, L., Small, G.J., *Anal. Chem.* 1988, *60*, 2692.

86. Marsch, G.A., Jankowiak, R., Suh, M., Small, G.J., *Chem. Res. Toxicol.* 1994, *7*, 98.

87. Marsch, G.A., Jankowiak, R., Farhat, J.H., Small, G.J., *Anal. Chem.* 1992, *64*, 3038.

88. Hofstraat, J.W., Jansen, H.J.M., Hoornweg, G.Ph., Gooijer, C., Velthorst, *Anal. Chim. Acta* 1985, *170*, 61.

89. van de Neese, R.J., Vinkenburg, I.H., Jonker, R.H.J,. Hoornweg, G.Ph., Gooijer, C., Brinkman, U.A.Th., Velthorst, N.H., *Appl. Spec.* 1994, *48*, 788.

90. Jankowiak, R., Zamzow, D., Stack, D.E., Todorovic, R., Cavalieri, E.L., Small, G.J., *Chem. Res. Toxicol.* 1998, *11*, 1339.

CHAPTER 2. FLUORESCENCE LINE-NARROWING SPECTROSCOPY (FLNS)

2.1. Homogeneous and Inhomogeneous Spectral Broadening

In solid-state molecular systems, molecules are frozen and have no freedom of rotation and translation, and should therefore provide much simpler optical spectra compared to gaseous or liquid samples. In the solid state, there are two possible contributions to spectral broadening: homogeneous (Γ_{hom}) and inhomogeneous (Γ_{inh}) [1], which are illustrated in Frames A and B of Figure 2-1, respectively. Depicted on the left in Figure 2-1A are three identical chromophores (guests) embedded in a perfect crystal lattice (host). The local microenvironments of the guest chromophores are identical, which results in the guests having identical absorption frequencies, $\omega_1 = \omega_2 = \omega_3$, and a Γ_{hom} width. The Γ_{hom} absorption profile has a Lorentzian line shape and predominantly originates from interactions of the guest molecules with lattice vibrations (phonons) of the host matrix [1]. Upon electronic excitation of the guest molecule from the ground state to the excited state, periodic movement of host molecules can destroy the phase relationship (guest-host equilibrium geometry) between the ground and excited state as defined by the total optical dephasing time (T_2), given by:

$$\frac{1}{T_2} = \frac{1}{2T_1} + \frac{1}{T_2'} \tag{2.1}$$

where T_1, so-called lifetime or natural broadening, originates from the excited-state lifetime of a single molecular electronic-vibrational (vibronic) transition terminating at

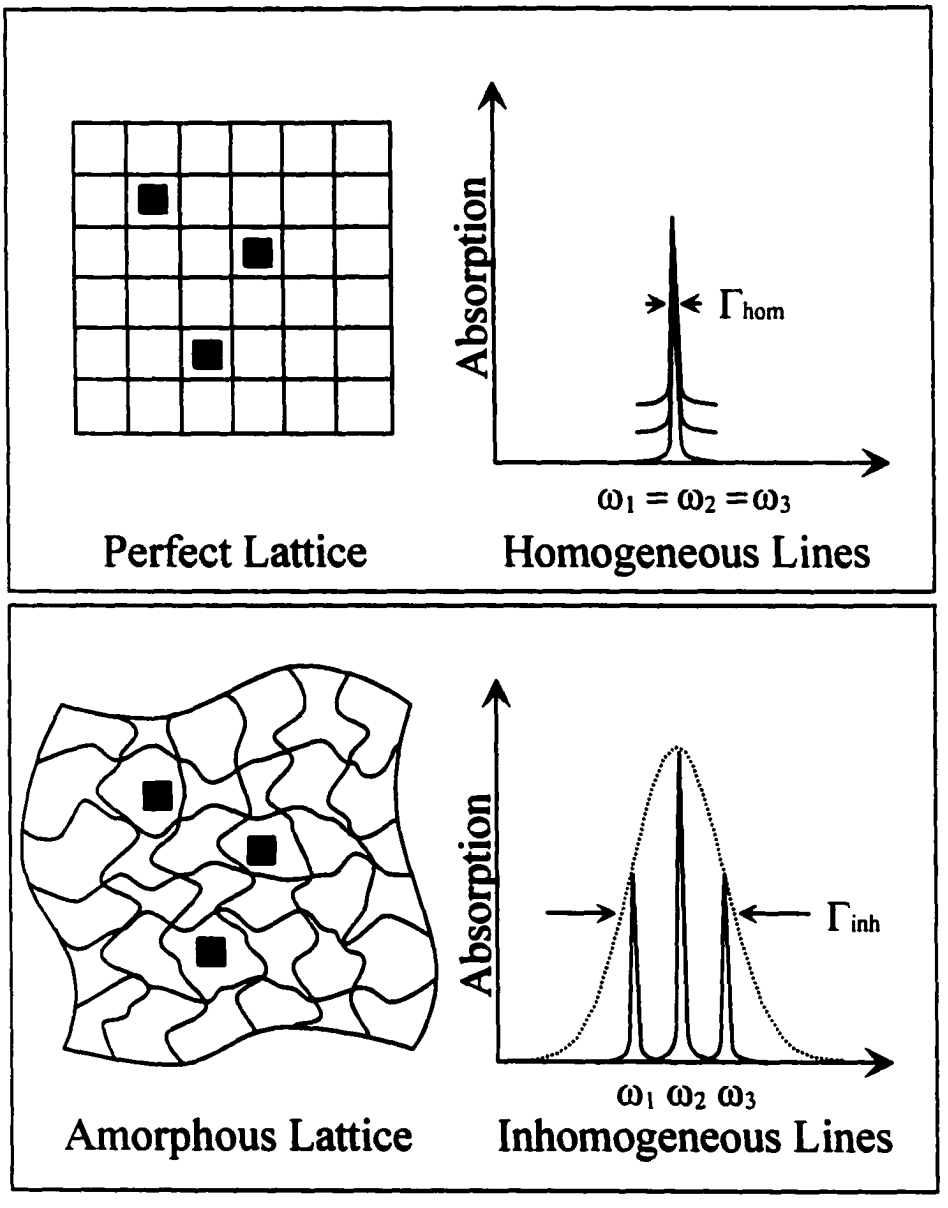

Figure 2-1. Schematic of the optical absorbance lines for three identical chromophores in a perfect crystal lattice (A) and in and amorphous host (B).

the zero-point level of the ground electronic state, and T_2' is the pure dephasing time. T_2' is the result of phonons that are excited by thermal motion and is therefore strongly temperature dependent. For this discussion, it suffices to say that T_2' is attibuted to a modulation of the single-site transition frequency that results from the interaction of the excited state with the bath phonons at high temperatures ($\geq$ 10 K) and other low-energy excitation modes at low temperatures ($\leq$ 10 K) of the host matrix. The contribution of T_2' to Γ_{hom} is much greater than that of T_1. Therefore, since Γ_{hom} ultimately dictates the achievable spectral resolution, low temperatures are required to minimize the number of thermally activated phonons responsible for T_2'. For example, in amorphous solids at room temperature Γ_{hom} from T_2' is ~ 200 cm^{-1} and is $\leq$ 0.1 cm^{-1} at 4.2 K, where the dependence of T_2' is proportional to $T^{1.3}$ at T $\leq$ 10 K. Therefore, the temperature-dependent homogeneous line width can be given (in cm^{-1}) as:

$$\Gamma_{hom} = (\pi T_2 c)^{-1} \tag{2.2}$$

where c is the speed of light in a vacuum (2.9979 x 10^{10} cm/s) and T_2 is comprised of T_1 and T_2' as described above.

Shown on the left of Figure 2-1B is an illustration of three identical chromophores in an amorphous lattice at low temperature. If the guest chromophore is embedded in an amorphous host, such as glasses, polymers, proteins, and DNA [1-3], each guest chromophore experiences energetically inequivalent microenvironments, forming an Γ_{inh} Gaussian distribution (~ 100-300 cm^{-1}) of Γ_{hom} transitions [1,4,5]. Even at low temperatures (< 10 K), to achieve high-resolution absorbance or fluorescence spectra under these conditions Γ_{inh} must be effectively eliminated or reduced. This can be

accomplished by either dissolving the guest in a uniform matrix of similar molecular dimensions to the guest (e.g., mixed crystal or Shpol'skii techniques) or by generally more applicable laser-based methods such as spectral hole burning or fluorescence line-narrowing spectroscopy (FLNS).

2.1.1. Zero-Phonon Lines and Phonon Sidebands

The coupling between electronic transitions of guest chromophores and the matrix phonons have major effects on the general shape of absorbance and fluorescence spectral lines. In what follows, these shapes will be discussed in terms of fluorescence since this thesis focuses on fluorescence detection. However, it should be noted that the principles described below are readily applicable to absorbance as well. Shown in Figure 2-2A is an inhomogeneously broadened fluorescence origin band [(0,0) band] at low temperature. The three relatively sharp lines within the fluorescence origin band are zero-phonon lines (ZPL), which refer to an electronic transition of a guest chromophore with no net change in the number of phonons in the host matrix [1]. Each single-site ZPL carries a homogeneous width, Γ_{hom}, which was described above for absorbance spectra in Figure 2-1. Building to the lower energy side of each ZPL is a broader (~ 30-40 cm^{-1}) phonon wing, known as the phonon sideband (PSB), which is a superposition of all lattice phonon transitions. Taking into account that phonons contribute to the overall fluorescence (0,0) band, the full width at half maximum (*fwhm*) of the Gaussian shown in Figure 2.2A is approximated as:

$$fwhm \approx \Gamma_{inh} + S\omega_m \tag{2.3}$$

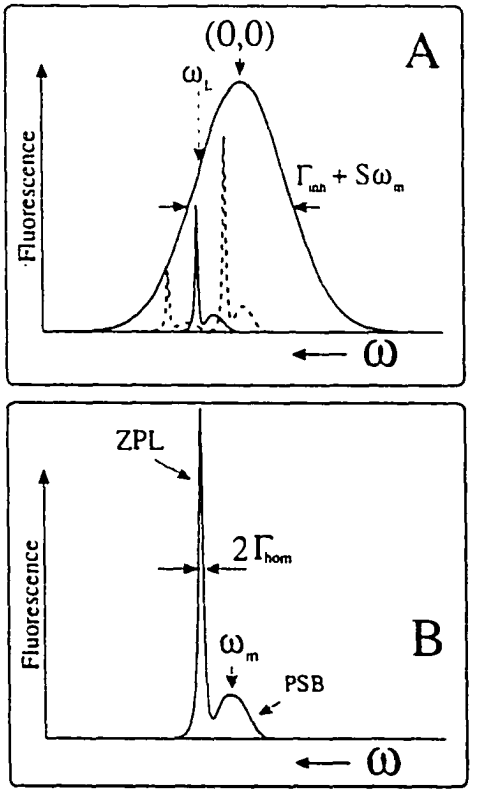

Figure 2-2. Frame A: Schematic representation of an inhomogeneously broadened (0,0) fluorescence origin band. The three sharp dashed lines are zero-phonon lines (ZPL), while the smaller, broader contribution to lower energy of the ZPLs are phonon sidebands (PSB). Inhomogeneous broadening is effectively eliminated by selective excitation with a tunable laser source at ω_L. Frame B: Resonant fluorescence ZPL and PSB from selective excitation within the inhomogeneously broadened spectrum in Frame A. The ZPL and PSB widths are enlarged relative to the inhomogeneous band to show detail.

where S is the Huang-Rhys factor, and ω_m is the mean phonon frequency [5,7,8]. The physical significance of $S\omega_m$, is most appreciated for fluorescence where $2S\omega_m$ corresponds to the Stokes shift for relaxed fluorescence. An expression for the single-site fluorescence profile in the low-temperature limit (T→ 0 K) has previously been derived and is given by [6,7]:

$$f(\omega) = e^{-S} I_0(\omega - \Omega) + \sum_{R=1}^{\infty} S^R \frac{e^{-S}}{R!} I_R(\omega - \Omega + R\omega_m) \qquad (2.4)$$

where Ω is the frequency of the ZPL, and $I_0(\omega-\Omega)$ describes the Γ_{hom} Lorentzian line shape of the ZPL. The second term describes the phonon sideband contribution, with R = 1,2,... terms corresponding to the one-phonon and multi-phonon ($R \geq 2$) transitions with I_1, the one-phonon profile. Frame B of Figure 2-2 shows the result of selectively exciting a narrow region of the inhomogeneous (0,0)-band in Frame A with a narrow laser excitation frequency, ω_L, such that $\Gamma_L << \Gamma_{hom} << \Gamma_{inh}$. The result is a [resonant] fluorescence line-narrowed (FLN) spectrum with a ZPL width of $2\Gamma_{hom}$, and a broad PSB centered at ω_m. By expanding Eq. (2.4) to include a distribution of phonons coupled to the electronic transition, the $I_R(R \geq 2)$ profile can be obtained by convolution of the one-phonon profile R times [6,7]. An expression for the FLN spectrum, $F(\omega)$, obtained by convolution of the single-site fluorescence profile with the site distribution function, $N(\Omega - \omega_c)$, and the absorption at the excitation frequency $I(\omega_L - \Omega + P\omega_m)$, can be given as:

$$F(\omega) = \sum_{R,P=0}^{\infty} \left(S^R \frac{e^{-S}}{R!} \right) \left(S^P \frac{e^{-S}}{P!} \right) \int d\Omega N(\Omega - \omega_c) I_R(\omega - \Omega + R\omega_m) I_P(\omega_L - \Omega - P\omega_m) \quad (2.5)$$

In this case, $N(\Omega - \omega_c)$ is taken as a Gaussian inhomogeneous distribution centered at ω_c with an excitation frequency ω_L and the R and P terms describe PSB transitions that build on the lower energy side of the ZPL, which itself (the ZPL) is defined as $R, P = 0$. In the case of $P = 0$, $R \geq 1$, the phonon transition is called a real-PSB. In the opposite case, $R = 0$, $P \geq 1$, the transition is a pseudo-PSB. Lastly, the multiphonon case of $R,P \neq 0$ results in a contribution building on the pseudo-PSB. However, each contribution cannot be determined experimentally by FLN, while it is possible with spectral hole burning. A complete physical description of the origins of the PSB contributions and ZPL line-width are beyond the scope of this discussion, but can be generalized here as the result of lifetime broadening, electron-phonon interactions, and spectral diffusion. For a complete discussion of ZPLs and PSBs, the reader is referred to Refs. 1, 6, 7, and 10.

Of analytical importance is the relative intensity ratio of the ZPL to the PSB, which is determined by the strength of electron-phonon coupling. In the low temperature limit, the Franck-Condon factors for the ZPL and PSB are given by exp(−S) and [1-exp(−S)], respectively. Weak electron-phonon coupling can be simply stated as $S < 1$, and strong coupling as $S > 1$. In the limit of very strong electron-phonon coupling, such that $S >> 1$, the resulting fluorescence spectrum will be dominated by the PSB emission with very weak ZPLs and fluorescence line-narrowing will be impossible. In a practical sense, the ZPL to PSB ratio is most easily determined experimentally, and depends not only on the host matrix, but also on intrinsic guest-host interactions. In terms of chromatography and electrophoresis, the host is the mobile phase or buffer, while the guest is the analyte.

2.2. Principles of FLNS

The key requirements for FLNS detection are: (*i*) low temperature to minimize homogeneous spectral broadening; (*ii*) selective excitation with a narrow laser source to effectively eliminate inhomogeneous broadening; (*iii*) weak electron-phonon coupling; and (*iv*) sufficiently low analyte concentration ($\leq 10^{-4}$ M) to prevent energy transfer. In conventional room-temperature fluorescence detection with a broadband excitation source, all mutually different sites within a (0,0) transition that overlap the excitation bandwidth fluoresce, resulting in a broad, featureless spectrum. However, as introduced above, in FLNS a narrow laser frequency excites only those sites whose (0,0) transitions overlap the laser profile (often referred to as selecting an "isochromat"), resulting in a fluorescence line-narrowed (FLN) spectrum as shown in Figure 2-2. At first glance, this would seem to make FLNS an insensitive technique, but the reduction in homogeneous broadening alone, in going from 300 to 4.2 K (from 200 to ≤ 0.1 cm^{-1}), more than compensates for the loss in being site selective.

Two types of excitation can be employed in FLNS: the chromophore can be excited in its inhomogeneously broadened origin absorption band (origin band excitation) or vibronic absorption bands (vibronic excitation). Figure 2-3 illustrates origin band excitation for the low temperature limit where the narrow bandwidth laser, with frequency ω_L, selectively excites chromophores within the (0,0) origin band. The resulting FLNS spectrum at the bottom of the top frame of Figure 2-3 is comprised of the highest energy ZPL which corresponds to the transition between the zero-point vibrational levels of the fluorescent (S_1) and ground electronic (S_0) states, and a series of vibronic ZPLs corresponding to transitions terminating at vibrational levels of S_0. This

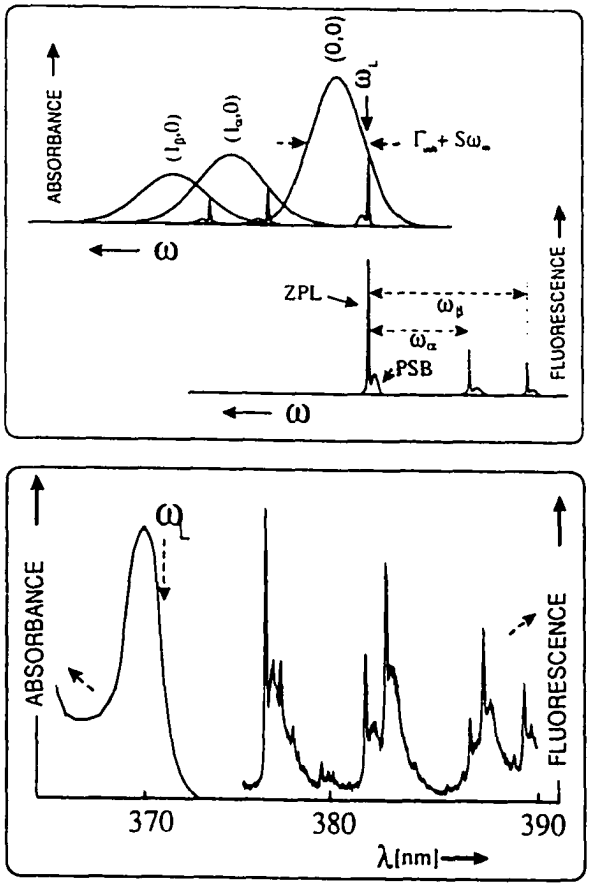

Figure 2-3. Origin band excitation in FLNS. Top frame: Γ_{inh} denotes the inhomogeneous broadening of the (0,0) band. S is the Huang-Rhys factor, and ω_m corresponds to the mean phonon frequency. Laser frequency, ω_L, excites only those chromophores whose (0,0) transition overlaps the laser profile. ω_α and ω_β correspond to the ground-state vibrational frequencies, in cm^{-1}. Bottom frame: (0,0) absorption band (left) and FLN spectrum (right) obtained for pyrene in ethanol glass at T = 4.2 K, λ_{ex} = 371.5 nm. The sharp peaks (ZPLs) in the fluorescence spectrum correspond to pyrene ground-state vibrational frequencies [12].

type of FLN spectrum provides ground-state vibrational frequencies (ω_α and ω_β) which, when combined with the relative vibronic intensities, serve as a "fingerprint" of the chromophore. In the bottom frame of Figure 2-3, an example of an origin-band excited FLN spectrum (right) is shown, along with the inhomogeneously broadened absorption spectrum (left) for pyrene embedded in ethanol glass at 4.2 K [12]. For clarity, only part of the FLN spectrum is shown; the narrow peaks are ZPLs, and their frequencies (not shown) correspond to the ground-state vibrations. The prominence of the ZPLs indicates weak electron-phonon coupling, i.e., $S < 1$. As the laser is tuned across the origin band, the fluorescence spectrum tracks the laser while maintaining the same vibronic structure.

Vibronically excited FLNS probes the S_1-state vibronic levels as shown in the top frame of Figure 2-4. The laser (ω_L) excites only two overlapping vibronic transitions, $(1_\alpha,0)$ and $(1_\beta,0)$, which are not resolved in the absorption spectrum. The two selected isochromats undergo vibrational relaxation to two different points (A and B) in the zero-point level of the S_1-state. This is followed by fluorescence from the energetically distinct isochromats, resulting in an FLN spectrum that consists of two strong ZPLs [$(0,0)_A$ and $(0,0)_B$]. This is often referred to as a "multiplet origin structure." The displacements between ω_L and the doublet components of the origin transition, [$(0,0)_A$ and $(0,0)_B$], yield the excited-state vibrational frequencies ω_α' and ω_β'. The vibronic bands that build on $(0,0)_A$ and $(0,0)_B$ to lower energy are not shown for simplicity. In an actual experiment, it is common to observe 6-8 ZPLs that contribute to the multiplet origin structure for each excitation frequency.

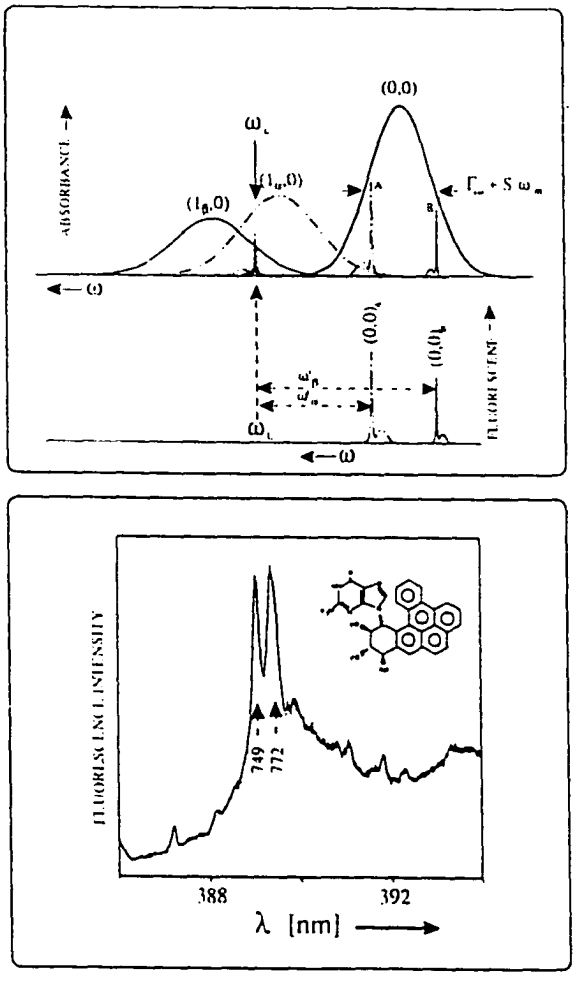

Figure 2-4. Principles of vibronic excitation in FLNS. Top frame: selective laser excitation (ω_L) of two subsets of molecules (A and B) within the vibronic region. Schematic of the resulting fluorescence spectrum with two $(0,0)_A$ and $(0,0)_B$ transitions is shown at the bottom of the top frame. ω_α' and ω_β' are the vibrational frequencies in the excited-state. Bottom frame: an example of vibronically excited FLN spectrum is shown for the *syn*-DB[*a,l*]PDE-14-N7Gua adduct; λ_{ex} = 376.0 nm, T = 4.2 K. The sharp ZPLs at 749 and 772 cm^{-1} correspond to excited state vibrational frequencies [12].

Vibronically-excited FLNS has been used almost exclusively for identification and conformational analysis of closely related analytes due to its superior ability (relative to origin-excited FLNS) to differentiate structurally similar molecules [3,11,12]. It has been established that the S_1-state vibrational frequencies and intensities are the most sensitive to subtle changes in the structure of the chromophore and its environment [11-13]. This sensitivity has a firm theoretical understanding based on the Duschinsky effect (a mixing of the normal coordinates in the excited state and vibronically induced anharmonicity) [14]. An example of a vibronically excited FLN spectrum obtained at 4.2 K for the *syn*-dibenzo[*a,l*]pyrene diolepoxide-14-N7Gua adduct is shown in the lower frame of Figure 2-4. Laser excitation at 378 nm selectively excites several modes; with the two strongest bands corresponding to 749 and 772 cm^{-1} excited state vibrations. The prominence of the vibronic ZPLs indicates weak electron-phonon coupling. By tuning ω_L across the $S_1 \leftarrow S_0$ absorption spectrum one can determine all active excited state vibrations [1,3,10,15]. For each excitation frequency ω_L, a distinct fingerprint of the analyte is obtained. Lastly, it is important to note that FLN is generally observed only with excitation frequencies located within the $S_1 \leftarrow S_0$ absorption spectrum at or near 4.2 K. Excitation of the higher-energy states (S_n, $n \geq 2$), or at temperatures larger than ~ 20 K results in S_1 fluorescence spectra that exhibit, at best, only a slight degree of line narrowing. This is a consequence of the site excitation energies of different electronic states being largely uncorrelated, and is often termed non-line-narrowed (NLN) fluorescence.

2.3. Off-Line Detection

By tradition, FLN and NLN detection is often accomplished in an "off-line" mode. In using FLN and NLN as an analytical technique to spectroscopically identify and characterize analytes (as is often the case in this laboratory) the basic procedure is to generate a reference library of spectra from a well-characterized standard. With this reference material, future identifications are possible by comparing sample data to previously generated reference data. In this laboratory, off-line FLN and NLN spectra are obtained using a Lambda Physik FL-2002 dye laser pumped by a Lambda Physik Lextra 100 XeCl excimer laser as an excitation source, as shown in the block diagram of Figure 2-5. The excimer laser provides high-energy (~ 150 mJ/pulse) pulses with a repetition rate up to 50 Hz at 308 nm. For time-resolved spectroscopy, a Lambda Physik EMG-97 zero-drift controller is used to trigger a high-voltage Roper Scientific FG-100 pulse generator, which controls both the adjustable delay time and the width of the temporal detection window. Detector delay times of 0-200 ns, with a gate width of 200 ns, are commonly used. The dye laser uses a Littrow style grating which provides a spectral line-width of ~ 0.2 cm^{-1}. For FLN spectra, several excitation wavelengths are used, each of which reveals a portion of the S_1 excited state vibrational frequencies of the analytes. NLN spectra are obtained using nonselective excitation at 308 nm from the excimer laser. Samples are cooled in a glass cryostat with quartz optical windows to 77 or 4.2 K. Fluorescence is dispersed by a McPherson 2061 1-m focal-length monochromator and detected by a Roper Scientific IRY 1024-GRB intensified photodiode array. For FLN measurements, the monochromator is equipped with a 2400 g/mm grating and for NLN a 150 g/mm grating is used. The resolution for FLN and

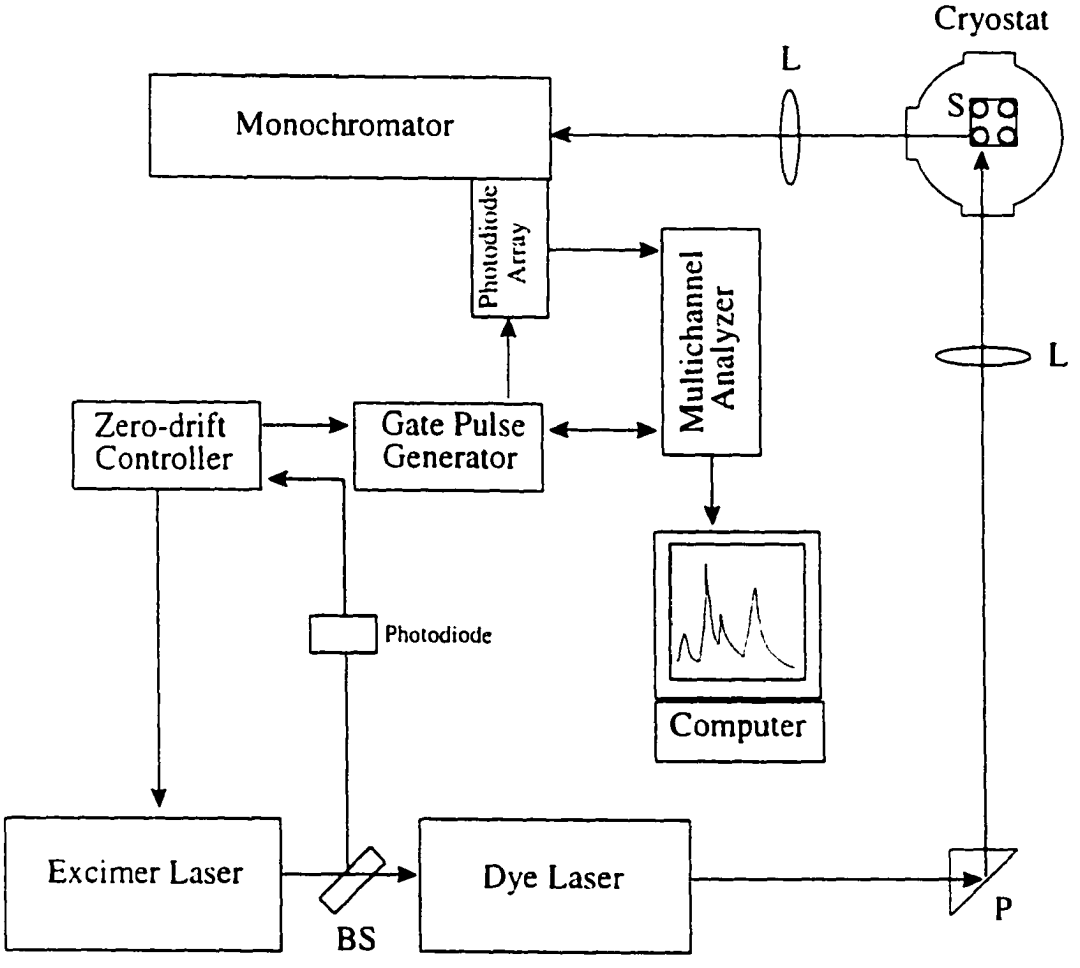

Figure 2-5. Block diagram of FLN and NLN spectroscopy instrumentation: S, sample in a copper holder; L, lens; P, prism; BS, beam splitter.

NLN spectra are 0.03 and 0.5 nm, respectively. Samples (ca. 20 μL) are transferred to quartz tubes (2 mm i.d.) and the tubes sealed with a rubber septum. Solvent matrices are of HPLC or spectrometric grade.

However, in many real-world analyses, samples can often be complex, unstable, and the analyte of interest present in small amounts. This can severely limit the applicability of the off-line experimental design described above for biological samples due to spectral interference [11]. For example, in studying metabolic pathways of polycyclic aromatic hydrocarbons, several structurally similar analytes are commonly encountered which need to be individually identified and quantified. For FLN and NLN to be operative under these conditions, sample constituents must first be separated and purified by, for example, extraction methods and/or preparative chromatography. This process generally requires ample amounts of sample and standard, reproducibility, and sufficient detection sensitivity by the preparative chromatography system. Moreover, most biological studies from *in vivo* experiments result in sample amounts that cannot sustain the losses associated with multiple sample-handling steps, or the losses associated with analyte degradation. To remedy these limitations and concerns, FLNS has been combined with various forms of chromatography and electrophoresis. The comparative performance of each combination will be discussed, beginning with the least expensive choice, thin-layer chromatography, and ending with the presentation of recent results by the candidate on the on-line combinations of FLNS with capillary electrophoresis and high-performance liquid chromatography. Similar to the above methods in off-line FLNS detection, identification of the chromatographically and electrophoretically separated analytes is made by comparison of sample spectra with reference spectra obtained (once)

from well-characterized standards. Excluding the relatively new separation method capillary electrophoresis (see Chapter 3), all the separation techniques discussed below are well known and the theory of their separation processes will only be briefly mentioned in the context of their performance when combined with FLNS.

2.4. Thin-Layer Chromatography (TLC) and FLNS

TLC is a well-established and inexpensive separations technique where chromatographic media is adhered to a glass plate. Samples are "spotted" on the plate and the plate placed in a TLC chamber containing an appropriate mobile phase. By capillary action, the mobile phase traverses up the TLC plate, separating components of the sample based on a dynamic equilibrium of the analyte between the stationary and mobile phases. TLC has been used in the analysis of many compounds including PAHs and DNA adducts, where analyte identification is generally accomplished by visualization of separated components on the TLC plate [16-26]. However, this method of identification is often difficult and ambiguous due to band broadening and/or incomplete separation of sample constituents. With FLNS, however, this limitation can be overcome by spatially analyzing the separated analyte zones with a focused laser beam to attain selectivity. The first experiments of TLC-FLNS were performed with PAHs and PAH-DNA adducts deposited on filter paper [16] and silica gel TLC plates [17,18]. For example, Cooper *et al.* [16] studied B[*a*]P derived deoxyguanosine (dG) adducts (B[*a*]P-C8dG) deposited on an octadecylsilate TLC plate. A detection level of ~10 femtomole was demonstrated. Shown in Figure 2-6 is a vibronically excited FLN spectrum obtained with an excitation wavelength (λ_{ex}) of 395.7 nm for B[*a*]P-C8dG on the TLC plate. The

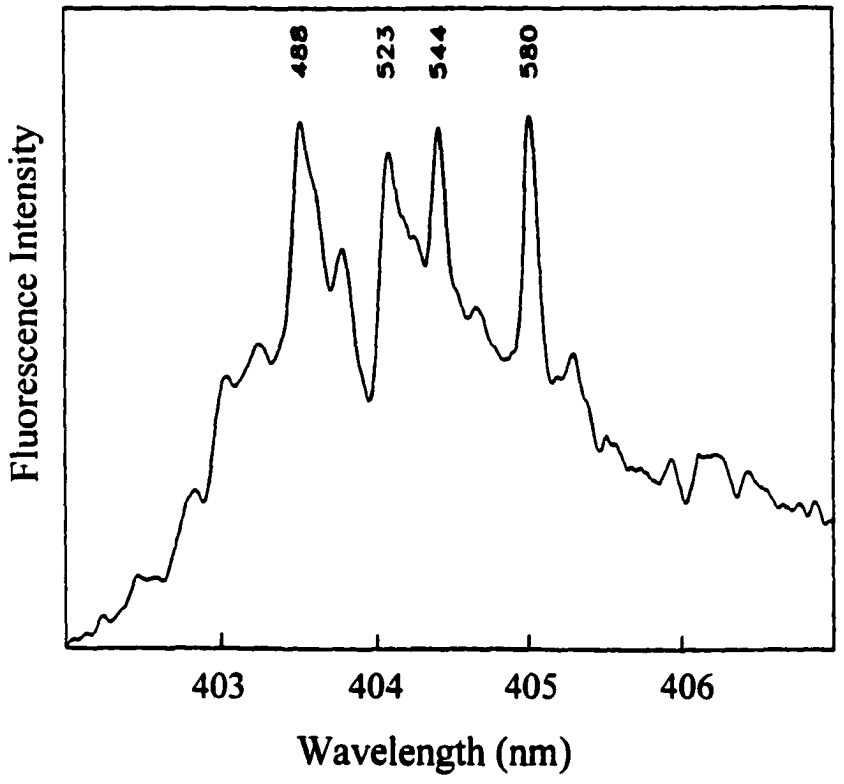

Figure 2-6. FLN spectrum of the B[*a*]P-C8dG nucleoside adduct on a TLC plate. λ_{ex} = 395.7 nm (vibronic excitation), T = 4.2 K. The numbers above the peaks correspond to excited state vibrations (in cm^{-1}). With permission from Ref. 17.

numbers above the peaks reflect the displacement of the ZPLs from the laser frequency in cm^{-1} and correspond to excited-state vibrational frequencies. These frequencies and the relative intensities of the ZPLs allowed for positive identification of B[*a*]P-C8dG.

Similarly, Velthorst and coworkers established that by coupling FLNS with HPLC-TLC in a semi-on-line arrangement (see below), pyrene and halogenated pyrene derivatives could be identified on the chromatographic media (e.g., silica gel, C18, and cellulose) of a TLC plate. The estimated limit of detection was in the low picomole range [19-21]. The same group demonstrated that a second separation (perpendicular to the HPLC deposition trace) on a TLC plate, prior to FLNS analysis, further improved the quality of chromatographic resolution and the FLN spectra [22,23]. The semi-on-line HPLC-TLC system is shown in Figure 2-7. A fused silica capillary is connected to the outlet of the HPLC detector flow cell, which is coupled to a heated spray jet assembly.

Heating the spray jet assembly with hot nitrogen gas up to 175°C allowed for the effluent to be gently deposited on the linearly translating TLC plate. Evaporation of the mobile phase limited the amount of diffusion of the deposited traces. Upon final drying, the TLC plate was placed in a closed-cycle refrigeration system (10-20 K) for FLNS analysis [22]. An example of FLN spectra from this methodology for stereoisomeric B[*a*]P-tetrol standards is shown in Figure 2-8. Detection limits were at the femtomole level [24]. With selective excitation at 364 nm, the FLN spectra of the *trans*- and *cis*-stereoisomers of the *anti*- and *syn*-BP-tetrols are clearly distinguishable at 12 K. The numbers in Figure 2-8 correspond to excited-state vibrational frequencies. These results demonstrate that B[*a*]P-derived tetrols (originating from PAH-DNA adducts) can be

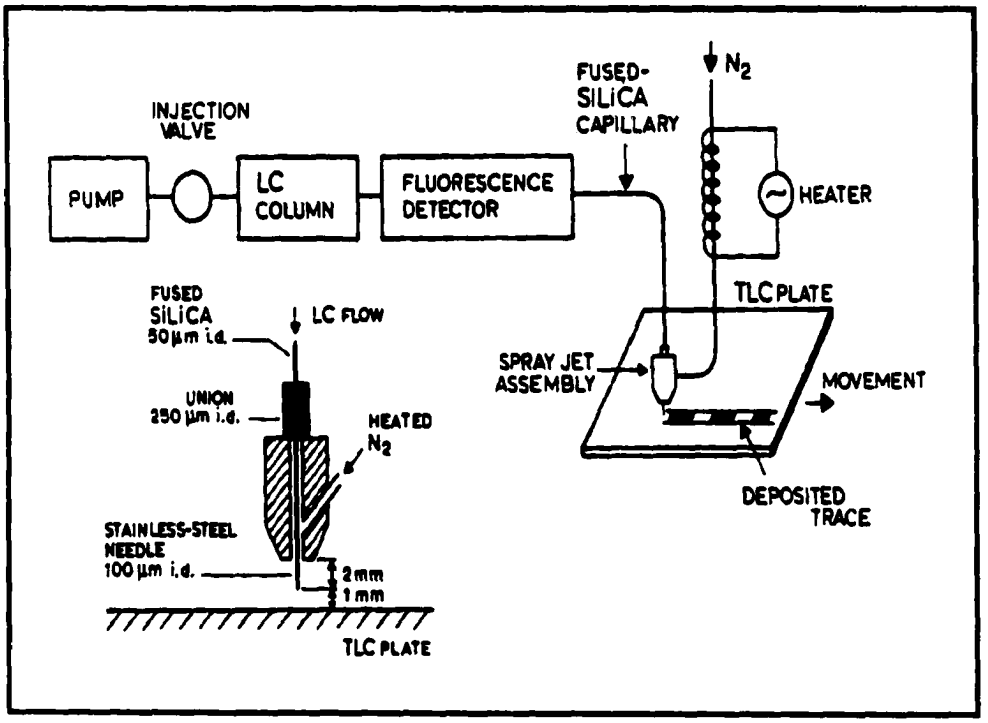

Figure 2-7. Schematic of the HPLC-TLC system and the coupling interface. The lower left corner shows an the spray jet assembly in more detail (see text). With permission from Ref. 22.

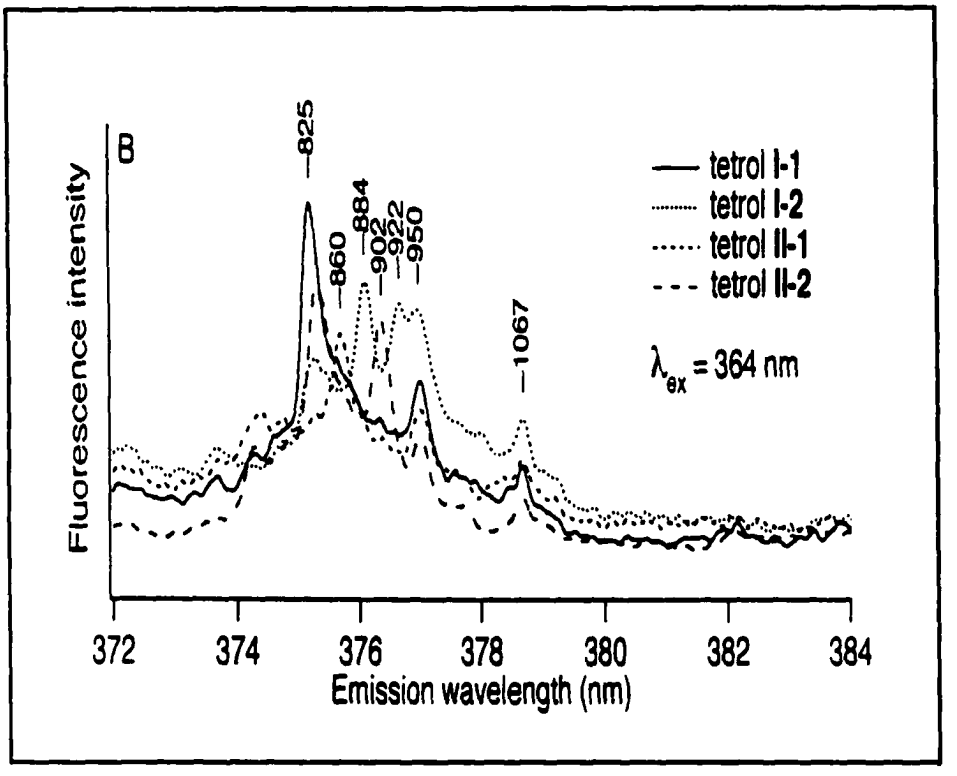

Figure 2-8. FLN spectra of *trans*- (1) and *cis*- (2) stereoisomers derived from the *anti*- (I) and *syn*-B[*a*]P-tetrols (II) obtained with the HPLC-TLC-FLNS. λ_{ex} = 364 nm; T = 12 K. The numbers correspond to excited state vibrational frequencies (in cm^{-1}). With permission from Ref. 24.

identified using TLC in combination with FLNS. However, drying the LC effluent with hot gas can lead to analyte decomposition and application of this methodology to real world samples has yet to be demonstrated.

TLC-FLNS was also utilized in combination with a ^{32}P-postlabeling (Randerath) procedure [25,26]. It is well known that DNA adducts can be enzymatically digested, labeled with ^{32}P, and separated on a polyethylenimine (PEI)-cellulose TLC plate. In ^{32}P-postlabeling identification is typically accomplished by measuring the relative positions of the separated components autoradiographically. The autoradiogram of BPDE adducted (1 adduct in 10^2 base pairs) and ^{32}P-postlabeled DNA digest on a PEI plate is shown in Figure 2-9A. Direct on-line FLNS analysis of spot A was not possible due to strong luminescence background of the PEI plates. The background was several orders of magnitude stronger than that observed for the octadecylsilate TLC plates discussed above [16,17]. Therefore, the analyte from spot A needed to be extracted from the TLC plate prior to off-line FLNS analysis [26]. An example of FLN spectrum obtained with an excitation wavelength of 361 nm is shown in Figure 2-9B (top). Since this FLN spectrum is similar to the FLN spectrum obtained for the *anti*-BPDE-dAMP standard (Figure 8B, bottom), it was concluded that the BPDE adduct formation was with -dAMP. However, the bottom FLN spectrum possesses additional weak ZPLs in the 377-381 nm region, which are not present in the top spectrum.

Similar experiments were performed in this laboratory where the B[*a*]P-DNA digest at the adduction level of ~ $1{:}10^4$ base-pairs was analyzed by on-line TLC-FLNS [unpublished results]. It was shown that extensively washing the plates with ethanol decreased the luminescent background of the PEI plates. Based on well-established

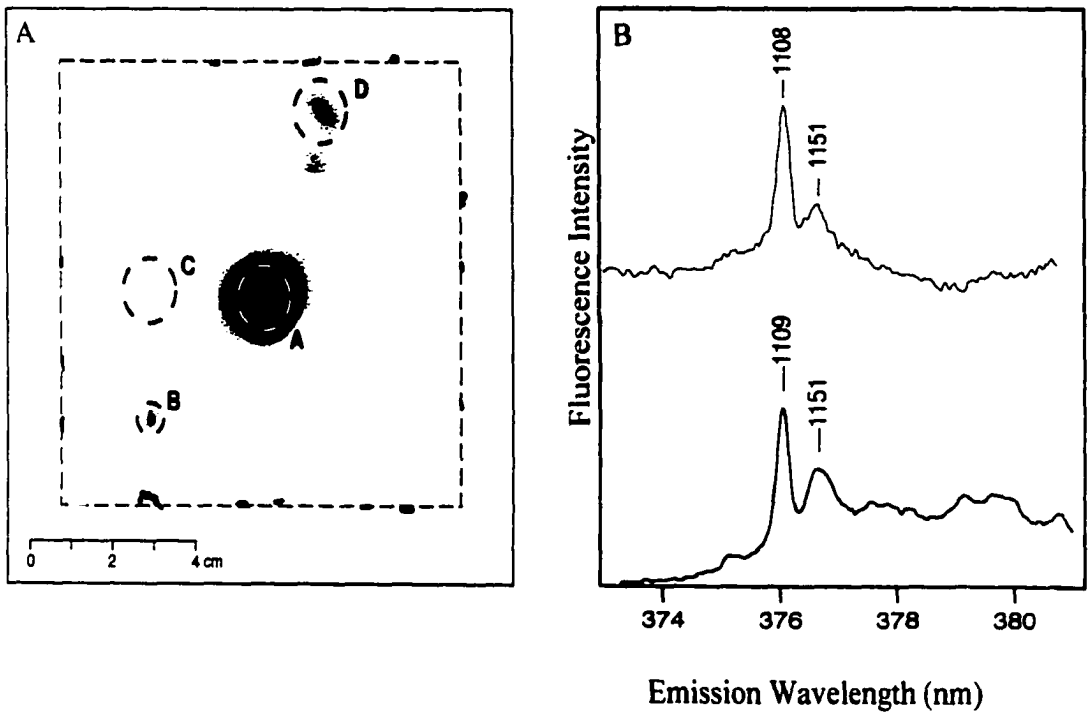

Figure 2-9. Frame A: Autoradiogram of BPDE adducted (~ $1:10^2$) and ^{32}P-postlabeled DNA after two-dimensional development on a PEI cellulose plate. Frame B, top: FLN spectrum of spot A extracted from the PEI plate of frame A. The bottom spectrum corresponds to the *anti*-BPDE-dAMP standard. T = 12 K; λ_{ex} = 361.0 nm. From Ref. 26 with permission.

migration times/distances for the TLC separation of *anti*-BPDE-dGMP [27], the same major spot as shown in Figure 2-9A was observed (data not shown). The on-line TLC-FLNS analysis revealed that the spot on the PEI-TLC plate corresponded to the *anti-trans*-BPDE-dGMP adduct isomer. This indicates, in agreement with a large number of ^{32}P-postlabeling studies [28-30], that the top FLN spectrum of Figure 2-9B most probably does not correspond to *anti*-BPDE-dAMP but to *anti-trans*-BPDE-dGMP. In fact, the presence of the –dGMP adduct was anticipated since 90-95% of total *anti*-BPDE derived DNA adducts are formed with guanine rather than adenine [30].

These results show that although FLNS can be combined with TLC, providing additional selectivity in the analysis of TLC spots associated with structurally similar analytes, its practical application is often confounded by the luminescence background of chromatographic media and glass support. Moreover, band broadening in TLC separations further limits the sensitivity of this approach. Nonetheless, in cases where extremely low detection levels are not required, these methodologies can be utilized. In particular, the semi-on-line combination of HPLC-TLC-FLNS, where the coupling strategies have been extensively developed and tested, could be applicable to the analysis of complex mixtures.

2.5. Polyacrylamide Gel Electrophoresis (PAGE) and FLNS

PAGE is a well-established technique for separating intact DNA in a highly cross-linked acrylamide gel separation media under the influence of an applied electric field. In many instances PAH-DNA adducts are best studied in intact DNA as opposed to the procedures described above. This is made possible by combining PAGE with FLNS.

The performance of PAGE-FLNS was tested with stable *anti*-B[*a*]P diolepoxide (*anti*-BPDE) adducts of various oligodeoxynucleotides [32,33]. As with TLC-FLNS, fluorescence analysis of PAGE-separated bands directly on the separation media (polyacrylamide gel) was impractical due to background luminescence. Therefore, the separated DNA band had to be extracted and redissolved in glycerol/water for FLNS analysis. For the sequences studied, it was shown that the spectral features of the N^2-dG adducts of single-stranded (ss) and double-stranded (ds) oligomers were similar, limiting spectral differentiation between ss and ds oligomers. Nonetheless, conformational information could be obtained for both ss and ds oligomers, as shown in Figure 2-10. The autoradiogram (left) shows the modification of ss d(TTAAGGAATT) by *anti*-BPDE enantiomers (see figure caption for details). Frame A shows FLN spectra (λ_{ex}= 356.9 nm) of DNA ss oligomers adducted with (+)-*anti*-BPDE that were extracted from the polyacrylamide gel (lane 2 of the autoradiogram), bands a, b, and d. The slowly-migrating DNA oligomers (assigned as external type adducts, solid line of frame A) displayed prominent ZPLs, whereas the oligomers with the fastest electrophoretic mobilities exhibited weaker ZPLs (alternating dotted and dashed line) and the origin band shifted to ~381.5 nm, characteristic of highly base-stacked adducts [31,32]. Adducted oligomers with a fluorescence origin at 379.5 nm and intermediate electrophoretic mobilities possessed weaker ZPLs (dashed line) compared to the external adduct type, but stronger than those of highly base-stacked adducts. Therefore, this type of adduct was assigned as partially base-stacked [31].

Frame B shows spectra from two different (–)-*anti*-BPDE adducted oligomers (lane 1; bands a and c). The solid spectrum is from the major adduct (extract from band

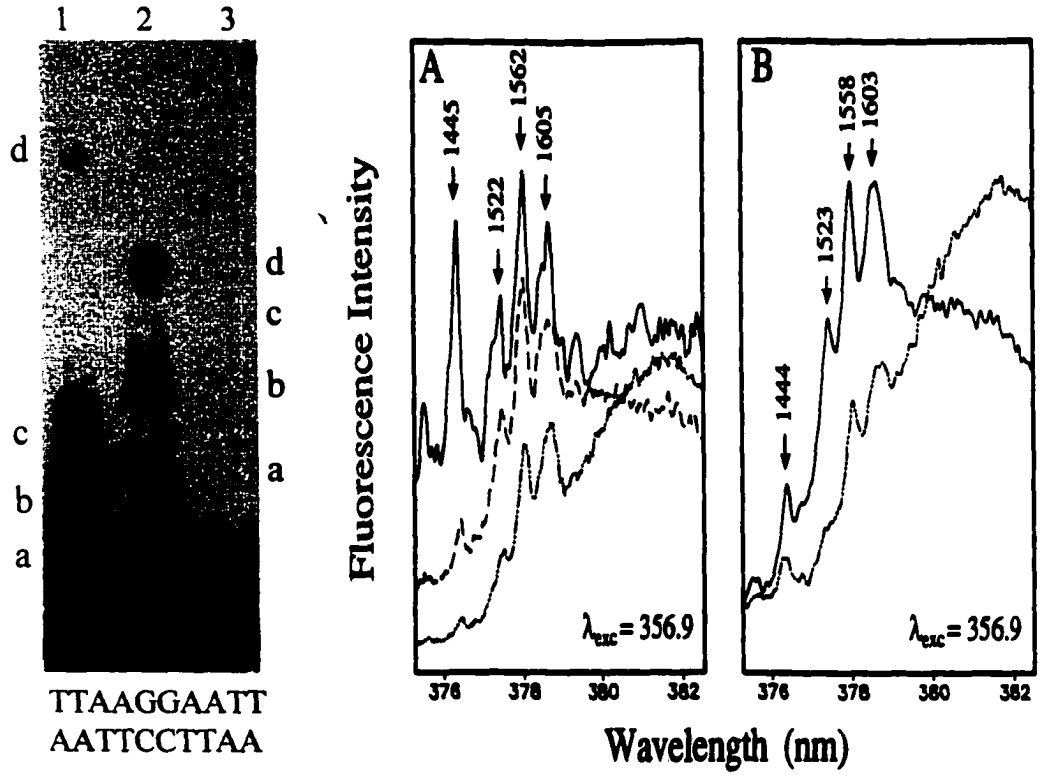

Figure 2-10. Left: autoradiogram of d(TTAAGGAATT) modified by (±)-*anti*-BPDE enantiomers. Lanes 1-3 correspond to (–)-*anti*-BPDE, (+)-*anti*-BPDE, and unreacted DNA oligomer, respectively. The anode is at the bottom of the figure; unmodified oligomer corresponds to the highly intense band exhibiting the fastest electrophoretic mobility. Bands of modified oligomers are labeled by lower-case letters. Frame A shows FLN spectra of (+)-*anti*- adducts corresponding to bands d (solid line), b (dashed line), and a (alternating dotted and dashed line) of lane 2. Frame B shows FLN spectra of (–)-*anti*-BPDE adducts corresponding to bands a (dotted-dashed line) and band c (solid line) of lane 1. FLN spectra from top to bottom correspond to external (top), partially base-stacked, and highly base-stacked adducts. λ_{ex} = 365.9 nm; T = 4.2 K. From Ref. 32 with permission.

c), and the alternating dotted and dashed spectrum is of the extract from the fastest-migrating band (a). Based on FLN and NLN spectra (data not shown), the conformations were assigned as partially- and highly base-stacked, respectively. The FLN spectrum of the extract from band d (line 1, data not shown) was very similar to the FLN spectrum of adduct extracted from spot d (lane 2), and therefore it was assigned as an external (-)-*anti*-BPDE-dGMP adduct.

PAGE-FLNS was also used to study the binding of (−)-*anti*- and (+)-*anti*-BPDE to several sequence-defined ds oligomers [31]. Two of the oligomers contained central 5′-RAGGAR-3′ sequences (R = purine), which appear to be frequently mutated by racemic (±)-*anti*-BPDE [33-35]. Two other oligomers contained a central 5′-CCGG-3′ or 5′-TGGT-3′ sequence, which are strongly preferred for covalent binding but are less frequently mutated. Binding of the two enantiomers to the latter two sequences (data not shown) yielded a distribution of BPDE-N^2-dG adduct conformations similar to those formed in random sequence DNA *in vitro*, which means that the external conformation of the N^2-dG adduct was dominant. PAGE-FLNS studies established that binding of (−)-*anti*-BPDE to the 5′-RAGGAR-3′ sequences yielded more of the partially base-stacked and less of the quasi-intercalated conformers than observed for random sequence DNA [31,32]. Importantly, the (+)-*anti*-BPDE bound to the more mutagenically inclined 5′-RAGGAR-3′ sequences yielded little external-type adduct in comparison to the other two sequences or random sequence DNA. However, the (+)-*anti*-BPDE adducts formed with the 5′-RAGGAR-3′ sequences yielded an unusually high proportion of partially base-stacked adducts. Since the (+)-*anti*-BPDE appears to be more mutagenic, this result suggests a possible role of partially base-stacked adduct conformations in mutagenesis.

In both TLC- and PAGE-FLNS, sensitivity is of large concern. If only small amounts of sample are available, which is commonly the case in studying the systems these combinations were intended for, either the background luminescence of the separation media or sample losses associated with analyte extraction will likely prevent these combinations from ever being useable for low-level detection. Moreover, TLC and PAGE can suffer from low separation resolution and efficiency, inherent to the techniques. Therefore, for FLNS to be useful in studying analytes in complex biological systems, more efficient separation techniques were needed that could accommodate small sample amounts, provide the necessary separation efficiency and resolution, and have minimal background interference in on-line detection. This was accomplished with capillary electrophoresis as presented in Chapters 3, 4, and 5 of this thesis, and then high-performance liquid chromatography as presented in Chapter 6.

References

1. Personov, R.I., in: Agranovich, V.M., Hochstrasser, R.M. (Eds.), *Spectroscopy and Excitation Dynamics of Condesned Molecular Systems*, North-Holland, Amsterdam, Vol. 4, 1983, pp. 555.

2. Fidy, J., Vanderkooi, J.M., in: Douglas, R.H., Moan, J., Rontó, Gy., (Eds.), *Light in Biology and Medicine*, Plenum Press, New York, Vol. 2, 1991, pp. 367.

3. Jankowiak, R., Small, G.J., in: Neilson, A.H., (Ed.), *The Handbook of Environmental Chemistry: PAHs and Related Compounds, Chapter 11.* Springer-Verlag, Berlin-Heidelberg-New York, 1998, pp. 119-145.

4. Weber, M.J., in: Yen, W.M., Selzer, P.M., (Eds.), *Topics in Applied Physics*, Springer-Verlag, New York, Heidelberg, Berlin, Vol. 49, 1986, pp. 1189-240.

5. Jankowiak, R., Hayes, J.M., Small, G.J., *Chem. Rev.* 1993, *93*, 1471.

6. Hayes, J.M, Lyle, P.A., Small, G.J., *J. Phys. Chem.* 1994, *98*, 7337.

7. Pieper, J., Voigt, J., Renger, G., Small, G.J. *Chem. Phys. Lett.* 1999, *310*, 296.

8. Riseberg, L.A., *Phys. Rev.* 1973, *A7*, 67.

9. Jankowiak, R., in: *Shpol'skii Spectroscopy and Other Site Selection Methods: Applications in Environmental Analysis, Bioanalytical Chemistry and Chemical Physics, Chapter 1.2*, John Wiley and Sons, New York, (in press).

10. Osadko, I.S., in: Dusek, K. (Ed.), *Advances in Polymer Science*, Springer-Verlag, Berlin, Heidelberg, Vol. 114, 1994, pp. 123.

11. Jankowiak, R., Small, G.J., *Chem. Res. Toxicol.* 1991, *4*, 256.

12. Jankowiak, R., Roberts, K.P., and Small, G.J. *Electrophoresis* 2000, *21*, 1251.

13. Jankowiak, R., Small, G.J., *Anal. Chem.* 1989, *61*, 1023A.

14. Dushinsky, F., *Acta Physiochem.* 1937, *7*, 551.

15. Hofstraat, J.W., Gooijer, C., Velthorst, N.H., in: Schulman, S.G., (Ed.), *Molecular Luminescence Spectroscopy: Methods and Applications, Part 2*, John Wiley and Sons, New York, 1988, pp. 383-459.

16. Vo-Dinh, T., Suter, G.W., Kallir, A.J., Wild, U.P., *Anal. Chem.* 1986, *58*, 3135.

17. Cooper, R.S., Jankowiak, R., Hayes, J.M., Pei-qui, L., Small, G.J., *Anal. Chem.* 1988, *60*, 2692.

18. Hofstraat, J.W., Engelsma, M., Gooijer, C., Velthorst, N.H., *Spectrochim. Acta* 1989, *45A*, 491.

19. Hofstraat, J.W., Jansen, H.J.M., Hoornweg, G.Ph., Gooijer, C., Velthorst, *Anal. Chim. Acta* 1985, *170*, 61.

20. van de Neese, R.J., Vinkenburg, I.H., Jonker, R.H.J,. Hoornweg, G.Ph., Gooijer, C., Brinkman, U.A.Th., Velthorst, N.H., *Appl. Spec.* 1994, *48*, 788.

21. Hofstraat, J.W., Engelsma, M., van de Neese, R.J., Gooijer, C., Velthorst, N.H., Brinkman, U.A.Th., *Anal. Chim. Acta* 1986, *186*, 247.

22. van de Neese, R.J., Hoogland, G.J.M., De Moel, J.J.M., Gooijer, C., Brinkman, U.A.Th., Velthorst, N.H., *J. Chromatogr.* 1991, *552*, 613.

23. Kok, S.J., Bakker, I., Gooijer, C., Brinkman, U.A.Th., Velthorst, N.H., *Anal. Chim. Acta*, 1999, *389*, 77.

24. Kok, S.J., Posthumus, R., Bakker, I., Gooijer, C., Brinkman, U.A.Th., Velthorst, N.H., *Anal. Chim. Acta* 1995, *303*, 3.

25. Randerath, K., Reddy, M.V., Gupta, R.C., *Proc. Natl. Acad. Sci. USA* 1981, *78*, 6126.

26. Kok, S.J., *Ph.D. Thesis: Identification Potential of Laser Induced Fluroescence Detection Coupled to CE and LC*, Vrije Universiteit, de Boelelaan, Netherlands, 1999.

27. Suh, M., Ariese, F., Small, G.J., Jankowiak, R., Hewer, A., Phillips, D.H., *Carcinogenesis* 1995, *16*, 2561.

28. Meehan, T., Straub, K., *Nature* 1979, *277*, 410.

29. Cheng, S.C., Hilton, B.D., Roman, J.M., Dipple, A., *Chem. Res. Toxicol.* 1989, *2*, 334.

30. Geacintov, N.E., Cosman, M., Hingerty, B.E., Amin, S., Broyde, S., Patel, D.J., *Chem. Res. Toxicol.* 1997, *10*, 111.

31. Marsch, G.A., Jankowiak, R., Suh, M., Small, G.J., *Chem. Res. Toxicol.* 1994, *7*, 98.

32. Marsch, G.A., Jankowiak, R., Farhat, J.H., Small, G.J., *Anal. Chem.* 1992, *64*, 3038.

33. Yang, J.-L., Maher, V.M., McCormick, J.J., *Proc. Natl. Acad. Sci. USA* 1987, *84*, 3787.

34. Maher, V.M., Yang, J.-L., McCormick, J.J., *Mol. Cell Biol.* 1987, *7*, 1267.

35. Marsch, G.A., *Sequence Preference Motifs of Covalent DNA Binding by Intercalating Drugs and Cartcinogens, Ph.D. Thesis*, Florida State University, 1990.

CHAPTER 3. CAPILLARY ELECTROPHORESIS WITH ON-LINE FLNS (CE-FLNS)

3.1. Principles of Capillary Electrophoresis

Capillary electrophoresis (CE) is a modern separation technique that permits rapid and efficient separation of components under the influence of an applied electric field. The first highly efficient CE separations were demonstrated by Jorgenson and Lukas in the early 1980s [1,2], and the first commercial CE instruments arrived later that same decade. Since its inception, CE has established itself as a widely used analytical and bioanalytical separations technique for a variety of applications such as inorganic anions [3-7], metal cations [8-11], drugs [12-14], carbohydrates [15-19], polycyclic aromatic hydrocarbons [20,21], peptides [22,23], proteins [24,25], DNA [26,27], DNA adducts [28,29], bacteria [30,31], and single cells [32,33]. Much like traditional electrophoresis, separation by CE is achieved when an external field is applied to a solution of charged species. Each ion is attracted to the electrode of opposite charge, and, at a given electric field, charged species travel with different velocities depending upon their size, valent charge, and environment [34]. This rate is known as the electrophoretic mobility of an analyte and is expressed in $cm^2/V \cdot s$ [1]. However, a unique feature of CE is the phenomenon known as electroosmosis (see below). Briefly, the occurrence of electroosmosis, originating on the inner wall of the glass capillary, provides a force that drives the flow of all species in the same direction within the capillary; usually from the positive to the negative electrode [35].

Traditionally, electrophoretic separations have been performed on semisolid support media such as slab gel or non-gelatinous material such as paper or cellulose

acetate [36]. The support media provide a physical support for the electrolyte buffer that maintains electrical conductance between the electrodes (cathode and anode). In CE, the capillary itself provides this support for the electrolyte and its small size (typically between 20 to 150 μm inner diameter) ensures rapid heat dissipation. A basic CE instrument schematic is shown in Figure 3-1, which consists of a high-voltage power supply, electrolyte-filled capillary placed between two electrolyte reservoirs, sample reservoir, and a detection system.

The most common way of classifying separation methods in CE is based on the background electrolyte (buffer) system. The two classification systems are either continuous or discontinuous [37]. Further sub-classifications are based on the constancy of the electrolyte. If the composition of a continuous background electrolyte is constant; as in capillary zone electrophoresis [1,2,38-41], micellar electrokinetic capillary chromatrography [41-45], and capillary gel electrophoresis [46-49], the resulting separation is a kinetic process. If the buffer composition is not constant, as in capillary isoelectric focusing [50-52], the result is a steady-state process [37]. In a constant electrolyte system, a constant electric potential and effective mobility for an analyte in the capillary is observed. Sample components will migrate (and separate) in a constant electric field according to their effective mobilities. In the case where the background electrolyte composition is not constant, effective mobilities will vary in the electric field along the capillary, focusing sample components at certain points (e.g., the isoelectric point for proteins). In contrast, a discontinuous electrolyte system is one in which the sample migrates between two different electrolytes as a distinct individual zone. As opposed to a continuous electrolyte system, conduction is accomplished by the

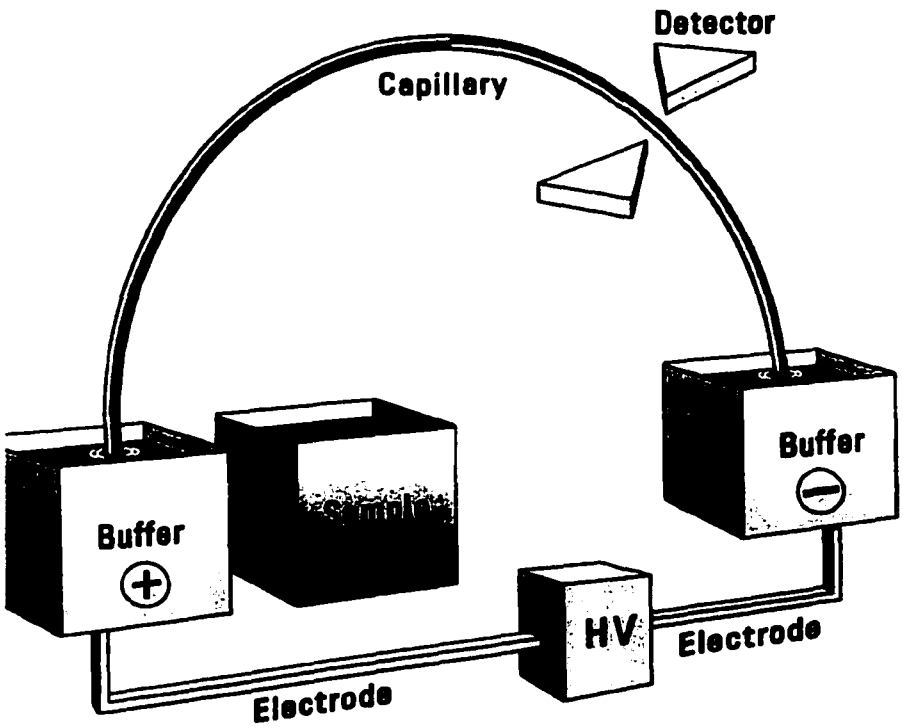

Figure 3-1. Basic schematic of a capillary electrophoresis setup, consisting of a high-voltage power supply, electrolyte-filled capillary placed between two electrolyte reservoirs, sample reservoir, and a detection system near the cathode.

sample ions in the analyte zone in a discontinuous system [53]. Capillary isotachophoresis is an example of a discontinuous system [54,55].

As stated above, movement of charged species in an applied electric field is characterized by the electrophoretic mobility, μ_{ep}, of the species. In capillary electrophoresis, the apparent mobility of an analyte is the sum of the electrophoretic mobility and the mobility of the electroosmotic flow, μ_{eo} [35,37]:

$$\mu = \mu_{ep} + \mu_{eo} \tag{3.1}$$

In the absence of electroosmosis the migration velocity (v) of a charged species is given by:

$$v = \mu_{ep}E = \frac{\mu_{ep}V}{L} \tag{3.2}$$

where μ_{ep} is the electrophoretic mobility, E is the field strength, V is the voltage applied across the capillary, and L is the length of the capillary. Under these conditions the time (t) needed for a solute to migrate from one end of the capillary to the other is given by:

$$t = \frac{L}{v} = \frac{L^2}{\mu_{ep}V} \tag{3.3}$$

Therefore, in the presence of electroosmotic flow, the migration velocity time can be written as:

$$v = \frac{(\mu_{ep} + \mu_{eo})V}{L} \tag{3.4}$$

and

$$t = \frac{L^2}{(\mu_{ep} + \mu_{eo})V} \tag{3.5}$$

As mentioned above, electroosmotic flow (EOF) is a unique phenomenon in CE that provides flow of a solution in contact with a solid surface in an applied electric field, and drives the flow of all species in the same direction within the capillary. Electroosmotic flow originates on the inner walls of fused silica capillaries when the silanol groups (SiOH) on the capillaries inner surface dissociates when in contact with the electrolyte, creating the negatively charged SiO^- surface [56]. A model of the silica-solution interface is shown in Figure 3-2. Hydrated cations in the electrolyte are attracted to the negatively charged silanol groups, creating a double layer. The first layer, the compact layer, is tightly bound to the negative capillary surface by electrostatic forces. A second layer, the more loosely bound diffuse layer, consists of mobile cations and is able to flow toward the cathode in an applied electric field at the plane of shear, dragging the bulk solution in the capillary. The potential formed across the double layer is called the zeta potential (ζ), which is given in the Helmholtz equation as [35]:

$$\zeta = \frac{4\pi\eta\mu_{eo}}{\varepsilon} \tag{3.6}$$

where η is the viscosity, ε is the dielectric constant of the solution, and μ_{eo} is the coefficient for electroosmotic flow. Therefore, electroosmotic mobility can be defined as:

$$\mu_{eo} = \frac{\varepsilon\zeta}{4\pi\eta} \tag{3.7}$$

Factors that can affect electroosmotic flow are electrolyte pH, ionic strength, organic solvent composition, choice of buffer anions/cations, and applied voltage [37]. The double layer thickness is generally only a few hundred nanometers and the potential

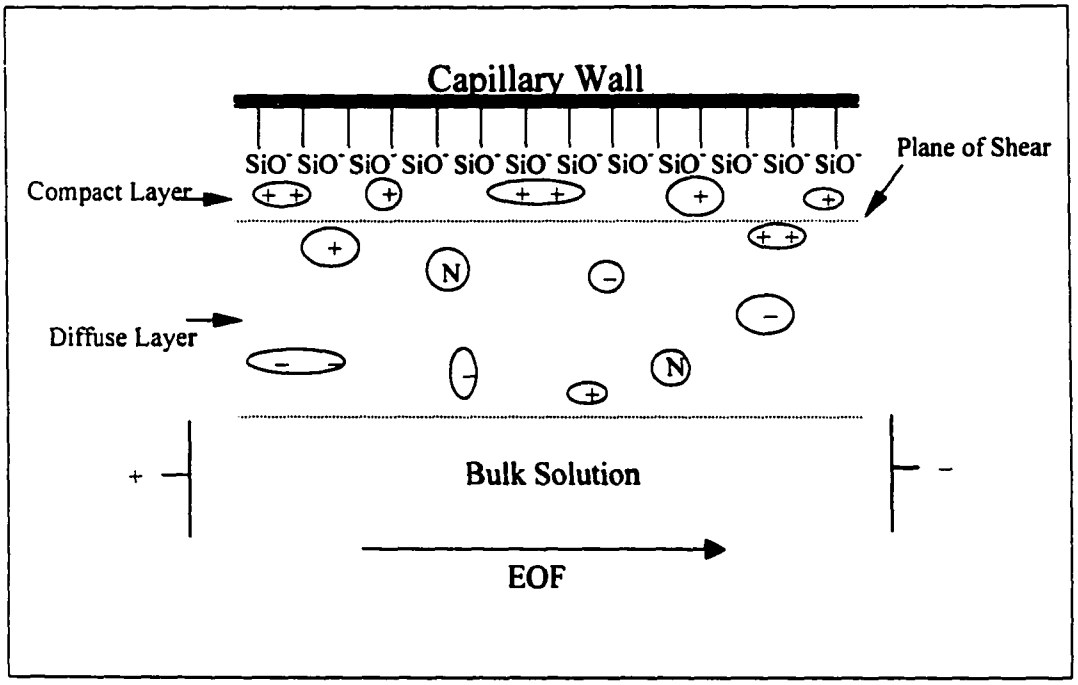

Figure 3-2. Scheme showing the formation of electroosmotic flow (EOF) within a glass capillary. The negatively charged SiO^- groups on the inner wall of the capillary attract cations, forming a tightly bound compact layer. Further into the capillary a loosely bound diffuse layer is formed, where hydrated cations drag the bulk solution toward the cathode.

drop results in a flat bulk flow profile of solvent toward the cathode. The resulting flat flow-profile creates an extremely efficient "pumping" mechanism when compared to the parabolic flow profile associated with pressure-driven separation techniques such as high-performance liquid chromatography. Therefore, the zone variance (σ^2) and number of theoretical plates (N) can be expressed as [35]:

$$\sigma^2 = \frac{2DL^2}{(\mu_{ep} + \mu_{eo})V} \tag{3.8}$$

and

$$N = \frac{(\mu_{ep} + \mu_{eo})V}{2D} \tag{3.9}$$

where D is the diffusion coefficient of the solute. Factors that can influence separation efficiency are: the length of the injection plug, axial diffusion, electromigration dispersion, solute-wall interactions, and Joule heating, to name a few. Axial diffusion is minimized when operating at high voltages, however, band broadening from Joule heating can occur from the electric current generated in the electrophoresis buffer. Therefore, optimal conditions are achieved by operating at voltages that create minimal heat and minimal diffusion [37]. Moreover, the small dimensions of the capillary used in CE allow heat to efficiently dissipate to the surrounding environment. Therefore, the control of Joule heating, along with the flat plug-like flow profile in CE create a highly efficient separation mechanism with separation efficiencies as high as 10^5-10^6 theoretical plates.

Resolution (R) of two zones in CE is a function of selectivity, column efficiency, and migration time [57] and is given by:

$$R = \frac{1}{4(2)^{1/2}} \cdot (\mu_{ep,2} - \mu_{ep,1}) \cdot \left[\frac{V}{D(\mu_{ep,ave} + \mu_{eo})} \right]^{1/2} \qquad (3.10)$$

where $\mu_{ep,1}$ and $\mu_{ep,2}$ are the electrophoretic mobilities for the two solute zones and $\mu_{ep,ave}$ is the average electrophoretic mobility. From this equation the highest resolution is obtained when $\mu_{eo} = -\mu_{ep}$; however, the trade-off is analysis time.

3.2. CE-FLNS System

In interfacing CE with on-line FLNS detection, the primary challenges were to develop a cryostat that could easily be adapted to a commercial CE instrument, and quickly be cooled to cryogenic temperatures to not introduce significant band-broadening of the separated analyte zones. This was accomplished in 1996 by Jankowiak *et al.* [58] with the CE-FLNS design shown in Figure 3-3. The apparatus consists of a modular CE apparatus, FLNS instrumentation, and a capillary cryostat (CC) mounted to an automated translation stage. The modular CE apparatus is a fully automated, high-voltage ATI Unicam Model 310 instrument. The inlet of a UV-transparent capillary is placed in the CE instrument with the outlet threaded axially through the CC and affixed at either end of the CC with plastic tubing. The capillary terminates in an outlet CE-buffer vial. CE separations are monitored using a model Innova 90C (Coherent, Santa Clara, CA) CW argon-ion laser excitation source operating at 351.1 nm (100 mW output power).

Fluorescence emission is collected at a 90-degree angle to the excitation beam with a reflecting objective (25-0506 X 15, Ealing, Holliston, MA), focused into a 0.3-m monochromator (McPherson, Acton, MA), and detected with an intensified charge-

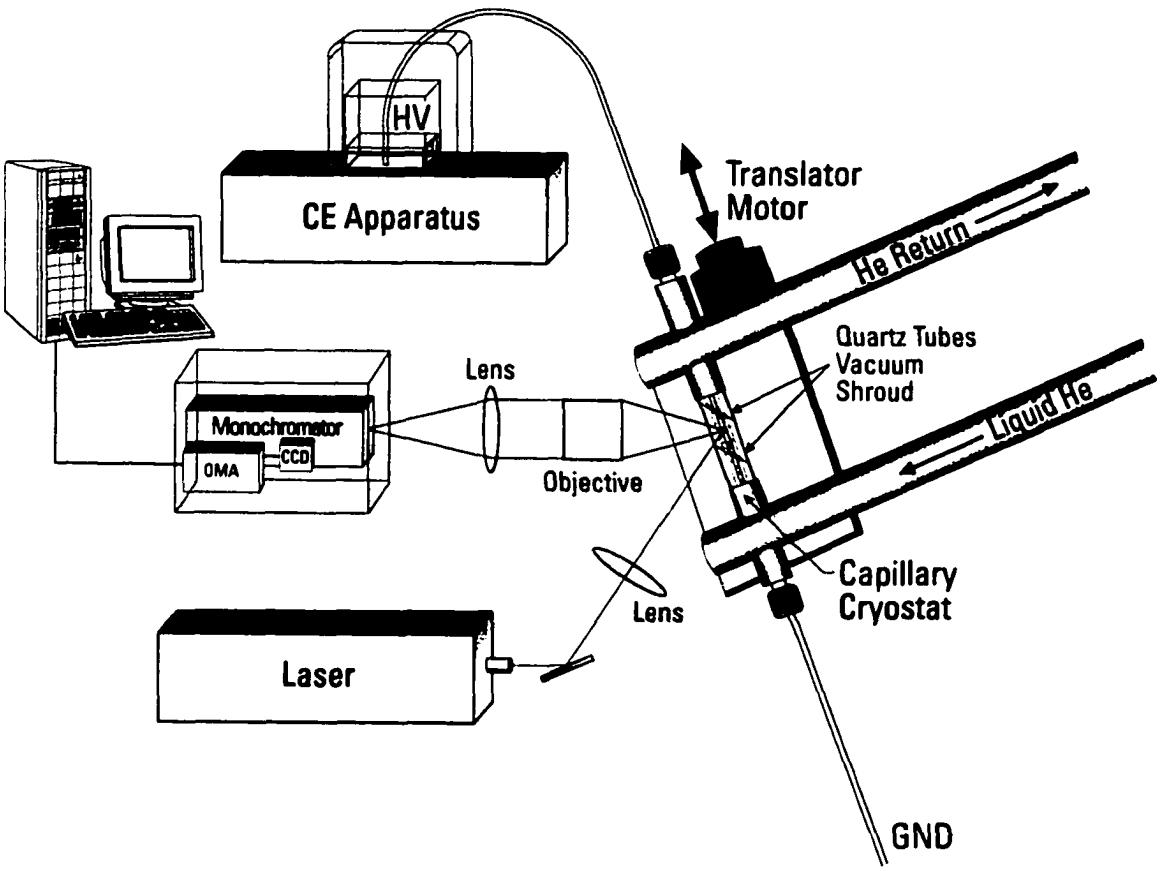

Figure 3-3. Schematic diagram of the CE-FLNS system. The instrumentation consists of a CE apparatus, capillary cryostat, translation stage, laser excitation source, a monochromator, and either an intensified photodiode array or charge-coupled device for detection. Pulse generators are employed for time-resolved spectroscopy. From Ref. 58 with permission.

coupled device (Roper Scientific, Trenton, New Jersey) that is triggered by a high-voltage pulse generator (Roper Scientific Model PG200). When the analyte of interest enters the detection cell, the cryostat is quickly cooled (see below) to liquid helium temperature (4.2 K). Automated translation of the cryostat is accomplished with a micron step-size translation stage having a 10-cm travel distance (New England Affiliated Technologies, Lawrence, MA). The excitation source for FLNS studies is a Lambda Physik FL-2002 pulsed dye laser (line-width of ~ 0.2 cm^{-1}), pumped by a Lambda Physik Lextra 100 XeCl excimer laser (Lambda Physik, Ft. Lauderdale, FL) at a repetition rate of 10 Hz. FLN spectra are obtained using various delay times with a gate width of 200 ns. The spectral resolution for FLN in this set-up is 0.09 nm.

3.2.1. Capillary Cryostat

The CC consists of a double-walled quartz cell with inlet and return lines for introducing liquid nitrogen or liquid helium (see Figure 3-3). The outer portion of the CC is evacuated. The capillary, positioned in the central region of the CC, is cooled by a continuous flow of liquid nitrogen (77 K) or helium (4.2 K). The low thermal capacity of the capillary along with the small dimensions of the CC (inner portion, 4 mm ID x 22-cm length) allow rapid cooling to 4.2 K. To discriminate against scattered and reflected laser light, the CC is tilted 20° with respect to the laser beam. An example of the cooling rate is shown in Figure 3-4, where fluorescence spectra of pyrene, acquired as a function of time after opening the helium transfer line valve, are shown [59]. Spectrum (a) was obtained at room temperature and spectra (b)-(e) were obtained 30, 35, 40, and 50 seconds after opening the valve. The five spectra, plotted using the same y-axis scale

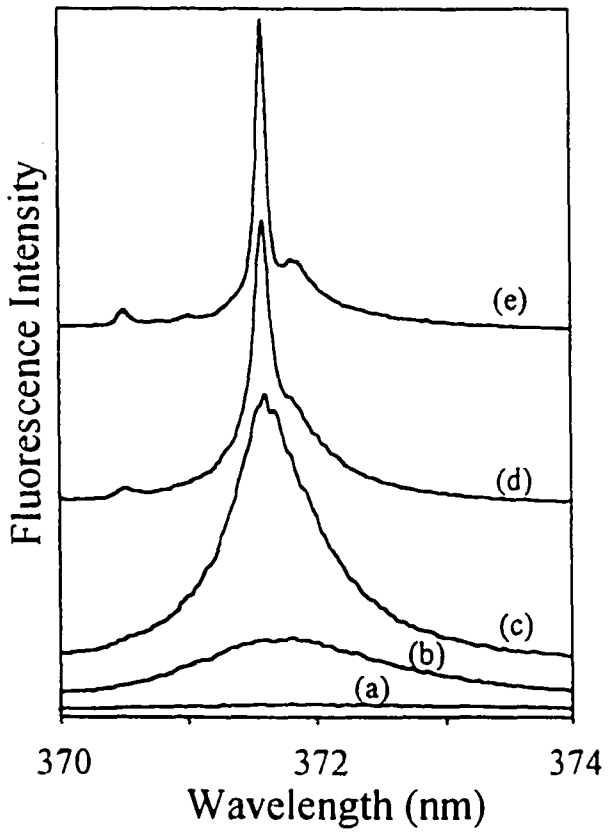

Figure 3-4. FLN spectra of pyrene as a function of time (temperature) after opening the valve of the helium transfer line to the capillary cryostat; $\lambda_{ex} = 364.0$ nm. Spectrum (a) was obtained at room temperature and spectra (b) - (e) were obtained 30, 35, 40, and 50 seconds, respectively. From Ref. 59 with permission.

expansion (offset for clarity), illustrate a fast cooling rate (minimizing analyte zone dispersion) and a significant increase in fluorescence with decreasing temperature. Spectrum (e), obtained at 50 seconds, is identical to the FLN spectrum of pyrene obtained in a regular helium immersion cryostat.

In CE-FLNS, when the analytes enter the CC optical window, the capillary is rapidly frozen in the CC to 4.2 K with liquid helium. Once frozen, long residence/detection times (up to hours) are available to completely characterize the analyte zones via FLNS. A precision stage provides translation of the CC along the capillary axis by ± 4 cm allowing the separated analytes to be sequentially characterized by FLNS. With this setup, the LOD of the CE-FLNS system is at the low-attomole level for moderately fluorescent chromophores [29]. When the fluorescence analysis is complete, efficient warming of the CC and capillary can be achieved by closing the valve of the helium transfer line and introducing (warm) helium gas into the CC [58].

3.2.2. Preliminary Test

The CE-FLNS system was first tested by Jankowiak and co-workers [58] with a mixture of five PAHs [benzo[*a*]pyrene (B[*a*]P), benzo[*e*]pyrene (B[*e*]*P*), pyrene, 1-hydroxypyrene, and benz[*a*]- anthracene (BA)], as shown in Figure 3-5. The CE electropherogram is shown in frame 3-5A, while the on-line FLN spectra of the five separated PAHs are shown in frames 3-5B and 3-5C. Identification was based on comparison of the vibronically excited FLN spectra of the CE-separated peaks with those of off-line generated reference spectra of the five compounds.

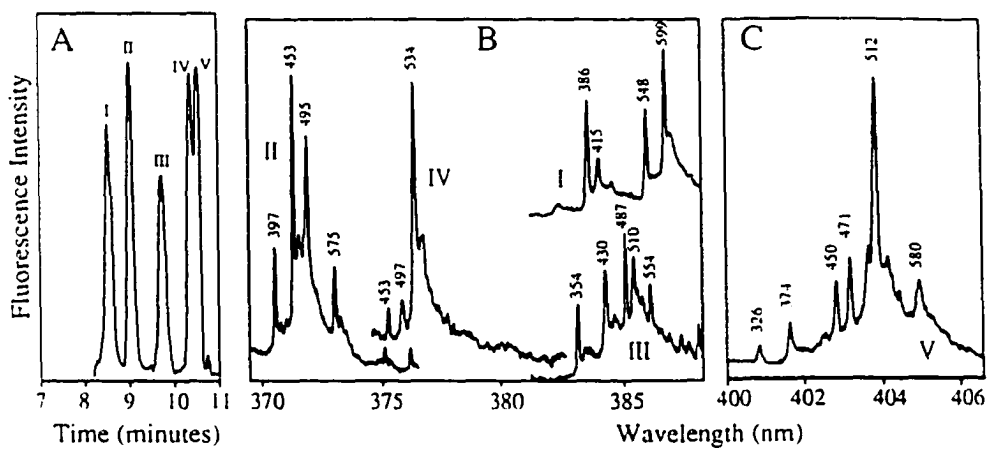

Figure 3-5. Fluorescence based CE electropherogram of the PAH mixture (frame A) and FLN spectra of the CE-separated PAHs (frame B); see Ref. 58 for separation conditions. Based on FLNS analysis the labeled peaks correspond to 1-hydroxypyrene (I), pyrene (II), BA (III), and B[*e*]P (IV), and B[*a*]P (V). Laser excitation wavelength 378.0 nm, 365.2 nm, 378.0 nm, 369.0 nm, and 395.7 nm respectively; T = 4.2 K. Peaks are labeled with their excited-state vibrational frequencies, in cm^{-1}; from Ref. 58 with permission.

More rigorous testing of the CE-FLNS by Zamzow *et al.* [59] was conducted, an example of which is shown in Figure 3-6 for a mixture of protonated and deuterated benzo[*a*]pyrene (B[*a*]P-d_{12}). Frame 3-6A shows a portion of the room-temperature fluorescence electropherogram for a B[*a*]P-d_{12}/B[*a*]P mixture (10^{-5} M each). The 4.2 K FLN spectra for CE-separated peaks (a) and (b) obtained using selective laser excitation at 395.7 nm are shown in frames 3-6B (spectrum a) and 3-6C (spectrum b), respectively. The FLN peaks are labeled with their S_1 vibrational frequencies in cm^{-1}. Comparison of the CE-FLN spectra in Figure 3-6 shows that spectrum (a) is virtually indistinguishable from spectrum (c) of the B[*a*]P-d_{12} standard and that spectrum (b) is identical to spectrum (d) of the B[*a*]P standard. Obvious differences in vibrational frequencies and intensities between spectra (a) and (b) are observed. For example, there are strong modes at 353, 493, and 558 cm^{-1} for B[*a*]P-d_{12}, while B[*a*]P has strong modes at 510 and 580 cm^{-1}. Therefore, peaks (a) and (b) of the electropherogram were definitively identified as deuterated and protonated B[*a*]P, respectively.

A preliminary test of on-line FLNS detection system with capillary electrochromatography (CEC) was also conducted (data not shown). CEC is a hybrid separation technique where the same flat, electroosmotic flow profile is used as in CE; however, the capillary is filled with functionalized stationary phase particles (e.g., C8, C18, and phenol) as in HPLC. The result is a high performance separation technique that can improve resolution and reduce analysis time in comparison to standard CE. However, its drawbacks are that the packed capillaries are difficult to manufacture, fragile, and rather expensive. Nevertheless, CEC is rapidly gaining acceptance as a high

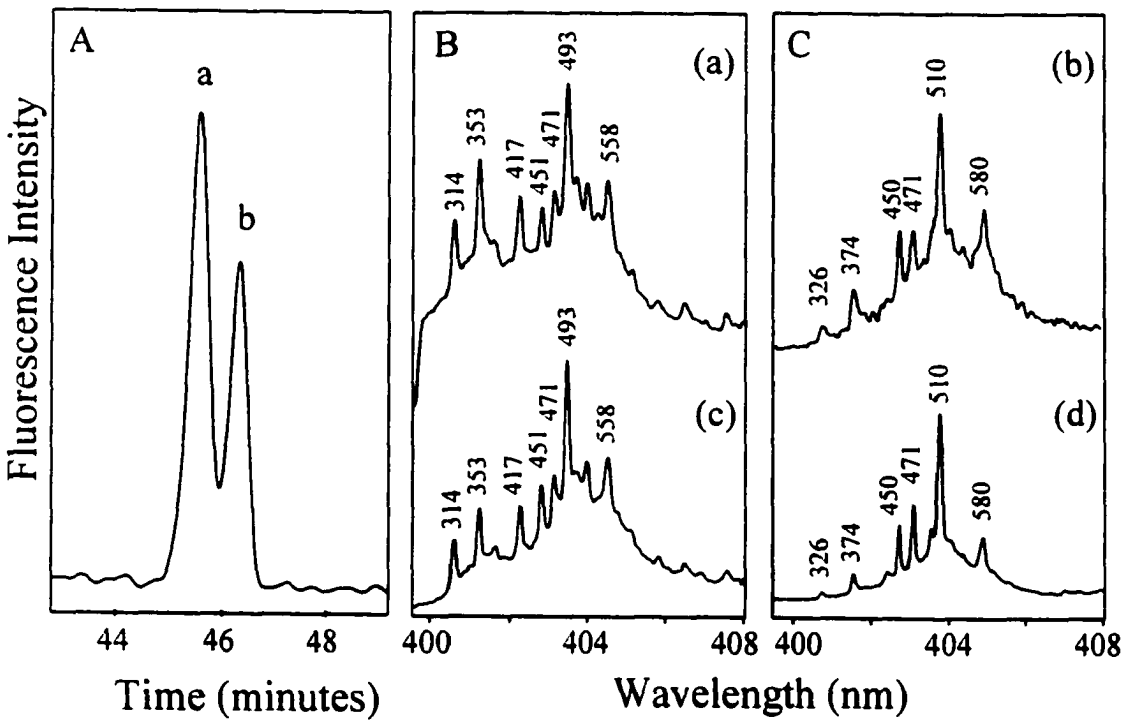

Figure 3-6. Frame A: room-temperature fluorescence electropherogram for a mixture of B[*a*]P-d_{12} (peak a) and B[*a*]P (peak b); see Ref. 59 for separation conditions. Frame B shows FLN spectra obtained for the CE-separated peak a (spectrum (a)), and the FLN spectrum from the reference library (spectrum (c)). Analogously, frame C shows the identification of the CE-separated peak b (see text for details). From Ref. 59 with permission.

performance analytical technique, especially with MS detection. A preliminary unpublished result from a CEC-FLNS experiment revealed that FLN spectra could be generated for a B[*a*]P-filled CEC (C18) capillary. However, the fragility of these capillaries makes their practical use for FLNS cost prohibitive, especially when most separations are possible with other, less expensive separation modes of CE.

The above tests of the CE-FLNS system indicated that in comparison to TLC- and PAGE-FLNS, on-line CE-FLNS is a more practical technique for real-world applications. CE-FLNS is fast, offers less background luminescence, and its nanoliter injection volumes are highly compatible for bioanalysis. In terms of separation performance, CE has very high separation efficiencies and resolving power. Moreover, with on-line CE-FLNS there is no post-separation extraction that could lead to sample losses from sample handling. In Chapters 4 and 5 of this thesis, CE-FLNS is applied for studies in chemical carcinogenesis: the analysis of diasteromeric DNA adducts from the most potent chemical carcinogen, dibenzo[*a,l*]pyrene; and to study the most common depurinating adducts of benzo[*a*]pyrene in humans exposed to coal smoke.

Furthermore, by interfacing FLNS with the well-established, versatile separation protocols of HPLC, it is anticipated that on-line HPLC-FLNS will significantly expand the bioanalytical applicability of FLNS and provide a complementary technique to CE-FLNS. This feasibility and design of this first-ever on-line combination of FLNS detection in HPLC is shown in Chapter 6. Its practicality is demonstrated with co-eluting geometric isomers of benzo[*a*]pyrene diols and a dibenzo[*a,l*]pyrene-deoxyadenosine adduct found in the skin of mice.

References

1. Jorgenson, J.W., Lukacs, K.D., *Anal. Chem*, 1981, *53*, 1298.

2. Jorgenson, J.W., Lukacs, K.D., *Science* 1983, *222*, 266.

3. Jandik, P., Bonn, B., *Capillary Electrophoresis of Small Molecules and Ions* VCH Publishers, New York, 1993.

4. Jones, W.R., Jandik, P. *Am. Lab.* 1990, *6*, 51.

5. Buchberger, W., Cousins, S.M., Haddad, P.R., *Trends in Anal. Chem.* 1994, *13*, 313.

6. Lamb, J.D., Huxford, T.L., Czirr, K.B. *J. Chromatogr.* 1996, *739*, 373.

7. Doble, P., Haddad, P.R. *Anal. Chem.* 1999, *71*, 15.

8. Weston, A., Brown, P.R., Jandik, P., Jones, W. R., Heckenberg, A.L. *J. Chromatogr.* 1992, *593*, 289.

9. Shi, Y., Fritz, J.S. *J. Chromatogr.* 1993, *640*, 473.

10. Shi, Y., Fritz, J.S. *J. Chromatogr.* 1994, *671*, 429.

11. Quang, C., Khaledi, M.G. *J. Chromatogr.* 1994, *659*, 459.

12. Nishi, H., Terabe, S. *J. Chromatogr.* 1996, *735*, 3.

13. Guzman, N.A., Berck, C.M., Hernadez, L., Advis, J.P. *J. Liq. Chromatogr.* 1990, *13*, 3833.

14. Trenerry, V.C., Robertson, J., Wells, R.J. *Electrophoresis* 1994, *15*, 103.

15. El Rassi, Z. *Adv. Chromatogr.* 1994, *34*, 177.

16. Honda, S., Yamamoto, K., Suzuki, S.M., U. Kakehi, K. *J. Chromatogr.* 1991, *588*, 327.

17. Linhardt, R.J., Liu, J., Han, X.-J. *Trends Glycosci. Glycotechnol.* 1993, *5*, 181.

18. Xu, X., Kok, W.T., Poppe, H. J. *Chromatogr.* 1995, *716*, 231.

19. Perez, S.A., Colón, L.A. *Electrophoresis* 1996, *17*, 352.

20. Nie, S., Dadoo, R., Zare, R.N. *Anal. Chem.* 1993, *65*, 3571.

21. Miller, J.L., Khaledi, M.G., Shea, D. *Anal. Chem.* 1997, *69*, 1223.

22. Schwer, C., Lottspeich, F. *J. Chromatogr.* 1992, *623*, 345.

23. Kornfelt, T., Vither, A., Okafo, G.N., Camilleri, P. *J. Chromatogr.* 1996, *726*, 223.

24. Simo-Alfonso, E., Conti, M., Gelfi, C., Righetti, pPG. *J. Chromatogr.* 1995, *689*, 85.

25. Ganzler, K., Greve, K.S., Cohen, A.S., Karger, B.L., Guttman, A., Cooke, A.S, *Anal. Chem.* 1992, *64*, 2665.

26. Guttman, A., Cohen, A. S., Heiger, D. N., Karger, B.L. *Anal. Chem.* 1990, *62*, 137.

27. He, Y. Pang, H.-M., Yeung, E. S. *J. Chromatogr. A.* 2000, *894*, 179.

28. Barry, J.P., Norwood, C., Vourous, P., *Anal. Chem.* 1996, *68*, 1432.

29. Roberts, K.P., Lin, C.-H., Singhal, M., Casale, G.P., Small, G.J., Jankowiak, R. *Electrophoresis*, 2000, *21*, 799.

30. Pfetsch, A., Welsch, T., *Fresenius' J. Anal. Chem.* 1997, 359, 198.

31. Avaniss-Aghajani, E., Jones, K., Chapman, D., Brunk, C., *Biotechniqes* 1994, 17, 144.

32. Lillard, S.J., Yeung, E.S., Lautamo, R.M.,A., Mao, D.T. *J. Chromatogr.* 1995, *718*, 397.

33. Chen, G.Y., Gavini, P.F., Luo, G.A., Ewing, A.G. *Neuroscience* 1995, *15*, 7747.

34. Hjerten, S. *Capillary Electrophoresis: Theory and Practice* Grossman, P.D. and Colburn, J.C., Eds., Academic Press, San Diego, 1992, *Chap. 7.*

35. Li, S.F.Y. *Capillary Electrophoresis: Principles, Practice and Applications* Elsevier Science, Amsterdam, 1992, *Chap. 1.*

36. Bruno, T.J. *Chromatographic and Electrophoretic Methods* Prentice-Hall, New Jersey, 1991, *Chap. 5.*

37. Weston, A., Brown, P.R. *HPLC and CE: Principles and Practice* Academic Press, San Diego,, 1997, *Chap. 4.*

38. Deng, Y., Fan, X., Delgado, A., Nolan, C., Kenneth, F., Zuo, Y., Jones, R.D. *J. Chromatogr. A*, 1998, *817*, 145.

39. Hutterer, K.M., Jorgenson, J.W. *Anal. Chem.* 1999, *71*, 1293.

40. Porras, S.P., Riekkola, M.-L., Kenndler, E. *J. Chromatogr. A*. 2001, *905*, 259.

41. Terabe, S., Otsuka, K., Ichikawa, K., Tsuchiya, A., Ando, T. Anal. Chem. 1984, 56, 111.

42. Burton, D.E., Sepaniak, M.J., Maskarinec, M.P. *J. Chromatogr. Sci.* 1987, *25*, 514.

43. Copper, C.L., Staller, T.D., Sepaniak, M. *Polycyclic Aromat. Compd.* 1993, *3*, 121.

44. Wiedmer, S.K., Riekkola, M.-L, Nyden, M., Soederman, O. *Anal. Chem.* 1997, *69*, 1577.

45. Wiedmer, S.K., Holopainen, J.M., Mustakangas, P., Kinnunen, P.K.J., Riekkola, M.-L. *Electrophoresis* 2000, *21*, 3191.

46. Guttman, A., Cohen, A.S., Heiger, D.N., Karger, B.L. *Anal. Chem.* 1990, *62*, 137.

47. Hjerten, S., *J. Chromatogr.* 1983, *270*, 1.

48. Hjerten, S. *J. Chromatogr.* 1985, *347*, 191.

49. Kim, Y., Morris, M.D. *Anal. Chem.* 1994, *66*, 1168.

50. Hjerten, S., Zhu, M.D. *J. Chromatogr.*, 1985, *346*, 265.

51. Mazzeo, J.R., Krull, I.S. *Anal. Chem.* 1991, *63*, 2852.

52. Martinovic, S., Berger, S.J. Pasa-Tolic, L., Smith, R.D. *Anal. Chem.* 2000, *72*, 5356.

53. Kleparnik, K., Bocek, P. *J. Chromatogr.* 1991, *569*, 3.

54. Emrmakov, S.V., Zhukov, M.Y., Capelli, L., Righetti, P.G. *Electrophoresis* 1995, *16*, 2149.

55. Gebauer, P. Bocek, P. *Electrophoresis* 2000, *21*, 3898.

56. Schwer, C., Kenndler, E. *Chromatographia* 1990, *30*, 546.

57. Cohen, A.S., Karger, B.L. *J. Chromatogr.* 1987, *397*, 409.

58. Jankowiak, R., Zamzow, D., Ding, W., Small, G.J., *Anal. Chem.* 1996, *68*, 2549-2553.

59. Zamzow, D., Lin, C.-H., Small, G.J., Jankowiak, R., *J. Chromatogr. A* 1997, *781*,73-80.

CHAPTER 4. ON-LINE IDENTIFICATION OF DIASTEROMERIC DIBENZO[*a,l*]PYRENE DIOL EPOXIDE-DERIVED DEOXYADENOSINE ADDUCTS BY CAPILLARY ELECTROPHOREIS - FLUORESCENCE LINE-NARROWING AND NON-LINE-NARROWING SPECTROSCOPY

A paper published in the *Journal of Chromatography A*, 1999, *853*, 159.

K. P. Roberts, C. -H. Lin, R. Jankowiak, and G. J. Small

4.1. Abstract

A capillary electrophoretic method for the separation and on-line identification of closely related analytes using low temperature fluorescence spectroscopy is reported for the eight diastereomeric deoxyadenosine (dA) adducts derived from dibenzo[*a,l*]pyrene diol epoxide (DB[*a,l*]PDE). Electrophoretic separation of stereoisomers was accomplished by application of a mixed surfactant buffer (dioctyl sulfosuccinate (DOSS) and Brij-S), which was below the critical micelle concentration (CMC) due to the high concentration (~25%) of organic solvent. Addition of multiple surfactant additives to the separation buffer provided electrophoretic resolution, which was unattainable under single surfactant conditions. It is shown that the CE-separated analyte zones could be identified on-line via low-temperature (4.2 K) fluorescence non-line narrowing and fluorescence line-narrowing (FLN) spectroscopy. In addition, it was determined that in CE buffer *trans-syn-*, *cis-syn-*, and *cis-anti*-DB[*a,l*]PDE-14-N^{6}dA diastereomeric adducts exist mostly with the –dA and DB[*a,l*]P moiety in an 'open'-type conformation while the *trans-anti*-DB[*a,l*]PDE-14-N^{6}dA adducts exist in two different conformations whose relative distribution depends on matrix composition. The above conformations have also

been revealed by selective laser excitation. Thus, the low-temperature methodology not only provides fingerprint structure via vibrationally resolved 4.2 K fluorescence spectra for adduct identification, but also provides conformational information on the spatial relationship of the carcinogen and dA moiety. These results, taken together with those for DB[*a,l*]P-DNA adducts formed in standard glasses and mouse epidermis exposed to DB[*a,l*]P, support our earlier findings that DB[*a,l*]P-derived adducts exist in different conformations [Jankowiak et al., *Chem. Res. Toxicol.*, 1998, *11*, 674]. Therefore, the combination of the separation power of CE and spectral selectivity of low temperature fluorescence spectroscopy at NLN and FLN conditions provides a powerful methodology that should prove useful for identification of closely related DNA adducts formed at low levels in biological systems.

4.2. Introduction

The polycyclic aromatic hydrocarbons are an important class of carcinogen. They are activated by two main pathways: one-electron oxidation to yield radical cations [1-4] and monooxygenation to produce bay region diol epoxides [5-10] which react with the nucleophilic centers of DNA bases, particularly those associated with guanine and adenine. It is widely accepted that the formation of DNA-PAH adducts is the initial event that leads to mutations that result in cancer [11,12]. In this paper we present results on DNA adducts formed from dibenzo[*a,l*] pyrene (DB[*a,l*]P), the most potent member of the PAH class of carcinogens [13,14]. It is found in river sediment [15] and indoor/outdoor air samples [16,17]. The technique used to obtain the results was capillary electrophoresis–fluorescence line narrowing spectroscopy (CE-FLNS) that has

recently been developed by our laboratory [18]. The technique allowed, for the first time, on-line structural characterization of DNA-carcinogen adducts. Capillary electrophoresis can also be interfaced with non-line narrowed fluorescence (NLNF) spectroscopy.

Prior to our development of CE-FLNS we had employed HPLC with FLNS to characterize and quantify a wide variety of DNA-PAH adducts in an off-line mode. The results obtained, when combined with the results of computational chemistry had shown that DB[*a,l*]P leads to a diverse spectrum of stable DNA adducts formed by the diolepoxide metabolic pathway [19]. Conformational information has been obtained for DB[*a,l*]PDE-14-N7Ade, –N7Gua [20], DB[*a,l*]P tetrols [21], and various DB[*a,l*]PDE-14-N^6deoxyadenosine (dA) stereoisomeric adducts [22,23]. It was shown that *anti*- and *syn*- derived DB[*a,l*]PDE-14-N^6dA adducts in ethanol and glycerol/water glasses can adopt various 'open'- and 'folded'-type conformations between the dA and carcinogen moiety; only the folded conformation allows significant interactions between the dA and aromatic portion of the carcinogen [23].

Off-line fluorescence studies, however, indicated that in some instances the purity of the DB[*a,l*]PDE-derived adducts being analyzed poses a problem, especially if the analytes are unstable and/or cannot be HPLC baseline resolved. To circumvent this problem we developed and applied the methodology, which interfaces CE with FLNS for on-line spectral characterization and identification of these closely related species. It has been shown that CE-separated fluorescent analytes can be identified on-line via fingerprint structure of vibrationally resolved FLN spectra at 4.2 K [18,24,25].

CE has also been coupled to MS and NMR for on-line analyte characterization. Both have yielded interesting results without the requirement of standards present for

analysis, although some difficulties exist [26-32]. In the case of CE-MS some of the issues have been circumvented with the introduction of capillary electrochromatography (CEC) [33-35]. CEC incorporates the packed stationary phase of LC (minimizing the need for surfactants) and the efficient electroosmotic flow mechanism of CE.

In this respect, we note that FLNS can also be coupled with CEC [36], and emphasize that the CE-FLNS approach mentioned above does not require standards each time a qualitative determination is to be made, but relies on an established reference library of spectra. This attribute of CE-FLNS is particularly important in the biomedical/biochemical sciences, where many standards (e.g., DNA and protein adducts/metabolites) are difficult/expensive to synthesize, and/or possess poor stability over time. These features of CE-FLNS, along with arbitrary detection times, selective determination in the frequency and time space, as well as increased fluorescence signal and/or decreased photodegradation (due to the low temperatures used), indicate that CE-FLNS is an appropriate methodology for identification, characterization, and quantitation of closely related analytes [18,24,25].

To complement the CE-FLNS methodology, it is shown here that adduct identification can also be achieved via CE and low-temperature fluorescence spectra obtained under non-line-narrowing conditions. With this approach, expensive tunable lasers are not required, i.e., a single-frequency excitation source can be used, expanding the applicability of low-temperature wavelength-resolved laser-induced fluorescence (LIF) detection in capillary electrophoresis [37]. Utilization of low-temperature in obtaining LIF spectra provides spectral resolution that is not possible at room temperature. At room temperature, fluorescence signals are spectrally broad and often

featureless, rendering them useless for identification purposes due to the nearly identical emission spectra of structurally similar analytes. In CE-FNLN spectroscopy, reduction in sample temperature to 4.2 K effectively eliminates thermal broadening contribution, which for a single vibronic transition is approximately equal to kT~ 200 cm^{-1} at room temperature. In the case of FLNS, a further reduction in line-width by a factor of 10-100 is achieved by selective excitation of a uniform subset of molecules [3,38,39]. The selective excitation eliminates inhomogeneous broadening which is typically about 100-500 cm^{-1} in amorphous solids [39].

In this paper, we report on the separation of eight DB[*a,l*]PDE-14-N^6dA diastereomeric adducts (see Figure 4-1), and their on-line identification via low temperature NLN fluorescence spectra. An example of analyte identification via FLN spectra is also shown for completeness. The main goal, however, is to establish a protocol for the separation and spectral characterization of closely related diastereomeric DB[*a,l*]PDE-derived dA adduct standards in CE buffer, and to provide a library of the NLN spectral fingerprints for future on-line *in vivo* and *in vitro* studies of –dA adducts derived from DB[*a,l*]P by CE-FNLN/FLN.

4.3. Experimental

Caution. anti- and syn-DB[a,l]P diolepoxides are extremely hazardous chemicals and should be handled carefully in accordance with NIH guidelines.

4.3.1. Materials

Sodium tetraborate (STB), sodium dioctyl sulfosuccinate (DOSS), and Brij 30 were obtained from Aldrich Chemical Co. (Milwaukee, WI). Acetonitrile (ACN) and

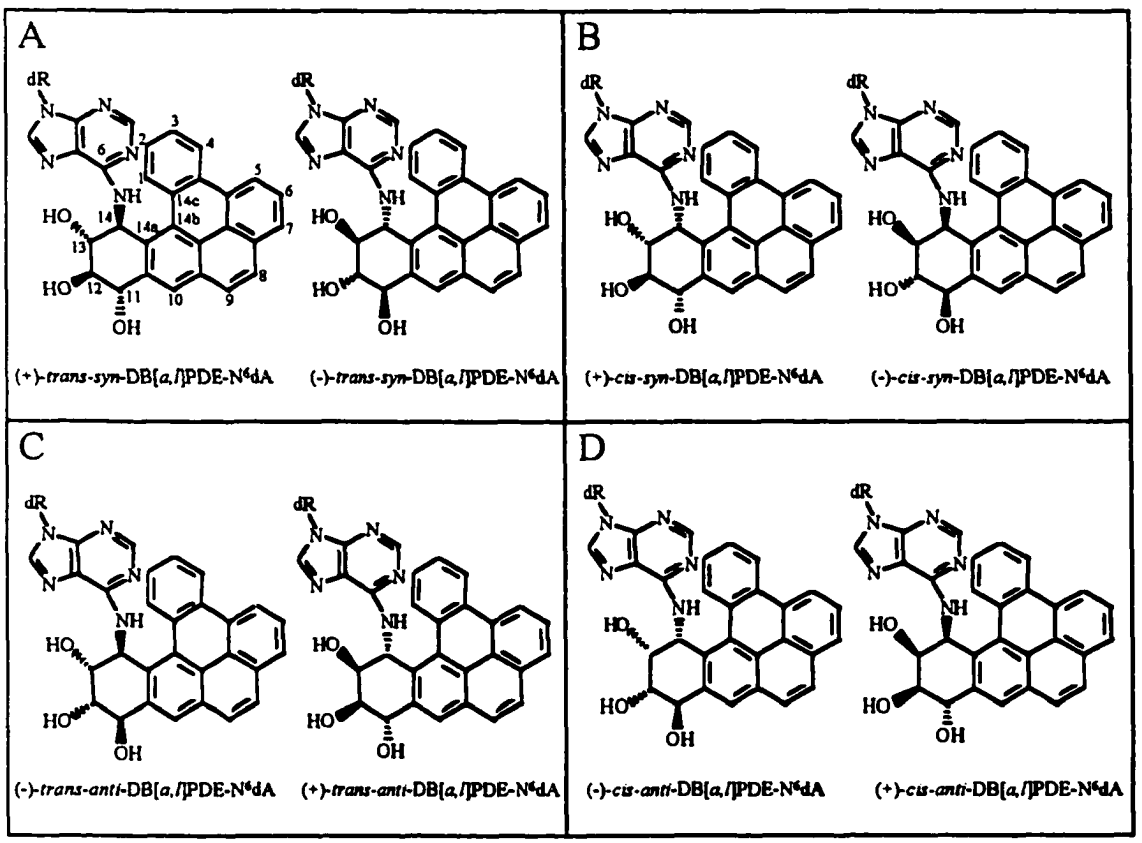

Figure 4-1. Molecular structures of the eight DB[*a,l*]PDE-14-N^{6}dA adducts investigated: A) (+/−)-*trans-syn*-DB[*a,l*]PDE-14-N^{6}dA; B) (+/−)-*cis-syn*-DB[*a,l*]PDE-14-N^{6}dA; C): (+/−)-*trans*-anti-DB[*a,l*]PDE-14-N^{6}dA; and D): (+/−)-*cis-anti*-DB[*a,l*] PDE-14-N^{6}dA. dR corresponds to deoxyribose.

sodium hydroxide (NaOH) were obtained from Fisher Scientific (Fair Lawn, NJ). All buffrs were prepared with water purified with a NANOpure II (Barnstead, Dubuque, IA) purification system. Capillaries were 75 μm i.d., 375 μm o.d. UV-transparent bare silica purchased from Polymicro Technologies Inc. (Phoenix, AZ). Glycerol was obtained from Spectrum Chemical Mfg. Corp. (Gardena, CA).

4.3.2. Sample Preparation and Buffers

The DB[*a,l*]PDE derived stereomeric adducts *trans-anti-*, *cis-anti-*, *trans-syn-*, and *cis-syn*-DB[*a,l*]PDE-14-N^{6}dA were synthesized by a reaction of *anti-* and *syn*-DB[*a,l*]PDE with dA. The (+/–)-*anti*-DB[*a,l*]PDE was reacted with optically-active dA in dimethylformamide at 100°C for 30 min to give four diastereomeric *anti*-DB[*a,l*]PDE-14-N^{6}dA adducts. Likewise, the (+/–)-*syn*-DB[*a,l*]PDE was reacted with optically-active dA under the same conditions, to yield the four *syn*-DB[*a,l*]PDE-14-N^{6}dA diastereomeric adducts. Further details on the synthesis and structural characterization are described elsewhere [22].

The CE buffer consisted of an ACN-water solution (25.5% v/v) containing 34 mM DOSS, 7.5 mM Brij-S (sulfonated Brij 30 as described by Ding and Fritz [37]), and 6.8 mM sodium tetraborate to form a mixed surfactant solution. Aqueous NaOH was used to adjust the pH to 9. Before injection, the separation buffer was filtered through a 0.22 μm syringe filter (Costor) and then degassed for 5 minutes.

Matrix dependent (off-line) studies of the dA standards at 77 and 4.2 K were performed in both 100% CE buffer and 20% CE buffer / 80% glycerol (v/v) to determine how the matrix affected the conformational distribution of the stereoisomers. Samples were diluted to equal concentrations in the appropriate matrix, placed in 2 mm i.d. quartz

tubes, and brought to 4.2 K for LIF measurements. Approximately 20 μL sample volumes were sufficient for the off-line analysis.

4.3.3. Instrumentation

A schematic of the CE-FLN/FNLN system is shown in Figure 4-2. A modular capillary electrophoresis system (Crystal 300 series, Model 310, ATI Unicam, Boston, MA) was used for the electrokinetic separations. Capillaries were 85 cm in length with a 75 cm effective length for LIF detection. Capillaries were conditioned with 100 mM NaOH for 15 minutes (30 minutes for new capillaries), water for 5 minutes, and separation buffer for 15 minutes. The sample was hydrodynamically injected with 20 mbar pressure for 3 seconds resulting in approximately a 10 nL injection volume. Separations were carried out at 20 kV resulting in a 40 μA current.

Room-temperature, LIF electropherograms were obtained with a CW excitation source (Model Innova 90C argon ion laser, Coherent, Santa Clara, CA) equipped with UV optics and an intracavity prism for single line selection. Pulsed excitation was accomplished with a Lambda Physik FL-2002 dye laser, pumped by a Lambda Physik Lextra 100 XeCl excimer laser (Lambda Physik, Ft. Lauderdale, FL). When the molecules of interest electrokinetically migrated into the observation window, the temperature of the capillary, housed in a specially designed capillary cryostat (CC) [18,24,25], was reduced to 4.2 K for low-temperature, on-line analysis. The cooling process took less than one minute. Individual analyte zones in the capillary were selectively probed by automated translation of the CC. Fluorescence was collected with a specially designed objective (Ealing, Holliston, MA), passed through a Model 218 0.3 meter monochromator (McPherson Inc., Acton, MA), and detected with an intensified

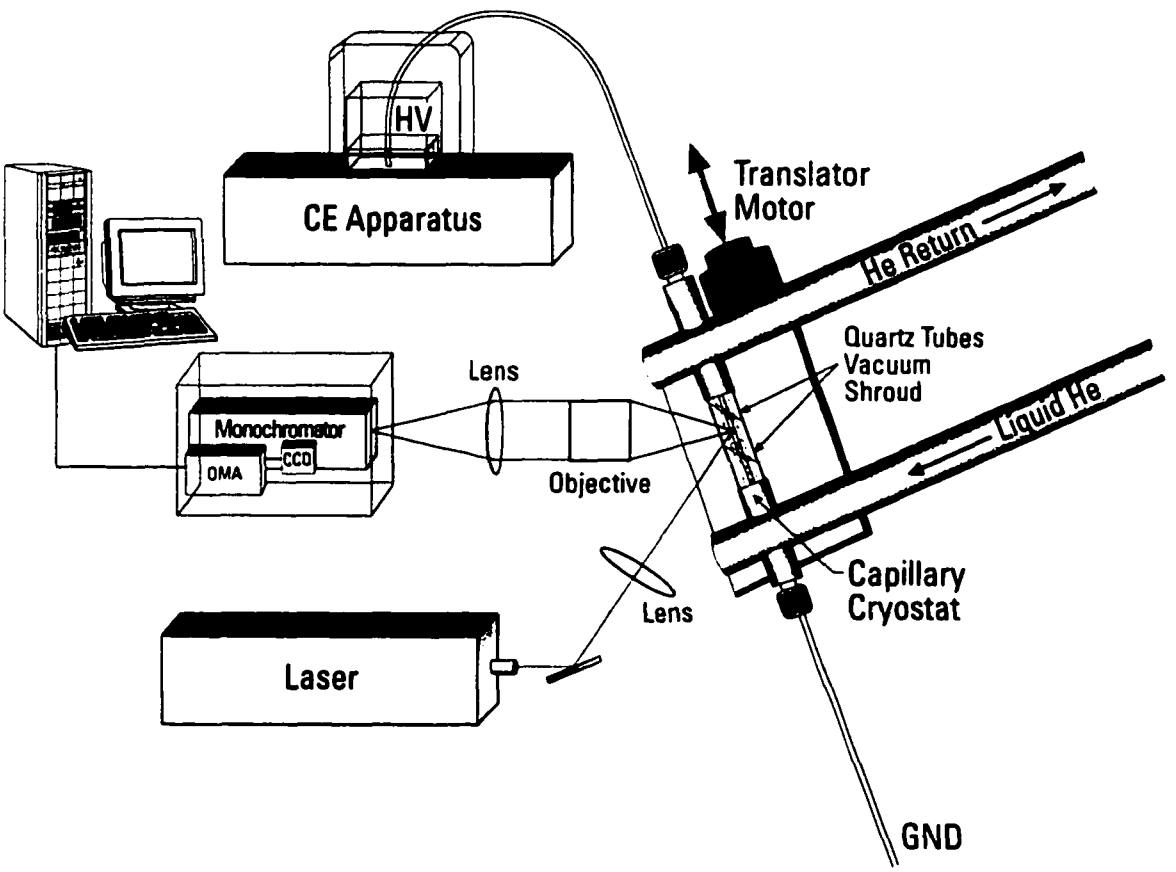

Figure 4-2. Schematic apparatus of the CE-FLNS system used for structural characterization of CE-separated analytes.

CCD camera (Princeton Instruments, Trenton, NJ) using gated and non-gated modes of detection. Spectral resolution for FLN and NLN were 0.09 and 0.8 nm, respectively. Further details of the experimental setup are given in Ref. [18].

4.4. Results and Discussion

4.4.1. Off-line NLN fluorescence spectra in CE buffer

In this section we present NLN fluorescence spectra obtained using a CE buffer in order to determine whether or not the spectra allow for distinction between the isomers of *anti*- and *syn*-DB[*a,l*]PDE-14-N^{6}dA. A reference library was established for the DB[*a,l*]PDE-14-N^{6}dA adducts in CE buffer, as shown in Figure 4-3. Spectra a-d, correspond to the (−)-*trans-anti*-, (−)-*cis-anti*-, (+)-*trans-syn*-, (+)-*cis-syn*-dA adducts, respectively. Identical spectra for the corresponding optical conjugates were obtained (not shown). However, the NLN spectra of the above four stereoisomeric adducts are clearly distinguishable, and can therefore be used for on-line identification of DB[*a,l*]PDE-derived deoxyadenosine adducts.

As shown in spectrum a, the (−)-*trans-anti*-dA adduct (in CE buffer) favors a conformation with a (0,0) origin band at 383.5 nm, in sharp contrast to the spectra obtained recently in ethanol and glycerol/water glasses where the major origin band of the same adduct was red-shifted to ~388 nm [23]. This large shift cannot be accounted for by simple matrix-dependent spectral shifting. Rather, it is due to matrix-induced conformational changes [20,21]. This is supported by the fact that a minor conformation, with an origin band at ~383 nm, was also observed in an ethanol matrix (see Table 1). The remaining adducts spectra (b, c, and d), though all in conformation I, still reveal

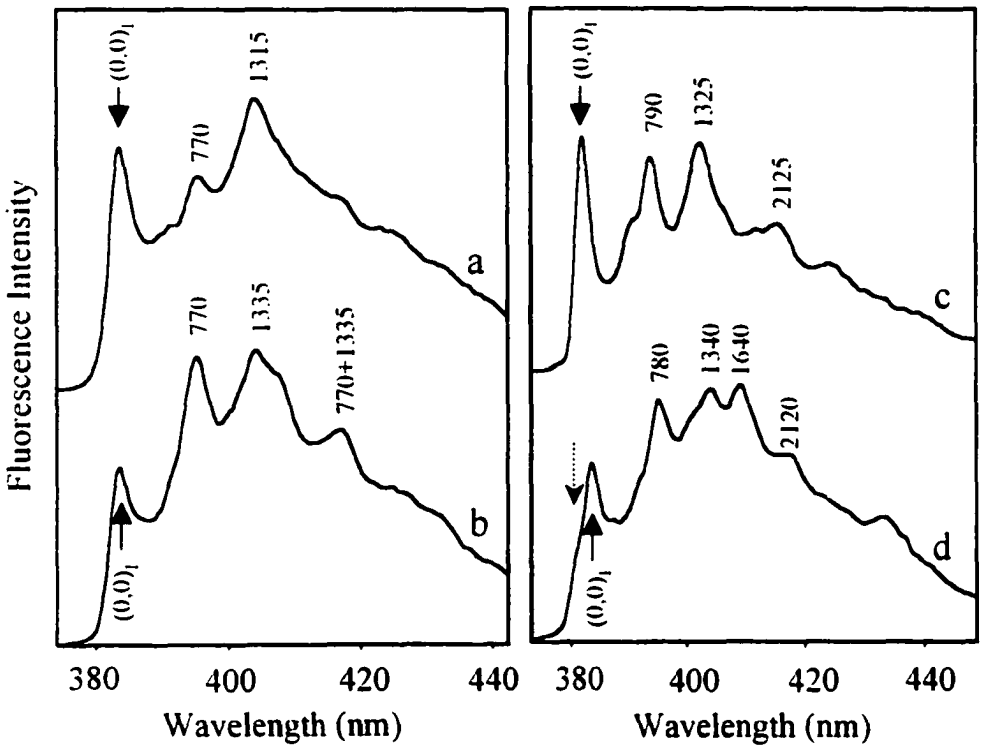

Figure 4-3. NLN fluorescence spectra obtained off-line for (−)-*trans-anti*-DB[*a,l*]PDE-14-N^{6}dA (spectrum a), (−)-*cis-anti*-DB[*a,l*]PDE-N^{6}dA (spectrum b), (+)-*trans-syn*-DB[*a,l*]PDE-14-N^{6}dA (spectrum), and (+)-*cis-syn*-DB[*a,l*]PDE-N^{6}dA (spectrum d) adducts in CE-buffer. T = 4.2 K, λ_{ex} = 308 nm, delay time = 80 ns, and gate width = 200 ns. The numbers correspond to the ground state (S_0) vibrational frequencies.

Table 4-1. Fluorescence origin band comparison observed for *syn-* and *anti-* DB[*a,l*]PDE-14-N^{6}dA adducts at 77 and 4.2 K in various matrices (λ_{ex} = 308 nm).

Stereoisomeric -dA Adducts	**Matrix**					
	Ethanol[a]		**Glycerol/Water[a]**		**CE Buffer**	
	(0,0) nm	**Conf.[b]**	**(0,0) nm**	**Conf.**	**(0,0) nm**	**Conf.**
(+)-*trans-syn-*	382.0	**I**[c]	382.0	**I**	381.9	**I**
	389.0	II	389.0	II	—	—
(+)-*cis-syn-*	383.6	**I**	384.0	**I**	383.4	**I**
	388.0	II	388.0	II	—	—
(−)-*trans-anti-*	383.0	**I′**	—	**I′**	383.5	**I′**
	388.1	**II′**	388.3	**II′**	390.1[e]	II′
(−)-*cis-anti-*	385.0	**I**	385.0[d]	**I**	383.5	**I**
	389.0	**II**	389.0	**II**	—	—

---

a) Observed at T = 77 K with an excitation wavelength of 308 nm[3].
b) Conf. = Conformation.
c) The bold Roman numerals indicate the major conformations observed by low-temperature fluorescence.
d) Minor conformation at the nucleoside level, but major conformation in single-stranded DNA [19].
e) This origin band corresponds to the unique conformation II′ clearly revealed in CE buffer when selectively excited at 351.1 nm. The same conformation was also observed in an 80% glycerol / 20% CE matrix (see Fig. 4-5 for details).

significant differences in their S_0 vibronic intensity distribution. The origin bands of the adducts discussed above are summarized in Table 1. The observed variations in the vibronic intensity distribution are not surprising given that the parent fluorophore B[e]P has C_{2v} symmetry, and the out of plane deformation, as well as the conformation of the cyclohexenyl ring depend on adduct stereochemistry [41,42]. Furthermore, the significant intensity of the 770, 790, and 780 cm^{-1} bands in spectra b, c, and d, respectively, of Figure 4-3 are due to electronic-vibrational coupling between the S_1 state and higher energy dipole-allowed states, and is a consequence of the $S_1 \leftarrow S_0$ absorption transition being only weakly allowed [42,43]. With regard to spectrum c, we note that the *trans-syn*-dA adduct exists mostly in conformation I with its NLN spectra being weakly matrix and excitation-frequency dependent (data not shown). The conformation of the cyclohexenyl ring of the *trans-syn-* dA has been previously assigned as being a unique half-boat configuration with the dA moiety in a pseudoaxial position [23]. Finally, spectrum d of Figure 4-3 is the NLN spectrum of the (+) *cis-syn-* adduct with a $(0,0)_I$ origin band at 383.5 nm. This adduct, in agreement with data previously obtained in ethanol and glycerol/water glasses [23], has been assigned as an open-type conformation with the cyclohexenyl ring in half-chair configuration and dA in a pseudoaxial position. A weak shoulder revealed in spectrum d of Figure 4-3 for the (+)-*cis-syn*-dA adduct, denoted with a dashed arrow, corresponds to a decomposition product (presumably DB[*a,l*]-tetrols) which is not observed in freshly synthesized samples. To generate a more accurate reference spectrum of the *cis-syn*-dA adduct, the decomposition product was electrokinetically separated from the adduct standard and an on-line reference spectrum of the "pure" *cis-syn*-dA standard was obtained as shown in Fig. 4-4.

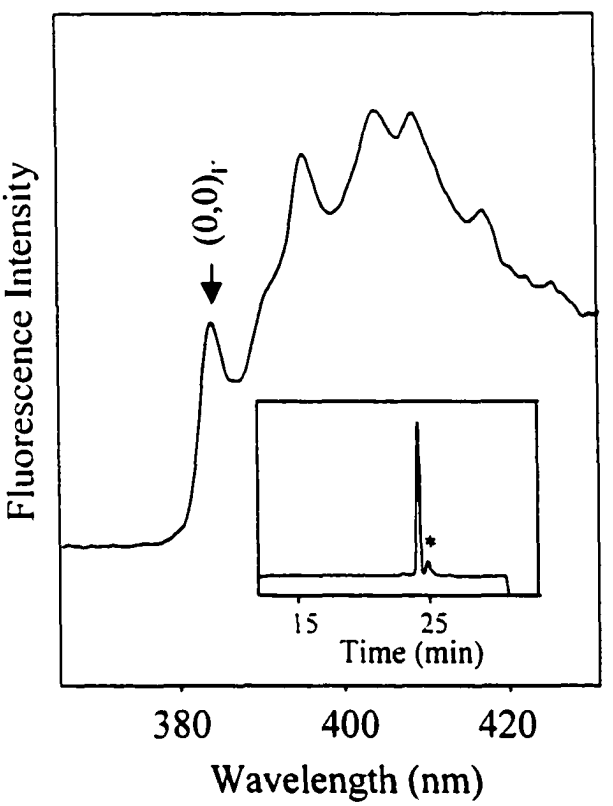

Figure 4-4. On-line NLN fluorescence spectrum of "pure" (+)-*cis-syn*-DB[*a,l*]PDE-14-N^6dA. Inset, an electropherogram of the standard revealing the pure *cis-syn*-dA adduct (large peak) and a small contribution from a decomposition product (denoted with an asterisk). T = 4.2K, λ_{ex} = 308 nm, delay time = 80 ns, and gate width = 200 ns.

4.4.2. Excitation and matrix dependent conformations

The existence of the conformations discussed above for the *trans-anti*-DB[*a,l*]PDE-14-N^6dA adducts is further confirmed below. Figure 4-5 shows the NLN (T = 77 K) fluorescence dependence of this –dA adduct on excitation wavelength and matrix composition. Spectra a and c were obtained (off-line) in CE buffer with excitation wavelengths of 308 nm and 351.1 nm, respectively. An excitation wavelength of 308 nm preferentially excites adducts in conformation I′, with a (0,0) origin band at 383.5 nm, revealing characteristic bands at 770, 1315, and 2085 cm^{-1}. In contrast, an excitation wavelength of 351.1 nm preferentially excites adducts in conformation II′ with a (0,0) origin band at 390.1 nm, and vibrational bands at 750, 1280, and 2030 cm^{-1}. A small contribution of conformation II′ in spectrum a is also observed as denoted by an asterisk. Thus, we conclude that *trans-anti*-dA adducts exist in two conformations (I′ and II′), whose relative distribution is not only matrix dependent, but can also be revealed by selective laser excitation. The small difference in the intensity distribution between spectra a of Figure 4-5 and 4-3 is due to a slightly different distribution of conformers I′ and II′ trapped at 4.2 and 77 K, respectively, and is the result of differences in cooling rates. The relatively strong bands at ~2085 cm^{-1} (curve a) and ~2030 cm^{-1} (curve c) correspond to the ~1315 and ~1280 cm^{-1} modes, which build on the intense Herzberg-Teller origin bands at 770 and 750 cm^{-1}, respectively; for more details see Ref. [21].

Spectrum b of Figure 4-5 was obtained under conditions identical to those used to obtain spectrum a except that in a 20/80 % (v/v) CE buffer/glycerol matrix. Comparison with spectrum a of Fig. 4-3 reveals that the (–) *trans-anti*-dA adduct preferentially adopts

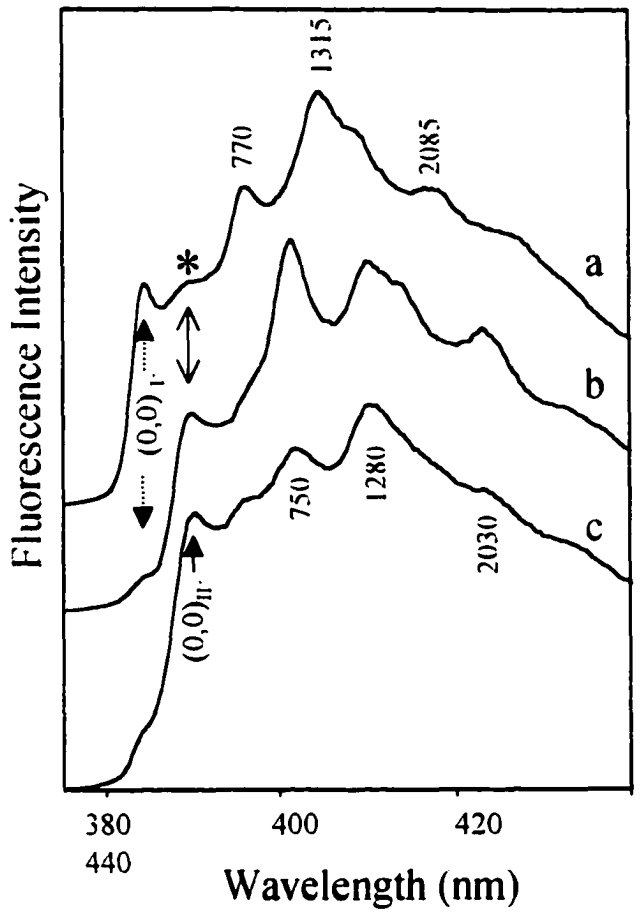

Figure 4-5. Excitation wavelength and matrix dependence of the NLN fluorescence spectra of (−)-*trans-anti*-DB[*a,l*]PDE-14-N^{6}dA adducts at 77 K. Spectra a and c were obtained in CE buffer with an excitation wavelength of 308 nm and 351.1 nm, respectively. Spectrum b was obtained in the 80 % glycerol / 20 % CE-buffer (v/v) solution with and λ_{ex} = 308 nm. Spectra a and b were obtained with a 0 ns delay time and 200 ns observation window (see text for details).

conformation I′ in CE buffer and conformation II′ ((0,0) origin band at 389.6 nm) in the predominantly (80 %) glycerol matrix. We emphasize that this conformation change is reversible (spectra not shown). Small differences in the vibronic intensity distribution observed in spectra b and c of Figure 4-5 are caused by solvent (matrix) dependent Herzberg-Teller coupling [41,42]. Therefore, based on data presented in Figure 4-5, we conclude that the *trans-anti-* DB[*a,l*]PDE-14-N^6dA adducts formed in CE buffer are trapped as a mixture of two adduct conformations. This provides additional support for the earlier assignment of these conformations as open- and folded-type, respectively. We recall that the cyclohexenyl ring in the above conformations possess a half-chair configuration with the dA moiety in a pseudoaxial and pseudoequatorial position, respectively [23]. Preliminary, matrix dependent, circular dichroism results support this assignment (data not shown).

4.4.3. CE separation

Despite considerable efforts, an electrokinetic separation of the –dA adducts was not achieved with either of the single surfactants, DOSS or Brij-S (data not shown). Therefore, we turned to mixed surfactant buffers, which were reported to be able to resolve structurally similar components that were inseparable under single surfactant conditions [44-46]. The buffer, which allowed for separation, consisted of 34.4 mM DOSS, 7.4 mM Brij-S, 6.8 mM sodium tetraborate, and 25.5 % acetonitrile (v/v). Altering the ratio of the two surfactants optimized electrophoretic resolution of the diastereomers. Utilizing the methodology described in Refs. [46,47], it was confirmed (data not shown) that at 25.5 % acetonitrile, micelle formation was inhibited. This suggests that the CE-separation mechanism involves a solvophobic association of the

PAH portion of the DB[*a,l*]PDE-14-N^{6}dA adducts with the hydrophobic chains of the surfactants.

Separation of a mixture of eight diastereomeric -dA adducts is shown in Figure 4-6. Since eleven peaks are nearly baseline resolved, three peaks of this electropherogram must belong to decomposition products or impurities.

4.4.4. On-line, low-temperature identification of CE-separated peaks

Figure 4-7 shows the low-temperature (4.2 K) on-line spectral identification of peaks 7 (spectrum a) and 11 (spectrum b) of the electropherogram shown in Figure 4-6. Peak identification is made based on comparisons with the library of the standard spectra. Spectrum a is identical to the off-line *trans-syn*-dA reference standard (spectrum c of Figure 4-3), and spectrum b is indistinguishable from the spectrum in Figure 4-4, which corresponds to the *cis-syn*-dA reference standard. Therefore, we conclude that peaks 7 and 11 of the electropherogram shown in Figure 4-7 can be unambiguously assigned as the *trans-syn*- and *cis-syn*-DB[*a,l*]PDE-14-N^{6}dA adducts, respectively.

Another example is shown in Fig. 4-8, where the identification of peaks 4 (spectrum a) and 5 (spectrum b) are illustrated. Both peaks reveal identical NLN spectra which are compared with the standard spectrum obtained for the (−)-*trans-anti*-dA (spectrum c). Since spectra a and b are nearly identical to the (−)-*trans-anti*-dA reference standard, we conclude that they must correspond to either the (+) or (−)-*trans-anti*-DB[*a,l*]PDE-14-N^{6}dA diastereomers. The increased broadening observed in spectra a and b, as compared to the standard spectrum c, is a consequence of a slight reduction in spectral resolution obtained in the on-line measurements. As mentioned earlier,

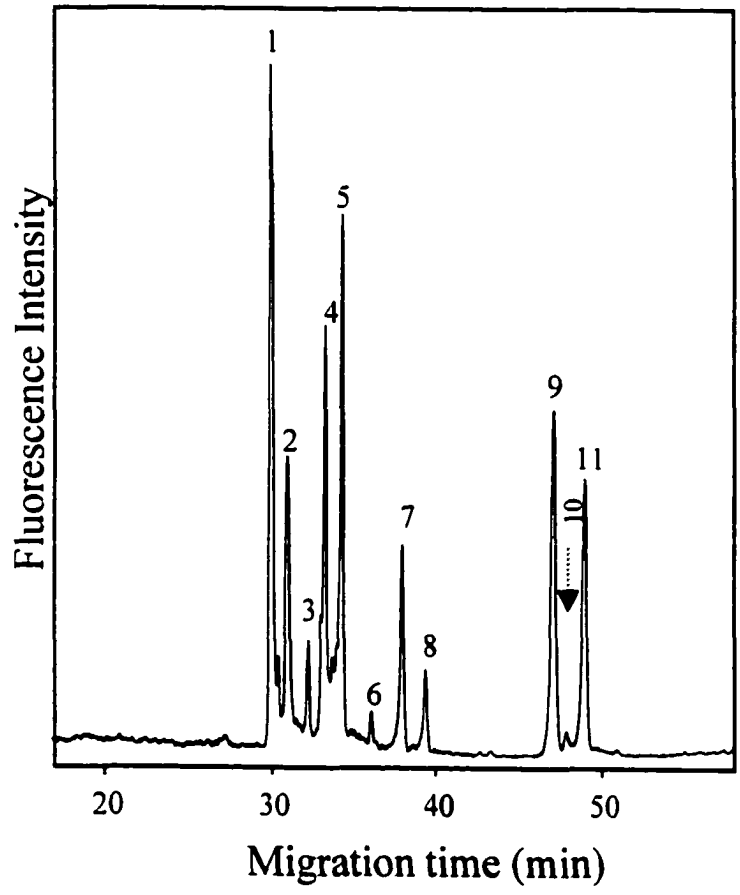

Figure 4-6. Room-temperature fluorescence electropherogram acquired during CE-separation of the eight HPLC purified DB[*a,l*]PDE-derived adduct standards. The peaks are identified in Table 4-2.

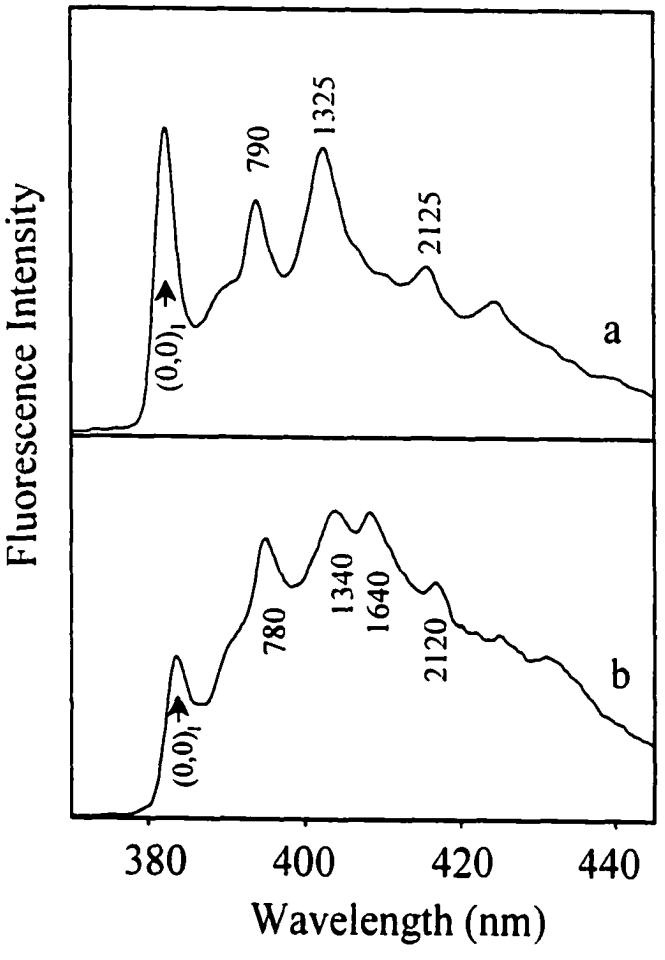

Figure 4-7. On-line NLN spectra (a and b) for the CE-separated peaks 7 and 11 of Figure 4-6. The bands are labeled with their ground-state vibrational frequencies, in cm^{-1}; T = 4.2 K, λ_{ex} = 308 nm.

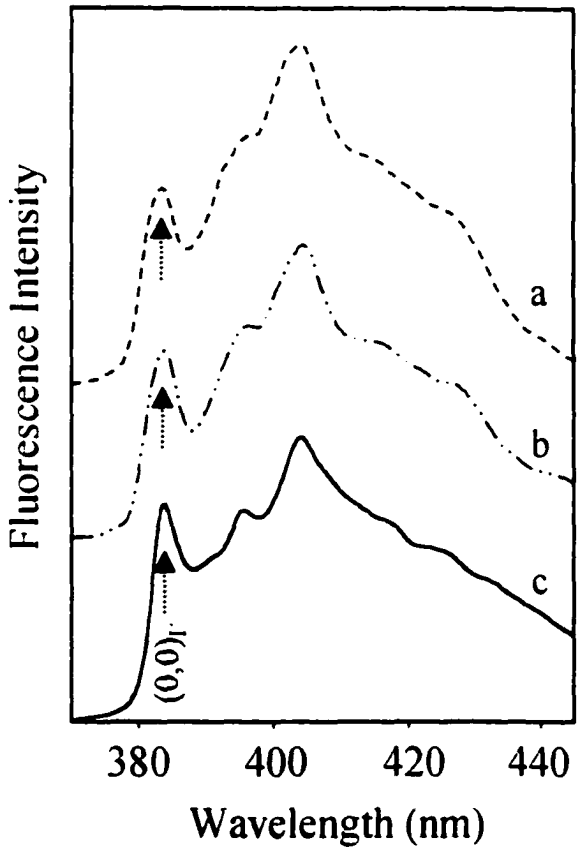

Figure 4-8. Spectra a and b were obtained on-line in the CE-buffer matrix (at T = 4.2 K, λ_{ex} = 308 nm) for peaks 4 and 5, respectively, of Figure 4-6. Spectrum c is from the library of NLN spectra and corresponds to the (−)-*trans-syn*-dA adduct. Spectra a and b were obtained with spectral resolution of 0.8 nm; spectrum c was 0.5 nm. The NLN bands are labeled with their ground-state vibrational frequencies, in cm^{-1}.

and as discussed in Ref. [48], the (+)-*trans-anti*- and (–)-*trans-anti*-type adducts possess indistinguishable fluorescence spectra [22,23]. Their differentiation has been accomplished via spiking with optically pure standards whose stereochemistry has been established by ^{1}H NMR and circular dichroism [22]. The latter revealed that peaks 4 and 5 correspond to (+)-*trans-anti* and (–)-*trans-anti*-dA adducts, respectively. The same methodology of differentiating the (+/–) diastereomers was utilized for the remaining (+/–) -dA adduct pairs.

As a final example, Fig. 4-9 shows the on-line identification of the CE-separated peaks 7 and 11 of Fig. 4-6 via FLN spectroscopy. Frame A of Fig. 4-9 shows the 4.2 K FLN spectra (λ_{ex} = 372.0 nm) of the CE-separated peak 7 (spectrum a) and the (+)-*trans-syn*-dA adduct standard (spectrum b). The comparison reveals vibronic modes at 720, 757, and 796 cm^{-1} in the on-line spectrum which are identical to those found in the (+)-*trans-syn*-dA adduct standard spectrum. Frame B of Fig. 4-9 compares the 4.2 K on-line FLN spectra (λ_{ex} = 372.0 nm) of the CE separated peak 11 (spectrum c) with that of the off-line (+)-*cis-syn*-dA adduct standard (spectrum d). Again, identical vibrational modes at 736, 796, 848, and 930 cm^{-1} are observed, proving that peak 11 corresponds to the (+)-*cis-syn*-dA adduct. Thus, Figures 4-7 and 4-9 demonstrate that *trans* and *cis* isomers of the *syn*-DB[*a,l*]PDE-14-N^{6}dA adducts are readily distinguishable and can be unambiguously assigned by both NLN and FLN spectra. The results obtained by combining CE with low-temperature fluorescence spectroscopy and spiking are summarized in Table 4-2.

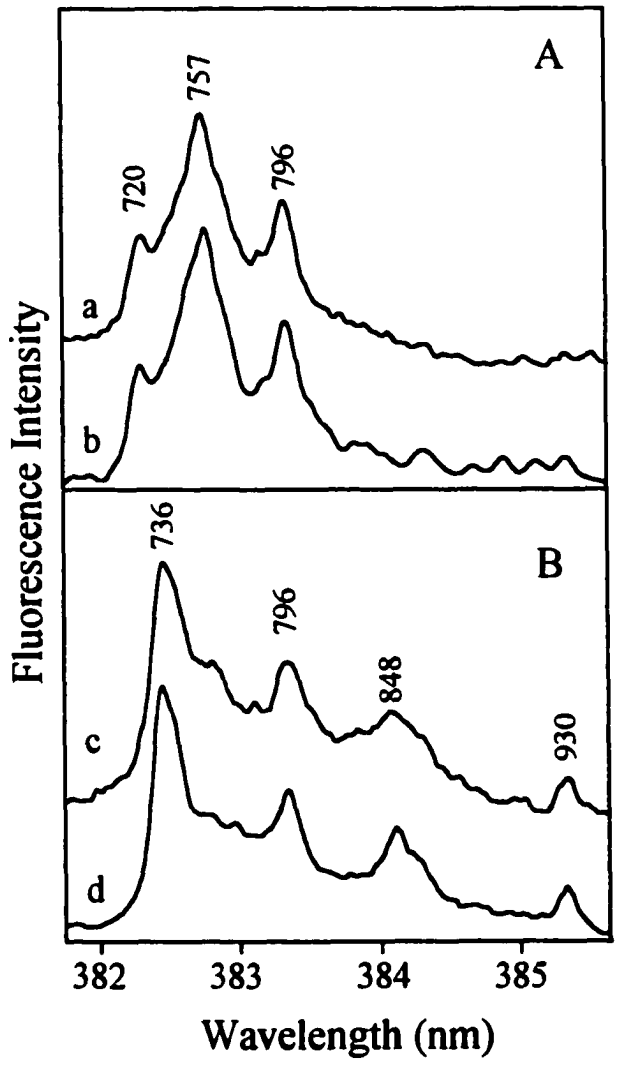

Figure 4-9. Spectra a and c were obtained on-line in CE-buffer for peaks 7 and 11 of Figure 4-6, with an excitation wavelength of 372.0 nm at T = 4.2 K. Spectra b and d are shown for comparison, and corresponds to FLN spectra of the (+)-*trans-syn-* and (+)-*cis-syn*-DB[*a,l*]PDE-14-N^6dA adduct standards, respectively. The detection delay time was 40 ns with a 200 ns gate width. The FLN peaks are labeled with their excited-state vibrational frequencies, in cm^{-1}.

Table 4-2. The identity of the peaks in the electropherogram shown in Figure 4-6.

Peak Number	Peak Assignment
1	(–) *cis-anti*-DB[*a,l*]PDE-14-N^{6}dA
2	(+) *cis-anti*-DB[*a,l*]PDE-14-N^{6}dA
3	decomposition product
4	(+) *trans-anti*-DB[*a,l*]PDE-14-N^{6}dA
5	(–) *trans-anti*-DB[*a,l*]PDE-14-N^{6}dA
6	decomposition product
7	(+) *trans-syn*-DB[*a,l*]PDE-14-N^{6}dA
8	(–) *trans-syn*-DB[*a,l*]PDE-14-N^{6}dA
9	(–) *cis-syn*-DB[*a,l*]PDE-14-N^{6}dA
10	decomposition product
11	(+) *cis-syn*-DB[*a,l*]PDE-14-N^{6}dA

4.5. Conclusions

The use of a capillary electrophoresis method for the separation and on-line spectral identification of closely related analytes, via low-temperature fluorescence spectroscopy, has been demonstrated for diastereomeric dA adducts derived from the DB[*a,l*]PDE. Successful separation of the eight stereoisomers was accomplished using an appropriate mixture of DOSS and Brij-S surfactants. Since the separation conditions inhibit micelle formation, it is concluded that the separation mechanism is the result of a solvophobic association of the PAH-dA adducts with the hydrophobic chains of the surfactants. It has been demonstrated that low temperature CE-FNLN/FLN methodology not only allows for on-line identification via vibrationally resolved 4.2 K fluorescence spectra, but also provides conformational information on the –dA adducts. We believe that the marriage of CE to low-temperature fluorescence spectroscopy will be useful in future *in vivo* and *in vitro* studies of DNA adducts derived from DB[*a,l*]P and other fluorescent carcinogens.

4.6. Abbreviations

Ade, adenine

CC, capillary cryostat

CCD, charge-coupled device

CE, capillary electrophoresis

CW, continuous wave

dA, deoxyadenosine

DB[*a,l*]P, dibenzo[*a,l*]pyrene

DB[*a,l*]PDE, dibenzo[*a,l*]pyrene diol epoxide

DB[*a,l*]PDE-14-N^2dG, dibenzo[*a,l*]pyrene diol epoxide-N^2-deoxyguanosine

syn-DB[*a,l*]PDE-14-N^6dA, *syn*-dibenzo[*a,l*]pyrene diol epoxide-14-N^6deoxyadenosine

anti-DB[*a,l*]PDE-N^6dA, *anti*-dibenzo[*a,l*]pyrene diol epoxide-14-N^6deoxyadenosine

DB[*a,l*]PDE-14-N7Ade, 14-(adenin-7-yl)-11,12,13-trihydroxy-11,12,13,14 tetrahydrodibenzo[*a,l*]-pyrene

DB[*a,l*]PDE-14-N7Gua, 14-(guanin-7-yl)-11,12,13-trihydroxy-11,12,13,14-tetrahydrodibenzo[*a,l*]pyrene

DB[*a,l*]P tetrol, 11,12,13,14-tetrahydroxy-11,12,13,14-tetrahydrodibenzo[*a,l*]pyrene

DE, diolepoxide

DOSS, dioctylsulfosuccinate

FLNS, fluorescence line-narrowing spectroscopy

LIF, laser-induced fluorescence

NLN, non-line-narrowing

PAH, polycyclic aromatic hydrocarbon

S_0 state, electronic ground state

S_1 state, lowest excited singlet state

4.7. Acknowledgements

Iowa State University operates Ames Laboratory for the U.S. Department of Energy under contract no. W-7405-Eng-82. The Office of Health and Environmental Research supported this research. C.H. Lin was funded by the National Institutes of

Health, grant # POI CA49210-0. The authors thank Dr. E.L. Cavalieri for providing adduct standards and J.S. Fritz for the helpful discussions.

References

1. K.-M. Li, R. Todorovic, E.G. Rogan, E.L. Cavalieri, F. Ariese, M. Suh, R. Jankowiak, and G.J. Small, Biochemistry, 34 (1995) 8043.

2. E. Cavalieri and E. Rogan, in A. H. Neilson (Editor), The Handbook of Environmental Chemistry, PAHs and Related Compounds, Springer-Verlag, Berlin Heidelberg, 1998, Vol. 3, Part I.

3. R. Jankowiak and G.J. Small, The Handbook of Environmental Chemistry, PAHs and Related Compounds, Springer-Verlag, Berlin Heidelberg, 1998, Vol. 3, Part I.
4. E.L. Cavalieri and E.G. Rogan, Pharmac. Ther., 55 (1992) 183.

5. S.L. Ralston, A. Seidel, A. Luch, K.L. Platt, and W.M. Baird, Carcinogenesis, 16, (1995) 2899.

6. A.H. Conney, Cancer Res., 42 (1982) 4875.

7. A. Luch, H. Glatt, K.L. Platt, F. Oesch, and A. Seidel, Carcinogenesis, 15 (1994) 2507.

8. R.G. Harvey, Polycyclic Aromatic Hydrocarbons: Chemistry and Carcinogenicity, Cambridge University Press, Cambridge, 1991.

9. S.L. Ralston, H.H.S. Lau, A. Seidel, A. Luch, K.L. Platt, and W.M. Baird, Cancer Res., 54 (1994) 887.

10. K.-M. Li, N.V.S. RamaKrishna, N.S. Padmavathi, E.G. Rogan, and E.L. Cavalieri, Polycyclic Aromat. Compd., 6 (1994) 207.

11. D. Chakravarti, R. Mailander, J. Franzen, S. Higgenbotham, E.L. Cavalieri, and E.G. Rogan, Oncogene, 16 (1998) 3203.

12. D. Chakravarti, E.L. Cavalieri, and E.G. Rogan, DNA and Cell Biology, 17 (1998) 529.

13. E.L. Cavalieri, S. Higginbotham, N.V.S. RamaKrishna, P.D. Devaneasan, R. Todorovic, E.G. Rogan, and S. Salmasi, Carcinogenesis, 12 (1991) 1939.

14. S. Higginbotham, N.V.S. RamaKrishna, S.L. Johansson, E.G. Rogan, and E.L. Cavalieri, Carcinogenesis, 14 (1993) 875.

15. I.S. Kozin, C. Gooijer, and N.H. Velthorst, Anal. Chem., 67 (1995) 1623.

16. J.L. Mumford, X. Li, F. Hu, X.B. Lu, and J.C. Chuang, Carcinogenesis, 16 (1995) 3031.

17. W.K. de Ratt, S.A.L.M. Kooijman, and J.W.J. Gielen, Sci. Total Environ., 66 (1987) 95.

18. R. Jankowiak, D. Zamzow, W. Ding, and G.J. Small, Anal. Chem., 68 (1996) 2549.

19. R. Jankowiak, F. Ariese, A. Hewer, A. Luch, D. Zamzow, N.C. Hughes, D. Phillips, A. Seidel, K.L. Platt, F. Oesch, and G.J. Small, Chem. Res. Toxicol., 11 (1998) 674.

20. F. Ariese, G.J. Small, and R. Jankowiak, Carcinogenesis, 17 (1996) 829.

21. R. Jankowiak, F. Ariese, D. Zamzow, A. Luch, H. Kroth, A. Seidel, and G.J. Small, Chem. Res. Toxicol., 10 (1997) 677.

22. K.-M. Li, E.L. Cavalieri, E.G. Rogan, M. George, M.L. Gross, A. Seidel, Chem. Res. Toxicol., in press.

23. R. Jankowiak, C.-H. Lin, D. Zamzow, K. Roberts, K.-M. Li, G.J. Small, Chem. Res. Toxicol., in press.

24. D. Zamzow, C.-H. Lin, G.J. Small, and R. Jankowiak, J. Chrom. A, 781 (1997) 73.

25. D. Zamzow, G.J. Small, and R. Jankowiak, Mol. Cryst. Liq. Cryst., 291 (1996) 155.

26. S. Pleasance, S.W. Ayer, M.V. Laycock, and P. Thibault, Rapid Comm. Mass Spectrom., 6 (1992) 14.

27. W. Lu, G.K. Poon, P.L. Carmichael, and R.B. Cole, Anal. Chem., 68 (1996) 668.

28. H. Ozaki, N. Itou, S. Terabe, T. Takada, M. Sakairi, and H. Koizumi, J. Chrom. A, 716 (1995) 69.

29. J. Cai and J. Henion, J. Anal. Toxicol., 20 (1996) 27.

30. S.J. Locke and P. Thibault, Anal. Chem., 66 (1994) 3436.

31. J. Cai and J. Henion, J. Chrom. A, 703 (1995) 667.

32. D.L. Olson, M.E. Lacey, and J.V. Sweedler, Anal. Chem., 70 (1998) 257A.

33. V. Pretoris, B.J. Hopkins and J.D. Schieke, J. Chrom., 99 (1974) 23.

34. J.W. Jorgenson and K.D. Lukacs, J. Chrom., 218 (1981) 209.

35. J. Ding and P. Vouros, Am. Lab., (1998) 15.

36. S. J. Kok, E.M. Kristensons, C. Gooijer, N.H. Velthorst, and U.A.Th. Brinkman, J. Chrom. A. 771 (1997) 331.

37. R. Jankowiak and G.J. Small, Chem. Res. Toxicol. 4 (1991) 256.

38. R. Jankowiak, J.M. Hayes, and G.J. Small, Chem. Rev., 93 (1993) 1471.

39. W. Ding and J.S. Fritz, Anal. Chem., 69 (1997) 1593.

40. J.C. Brown, J.A. Duncanson, and G.J. Small, Anal. Chem., 52 (1980) 1711.

41. G. Herzberg, Molecular Spectra and Molecular Structure, III. Electronic Spectra and Electronic Structure of Polyatomic Molecules, van Nostrand and Reinhold Co., New York, 1966, Ch. 2.

42. J.C. Brown, Ph.D. Thesis, Iowa State Univ., 131.

43. X. Li and J.S. Fritz, Anal. Chem., 68 (1996) 4481.

44. S.K. Poole and C.F. Poole, J. High Res. Chrom., 20 (1997) 174.

45. J.H.T. Luong and Y. Guo, Electrophoresis, 19 (1998) 723.

46. C.C. Ruiz, Coll. Poly. Sci., 273 (1995) 1033.

47. M. Suh, F. Ariese, G.J. Small, R. Jankowiak, T.-M. Liu, and N.E. Geacintov, Biophys. Chem., 56 (1995) 281.

CHAPTER 5. ON-LINE IDENTIFICATION OF DEPURINATING DNA ADDUCTS IN HUMAN URINE BY CAPILLARY ELECTROPHOREIS FLUORESCENCE – LINE-NARROWING SPECTROSCOPY

A paper published in *Electrophoresis*, 2000, *21*, 799.

K. P. Roberts, C. -H. Lin, M. Singhal, G. P. Casale, G. J. Small, and R. Jankowiak

5.1. Abstract

The benzo[*a*]pyrene (BP) derived 7-(benzo[*a*]pyren-6-yl)guanine (BP-6-N7Gua) depurinating one-electron oxidation adduct was identified in the urine extracts of coal-smoke-exposed humans for the first time. Urine samples were prepared by solid phase extraction and reverse-phase high-performance liquid chromatography. Subsequently, the BP-6-N7Gua adduct was identified on-line with capillary electrophoresis – fluorescence line-narrowing spectroscopy (CE-FLNS) at 4.2 K. The daily excretion of BP-6-N7Gua in human urine of individuals exposed to coal-smoke was about ~226 pmol per μmol of creatinine. Due to the high level of excretion we propose that BP-6-N7Gua adducts found in urine could serve as effective biomarkers for risk assessment of BP exposure. The results demonstrate that CE-FLNS allows for on-line separation and DNA adducts identification in complex fluid-extracts.

5.2. Introduction

Capillary electrophoresis (CE) is now a well established and widely used analytical and bioanalytical separation technique. Various protocols necessary for CE separation of molecular analytes have been established [1-4]. Using CE, polycyclic

aromatic hydrocarbon (PAH)-carcinogens were measured with a detection level of 0.1 attomole [5]. CE has also been successfully applied to the analysis of DNA adducts [3,6-9], nucleic acid bases, and DNA oligonucleotides [2]. Fluorescence line narrowing spectroscopy (FLNS) provides frequency selection by exciting a homogeneous ensemble of molecules, providing a means to overcome the inhomogeneous spectral broadening [10,11]. FLNS is capable of distinguishing between a given PAH metabolite covalently bound to different DNA bases and to different nucleophilic centers of a given base [10-14]. Furthermore, FLNS has been used to distinguish between a given metabolite bound in helix external, partially base-stacked, and intercalated conformations [10,11,15]. Sub-femtomole detection limits have been obtained, i.e. ~1 adduct in 10^8 base-pairs can be measured in about 100 μg of DNA [16]. Although excellent selectivity and sensitivity of FLNS indicate that this methodology is a powerful tool for the study of both stable and depurinating DNA adducts [10-17], it should be pointed out that a complex mixture of closely related adducts/metabolites cannot be resolved by FLNS alone.

Therefore, we recently demonstrated that CE can be interfaced with FLNS for on-line structural characterization. It was shown that detection by laser-induced fluorescence (LIF) under line-narrowing (FLN) conditions provided excellent spectral resolution, which allowed for structural characterization of various PAHs [4] and PAH-derived DNA adducts [3,8,9]. We emphasize that CE-FLNS does not require standards each time the analytes identification is to be made. Rather, it relies on an established reference library of spectra. This attribute is particularly important when standards (e.g. DNA adducts/metabolites) are difficult/expensive to synthesize, and/or exhibit poor stability. We have also shown that adduct identification can be achieved with CE-NLN

fluorescence spectroscopy at 4.2 K [3] (or at 77 K; unpublished results). For NLN spectroscopy non-selective excitation into the S_2 state with a single-frequency excitation source can be used, leading to excitation of all sites within the inhomogeneously broadened band. The resulting spectra are much more characteristic for analyte identification than room-temperature spectra. With this approach, expensive tunable lasers are not required, expanding the applicability of low-temperature LIF detection in CE [3].

Benzo[*a*]pyrene (BP), the carcinogen of interest in this manuscript, can be activated by one-electron oxidation to yield reactive intermediate radical cations and by monooxygenation to produce bay-region diol epoxides [17-21]. The active intermediates formed by one-electron oxidation and monooxygenation readily bind to DNA and have been shown to form adducts *in vitro* and *in vivo* [18,22]. Results obtained in recent years unequivocally demonstrated the importance of the one-electron oxidation pathway for the carcinogenic activation of PAHs [18]. For example, it was shown that the BP-radical cation (at the C6 position) binds *in vitro* to the N7 position of adenine or guanine to form unstable BP-6-N7Ade and BP-6-N7Gua adducts that are rapidly lost (depurinated) from DNA [21,23]. Mouse skin studies showed that the major BP-derived depurinating adducts formed are BP-6-N7Ade, BP-6-N7Gua, and BP-6-C8Gua; together, they account for 74% of all BP adducts formed [22,24-26]. The presence of the BP-6-N7Gua adduct was also demonstrated in urine and feces of rats exposed to BP, where the identification was made by off-line FLNS [21]. However, the question remains as to whether or not these adducts are formed in humans.

In this study, urine from coal smoke exposed individuals is analyzed by CE-FLNS for the presence of BP-DNA adducts, since BP is one of the major carcinogens found in coal smoke [27]. Previously, PAH-metabolites such as 1-hydroxypyrene-glucuronide and BP-tetraols were used as biomarkers of PAH exposure in urine assays of individuals exposed to coal tar [28]. However, identification of depurinated PAH-DNA adducts in human fluids, if formed at detectable levels, would be more relevant indicators of PAH exposure since they directly reflect PAH-induced DNA damage.

5.3. Experimental Section

Caution. BP is an extremely hazardous chemical and should be handled carefully in accordance with NIH guidelines.

5.3.1. Materials

Sodium tetraborate (STB), sodium dioctyl sulfosuccinate (DOSS), and dimethylsulfoxide (DMSO) were obtained from Aldrich Chemical Co. (Milwaukee, WI). Acetonitrile (ACN), methanol, and sodium hydroxide (NaOH) were obtained from Fisher Scientific (Fair Lawn, NJ). All buffers were prepared with water purified by a NANOpure II (Barnstead, Dubuque, IA) purification system. Capillaries were 75 μm i.d., 375 μm o.d. UV-transparent bare silica purchased from Polymicro Technologies Inc. (Phoenix, AZ). BP-6-N7Gua and BP-6-N7Ade standards were prepared via iodine oxidation reaction of BP with the individual DNA bases as described in detail elsewhere [18].

5.3.2. CE-FLNS instrumentation

The CE-FLNS instrumentation is described in Refs [3,5,6]. Briefly, the system consists of a modular CE (Crystal 300 series, Model 310, ATI Unicam, Boston, MA) system, FLNS apparatus, and a capillary cryostat (CC). A schematic of the CE-FLN/FNLN system is shown in Figure 5-1. The CC consists of a double-walled quartz cell with inlet and return lines for introducing liquid nitrogen or liquid helium. The outer portion of the CC is evacuated. The capillary, positioned in the central region of the CC, is cooled by a continuous flow of liquid nitrogen (77 K) or liquid helium (4.2 K). The low thermal capacity of the capillary and the small dimensions of the CC (inner portion, 4 mm ID x 22-cm length) allow rapid cooling to 4.2 K (in less than 1 min.) and the ability to form disordered matrices for FLN to be operative in typical CE buffers. A precision stage provides translation of the CC along the capillary axis by +/– 4 cm allowing the separated analytes to be sequentially characterized by LIF spectroscopy.

Room temperature, LIF electropherograms were obtained with a CW excitation source (Model Innova 90C argon ion laser, Coherent, Santa Clara, CA) equipped with UV optics and an intracavity prism for single line selection. The excitation wavelength was 351.1 nm with an output power of 100 mW. Fluorescence was collected with a reflecting objective (25-0506 x 15, Ealing, Holliston, MA; numerical aperture of 0.28), passed through a Model 218 0.3-m monochromator (McPherson Inc., Acton, MA), and detected with an intensified charge-coupled device (ICCD) (Roper Scientific, Trenton, NJ). The FLN spectra were obtained with a Lambda Physik FL-2002 pulsed dye laser, pumped by a Lambda Physik Lextra 100 XeCl excimer laser (Lambda Physik, Ft.

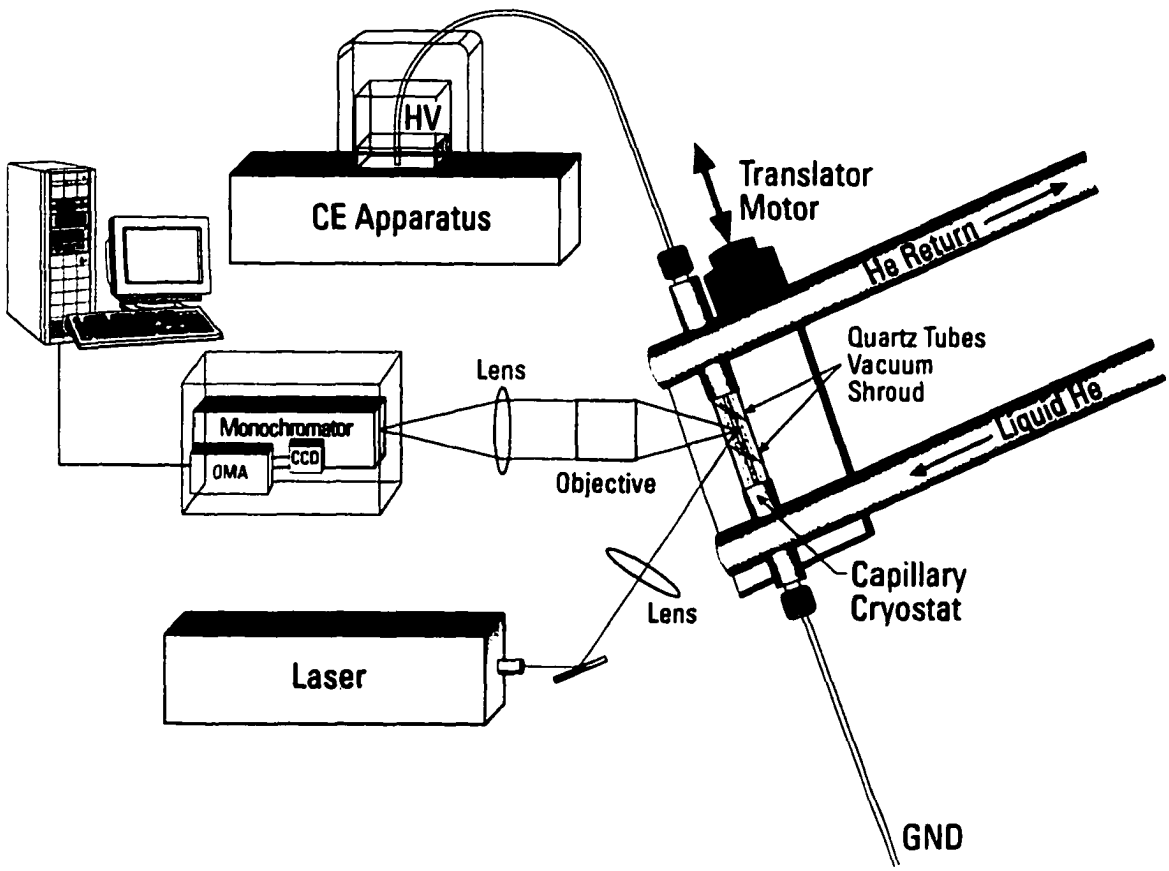

Figure 5-1. Schematic apparatus of the CE-FLNS system used for low temperature structural identification of CE-separated analytes.

Lauderdale, FL). Low-temperature spectra were obtained using gated and non-gated modes of detection. A gatewidth of 200 ns and various delay times, as specified in figure captions, were used. Spectral resolution for NLN fluorescence and FLN spectra was 0.8 and 0.09 nm, respectively.

5.3.3. Solid phase extraction (SPE) and reverse-phase high-performance liquid chromatography (RP-HPLC)

The (dominantly) hydrophobic BP derived adducts/metabolites from human urine was done by a multi-staged process (Casale *et al.*, in preparation). Urine samples were standardized to 100 mg creatinine as an internal standard. Extraction and preconcentration methods were employed with urine to minimize a large number of the (unwanted) endogenous species, which can chemically and spectrally interfere with the analytes of interest. The procedure was established with the extraction of adduct standards (BP-6-N7Gua and BP-6-N7Ade) added to human urine. The C-18 chains of the SPE cartridge efficiently retained the hydrophobic species, while a majority of unwanted components (e.g. salts) present in the urine samples eluted without retention. Adducts were released from the Sep-Pak columns when the 60/40 (v/v%) point was reached on the elution gradient. The standards were further isolated with a chloroform extraction, followed by evaporation to a volume of 10 μL. Then DMSO (200 μL) was added and evaporation continued until the chloroform was removed.

Based on the RP-HPLC (C-18) retention times established by BP-6-N7Gua/-N7Ade standards, maximum sample clean-up was achieved when 10-minute (70-80 minute retention window) eluate fractions were collected from the first HPLC separation (methanol/water gradient). After concentrating the effluent to 200 μL in DMSO, urine

samples were further purified with the second RP-HPLC (ACN/water gradient) separation. With this separation, optimal adduct isolation (i.e., maximum adduct recovery with minimal background components) was achieved by collecting a 10-minute fraction (30-40 minute retention window) established by the adduct standards. Finally, effluent collected from the second separation was concentrated to 30 μL in DMSO for CE-FLNS analysis.

5.3.4. CE-separation conditions

The CE buffer consisted of a 15% acetonitrile (ACN) solution (v/v) containing 20 mM DOSS, and 4 mM sodium tetraborate. Aqueous NaOH was used to adjust the pH to 9. Before injection, the separation buffer was filtered through a 0.22 μm syringe filter (Costor) and then degassed for 5 minutes. All CE experiments were carried out in the micellar electrokinetic chromatography (MEKC) mode [29]. Introduction of the organic modifier ACN to the separation buffer provided adduct solubility within the mobile phase and thus established the dynamic equilibrium needed for differential partitioning (resolution) of the analytes by the pseudo-stationary phase. Capillaries (85 cm in length with a 75 cm effective length) were conditioned with 100 mM NaOH for 15 minutes (30 minutes for new capillaries), water for 5 minutes, and separation buffer for 15 minutes. The samples were hydrodynamically injected with 20 mbar pressure for 3 seconds resulting in approximately a 10 nL injection volume. Electrokinetic separations were carried out at 22 kV resulting in a current of ~ 19 μA. To eliminate the possibility of contamination of adduct standards, room-temperature CE-LIF was used to confirm the purity of BP-6-N7Gua and B-6-N7Ade adduct.

5.3.5. Off-line FLNS experiments

Reference spectra of BP-derived adduct standards were performed in 100% CE buffer. The samples were placed in 2 mm i.d. quartz tubes, and brought to 4.2 K in a double nested liquid helium dewar for LIF measurements under NLN and FLN conditions. Approximately 20 μL sample volumes were sufficient for off-line analyses. The delay times and gate widths are specified in figure captions.

5.3.6. Molecular modeling

Molecular structures of BP-6-N7Gua and BP-6-N7Ade are shown in Figure 5-2. Structural optimization of one of these adducts (–N7Gua) was performed with HyperChem's molecular modeling program. The MM+ force field parameters developed for organic molecules and the Polak-Ribiere method for molecular mechanics optimization were employed. A quenched dynamics (i.e. simulated annealing) was used to explore the conformational space. Ten structures were minimized and then subjected to 100 ps of molecular dynamics at T = 400 K.

The dihedral angle α, defining the relative orientation of guanine in respect to the BP-moiety (see Figure 5-2), was used as a variable during the exploration of the conformational space. A Monte Carlo method was employed to determine the average value of α. Ten simulations were performed with 2000 steps at T = 400 K with a maximum allowed atomic displacement of 0.05 Å. Fifteen randomly selected structures were again subjected to a 100 ps run (at 400 K) and cooled to 0 K in 2 ps. The (0,0) transitions were calculated for the resulting fifteen structures using the ZINDO/S semi-empirical quantum mechanical method.

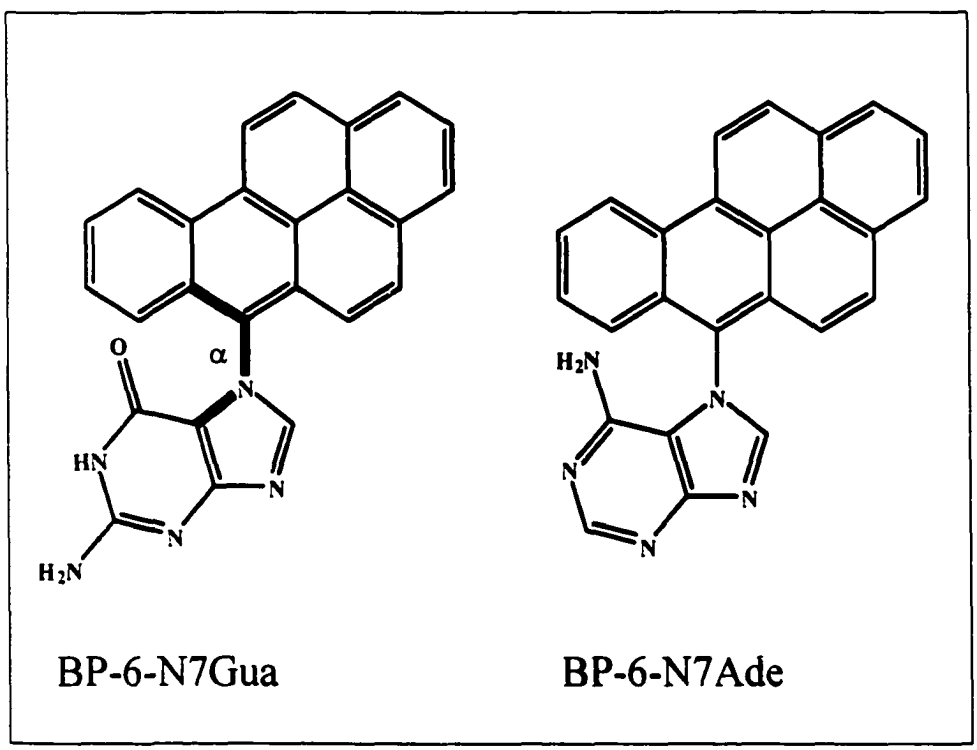

Figure 5-2. Molecular structures of one-electron oxidation BP-6-N7Gua and BP-6-N7Ade adducts. The dihedral angle α corresponds to rotation around the single bond that connects the two moieties.

5.4. Results and Discussion

5.4.1. Separation of BP-6-N7Gua and BP-6-N7Ade: limit of detection The room-temperature fluorescence electropherogram of the expected depurinated adducts standards (10^{-8} M) is shown in Figure 5-3. Peaks a and b correspond to BP-6-N7Gua and BP-6-N7Ade, respectively, as established by CE migration times. The small-unidentified peaks observed in the electropherogram of Figure 5-3, most probably correspond to adduct decomposition products, and/or impurities present in solvents used in purification and/or CE separation. The inset of Fig. 5-3 shows the CE electropherogram obtained for the BP-6-N7Ade standard at much lower concentration. Fluorescence was integrated in the 385-500 nm range. This result establishes an absolute limit of detection for the BP-6-N7Ade adduct (at room temperature) of approximately 2 attomole (~2 x 10^{-10} M; S/N ~3); the detection limit for BP-6-N7Gua was similar.

5.4.2. Identification and relative abundance of BP-6-N7Gua in human urine

Curve a of Figure 5-4 shows the CE separation of the 10-minute HPLC urine fraction (see section II.3) of an individual chronically exposed to coal smoke (i.e., ~30 μg of BP per day). Electropherograms b and c are those of the BP-6-N7Gua standard and a urine fraction from non-exposed individual, respectively. The data, based on migration times and standard additions, indicates that the intense peak (~23 minutes) in the electropherogram of the coal smoke-exposed individual (curve a) corresponds to BP-6-N7Gua at a level of ~0.9 fmol. No detectable amounts of the BP-6-N7Gua or BP-6-N7Ade were observed in the electropherogram of the urine extract from the non-exposed individual (curve c).

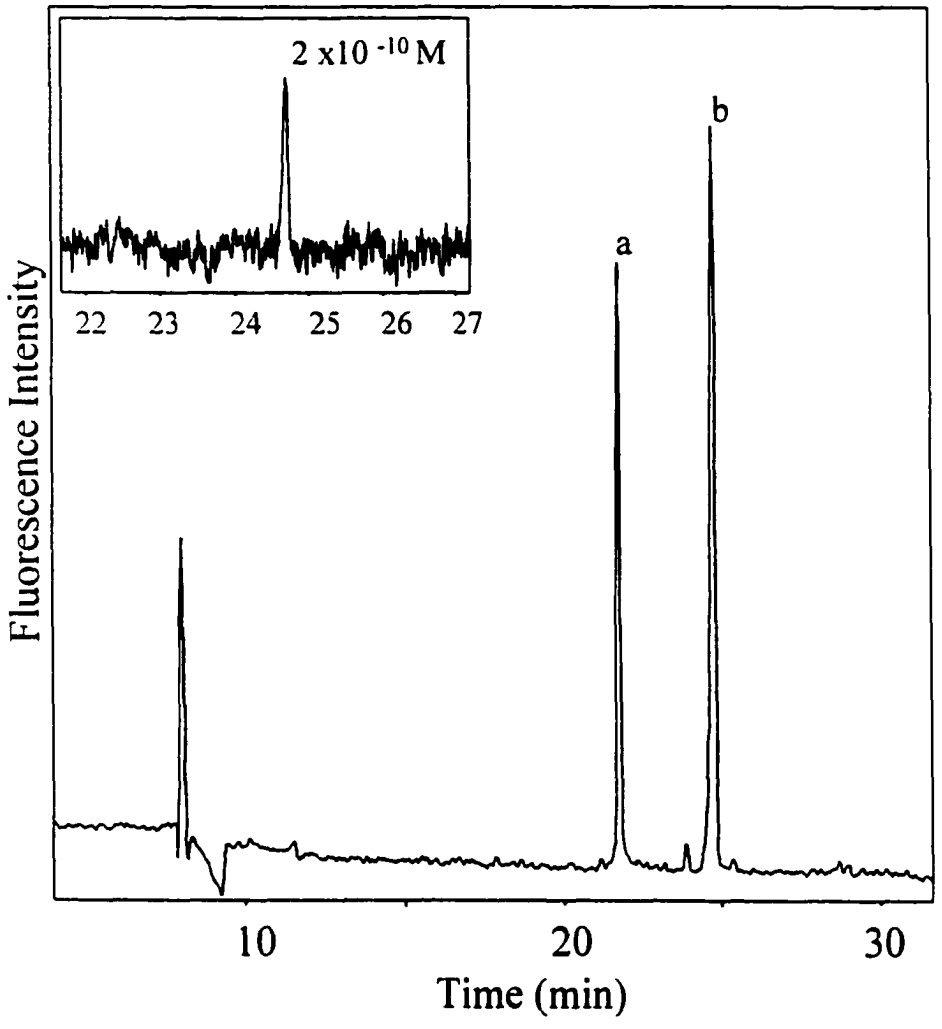

Figure 5-3. CE electropherogram of the BP adduct standards. Peak a corresponds to BP-6-N7Gua and peak b corresponds to BP-6-N7Ade. The small (unidentified) peaks in the electropherogram are presumed to be impurities and/or adduct decomposition products. Inset, a detection limit of 10^{-10} M is shown for the BP-6-N7Ade standard. Laser excitation wavelength = 351.1 nm with the power output set to 100 mW. The fluorescence intensity of the electropherogram was obtained by integration of the spectral region from 385-500 nm.

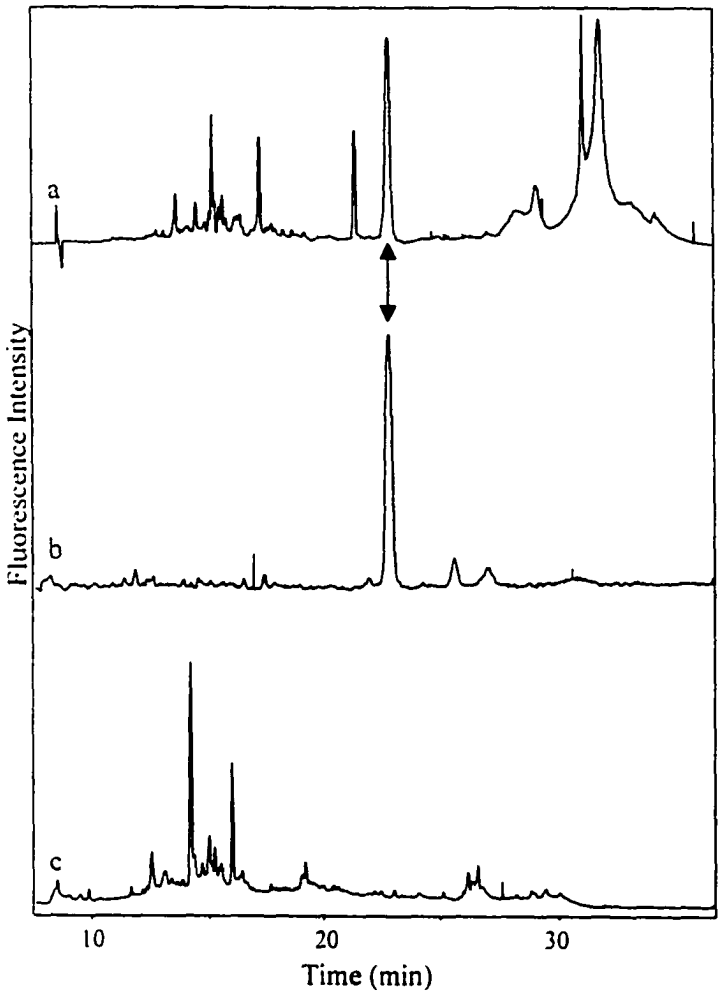

Figure 5-4. CE separations of urine extract of an individual exposed to coal smoke (a), BP-6-N7Gua standard (b), and the urine extract of a non-exposed individual (c). The arrow marks the location of the depurinated adduct, BP-6-N7Gua. The fluorescence intensity of the electropherogram was obtained by integration of the spectral region from 385-500 nm. Spectra were obtained with an excitation wavelength of 351.1 nm (output power of 100 mW).

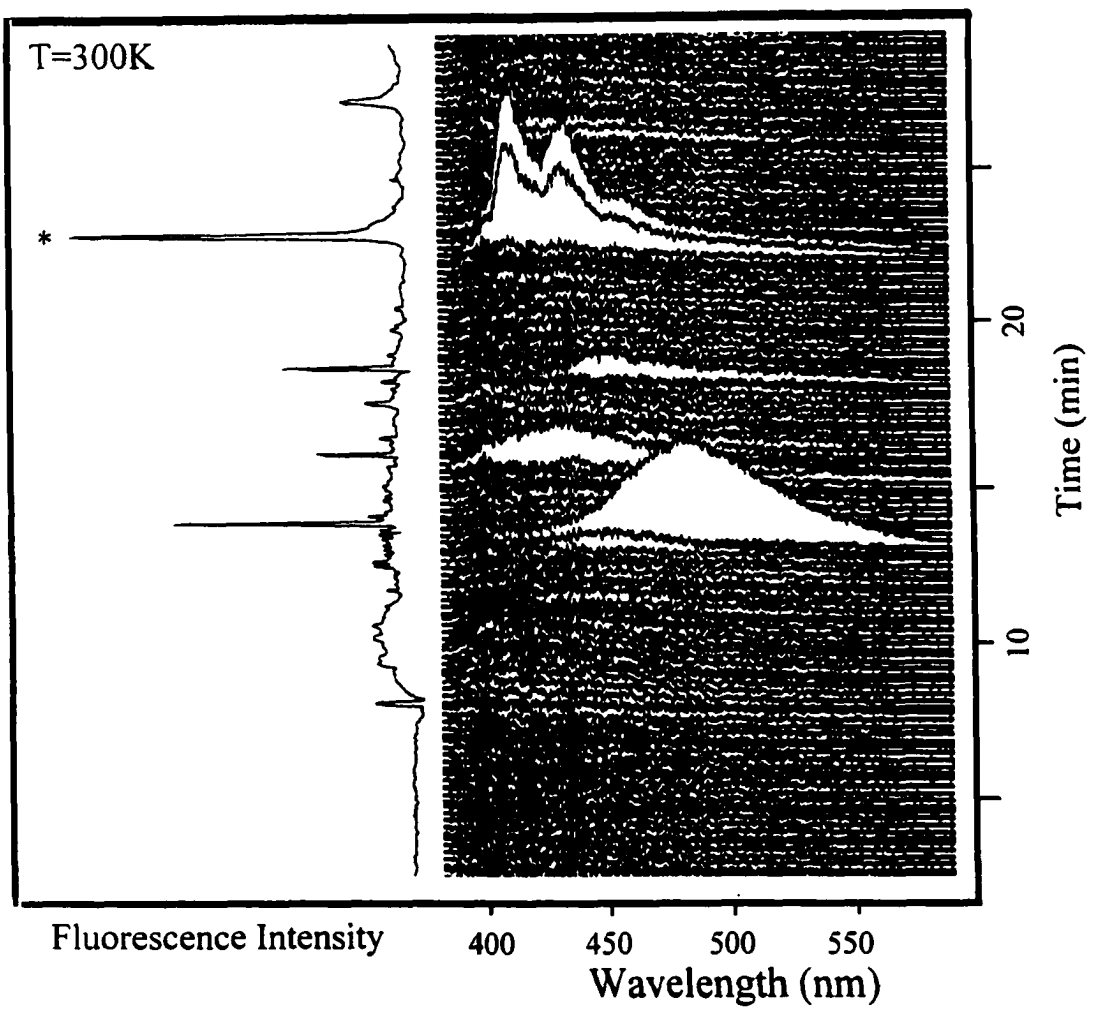

Figure 5-5. CE electropherogram, with fluorescence spectra corresponding to the CE-separated peaks obtained for urine-extract from an individual exposed to coal smoke (λ_{ex} = 351.1 nm). Fluorescence intensity of the electropherogram (left) was obtained by integration of the spectral region from 385-500 nm. The peak labeled with an asterisk correspond to the BP-6-N7Gua adduct (see text for details).

Figure 5-5 shows another example of an electropherogram (left) of a urine fraction from a second coal smoke-exposed individual. In addition to the electropherogram, NLN fluorescence spectra of the CE separated peaks were monitored in real-time. An intense peak at ~23 min (labeled with an asterisk) is also observed for this individual. The 4.2 K NLN spectrum of this peak is indistinguishable from that of the BP-N7Gua standard (not shown), suggesting again that BP-6-N7Gua is formed *in vivo*. The same quantitation procedure as described above revealed that the level of BP-6-N7Gua is ~0.6 fmol. It is worth pointing out that the peaks at ~ 13 and 16 minutes, with emission maxima at ~ 475 and ~ 430 nm, would likely prevent spectral characterization of the ~23 min peak had the analysis been performed using off-line NLN fluorescence. No attempts were made to identify the peaks whose spectra do not resemble BP-type fluorescence.

5.4.3. CE-FLNS analysis

The results in Figure 5-5 indicate that the one-electron oxidation BP-6-N7Gua adduct is probably formed in humans. Nevertheless, a more definitive identification is required. The 4.2 K NLN spectrum of the CE-separated peak (~ 23 minutes), obtained with an excitation wavelength of 351.1 nm, is shown in frame A of Figure 5-6. The spectrum is indistinguishable from that of the BP-6-N7Gua adduct standard (spectrum not shown). We note that at 4.2 K the fluorescence intensity increases by a factor of 10 due to the higher fluorescence quantum yield. The latter along with longer detection times for the frozen and stationary analyte zone provides sub-attomole detection limit. Figure 5-6 (Frame B) shows the 4.2 K high-resolution on-line FLN spectrum (λ_{ex} = 386.5

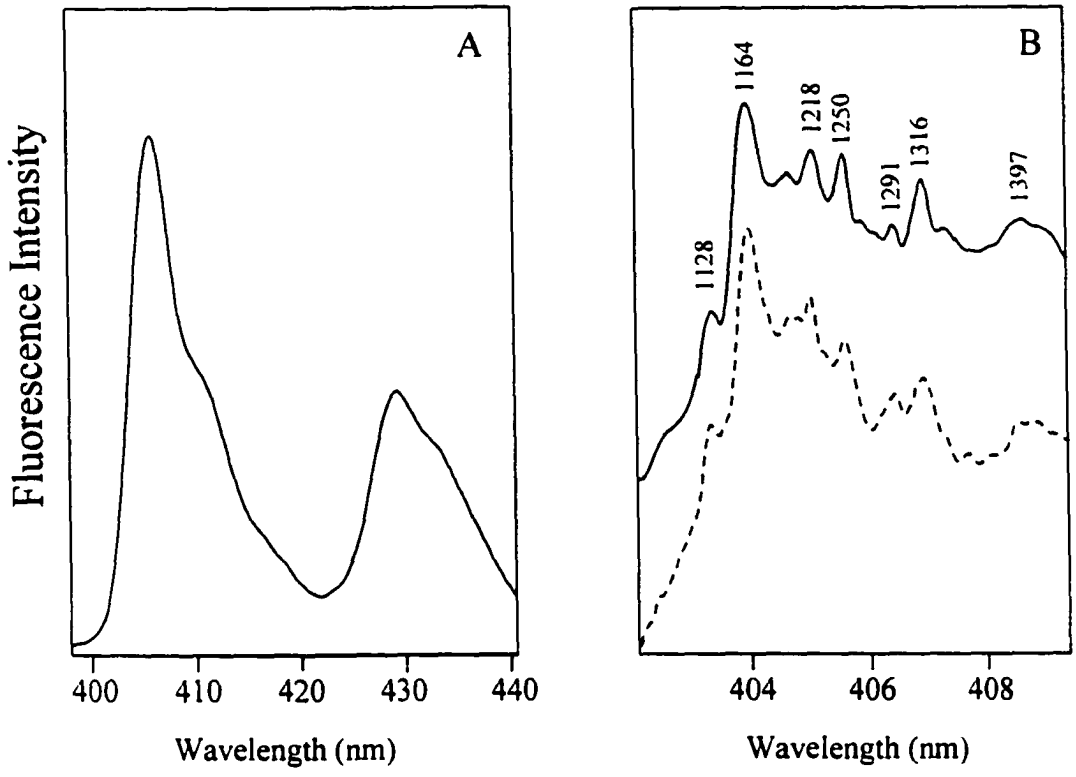

Figure 5-6. On-line, 4.2 K analysis of the CE-separated peak at ~ 23 minutes in the electropherogram of Figure 5-5. Frame A: NLN fluorescence spectrum of the CE-separated peak obtained with a CW Ar-ion laser; 351.1 nm. The origin, or (0,0) band, is at 406 nm. Frame B: Comparison the on-line FLN spectrum (solid line) for the CE separated peak to the FLN spectrum of BP-6-N7Gua standard. The FLN peaks are labeled with their excited-state vibrational frequencies, in cm^{-1}. T = 4.2 K, λ_{ex} = 386.5 nm, gate-width = 200 ns with a 40 ns delay.

nm) for the CE-separated peak (solid line) and the off-line FLN spectrum (dashed line) of the BP-6-N7Gua standard. The FLN spectra are nearly indistinguishable as revealed by the identical frequencies (and intensities) of the excited state vibronic modes at 1128, 1164, 1218, 1250, and 1316 cm^{-1}. This result provides conclusive proof that the DNA adduct is BP-6-N7Gua and, as well, underscores the high selectivity and sensitivity of CE-FLNS.

Quantitative studies revealed that the daily excretion of BP-6-N7Gua by the two individuals studied in this work was about 200 pmol per day. From spiking experiments, it was determined that adduct recovery was 65-85%, therefore, the daily excretion could be ~18-53 % higher. In terms of the creatinine level (an internal standard), the two coal smoke exposed individuals excreted about 226 pmol of BP-6-N7Gua per μmol of creatinine. By way of comparison, it was recently shown that psoriasis patients treated with coal tar medication excreted (in urine) 5-250 pmol of 1-hydroxypyrene [30] and 15.0 ± 29.5 pmol of BP-tetraols per μmol of creatinine [28]. The BP-tetraols were claimed to be relevant for PAH-cancer risk assessment because formation of BP-diolepoxide (which is known to form stable DNA adducts) precedes formation of BP-tetraols [31]. 1-hydroxypyrene (the metabolite most often used to assess PAH exposure) was measured in the urine of garbage incineration workers at the level of 0.05-0.41 pmol per μmol of creatinine [32]. However, we believe, due to the relatively high abundance of the BP-6-N7Gua adduct formed in coal smoke-exposed humans, that it is a more biologically relevant marker for PAH exposure since it reports directly on DNA damage.

5.4.4. Spectral characterization of the BP-6-N7Gua standard

The 4.2 K fluorescence origin bands of BP-6-N7Gua in CE-separation buffer obtained under NLN conditions are shown in Figure 5-7, frame A. The origin band maximum for 0 ns delay is at 407.1 nm shifting to 406.1, 405.6, 404.5 nm for 20, 40 and 80 ns delay times, respectively. The gate width was kept constant at 20 ns. Such a blue shift with increasing delay time has been observed for the BP-6-N7Ade adduct and was attributed to a distribution of BP-6-N7Ade adduct conformers [33].

Vibronically excited FLN spectra (Figure 5-7A, curves a-c), obtained with λ_{ex} = 386.5 nm and delay times of 0, 40, and 80 ns are shown in Fig. 5-7B. The observed narrowing of the FLN spectra and decreasing intensity of the zero-phonon lines in the long wavelength region with increasing delay time indicates that fluorescence originates only from BP-6-N7Gua adducts absorbing at the high-energy wing of the inhomogeneously broadened vibronic absorption band. The latter is in agreement with the observed distribution of fluorescence lifetimes (data not shown). Such narrowing correlates well with the NLN spectra shown Fig. 5-7A. From an analytical standpoint, the importance of the results is that adducts formed *in vivo* and corresponding adduct standards should be measured with identical delay times.

5.4.5. Modeling studies of BP-6-N7Gua

To provide some insight on the blue-shift of the fluorescence origin bands, a molecular modeling study was initiated. A typical structure obtained from molecular dynamics simulations (T = 0 K), and subsequent optimization, is shown in Figure 5-8. The dihedral angle α (defined in Figure 5-2) of the optimized BP-6-N7Gua structure at T = 0 K is 90.2°. Monte Carlo simulations performed at 400 K revealed that the average

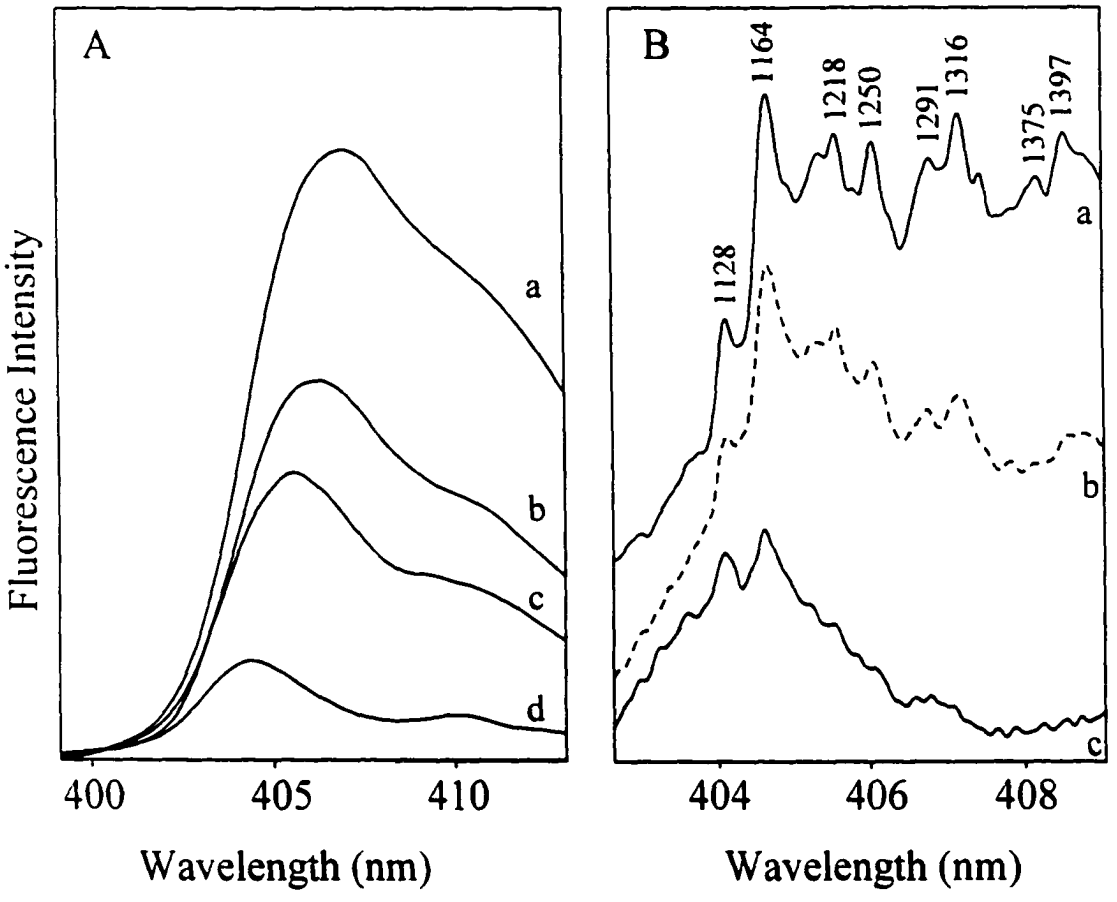

Figure 5-7. (A) NLN fluorescence spectra (curves a-d) of BP-6-N7Gua in CE buffer obtained at delay times of 0, 20, 40, and 80 ns, respectively; λ_{ex} = 308 nm. Spectra b, c, and d were multiplied by a factor of 2, 8, and 40, respectively. (B) FLN spectra obtained for BP-6-N7Gua in CE buffer with an excitation wavelength of 386.5 nm for 0 (spectrum a), 40 (spectrum b), and 80 ns (spectrum c) delay times. The numbers correspond to excited-state vibrational frequencies in cm^{-1}. T = 4.2 K; gate width = 200 ns.

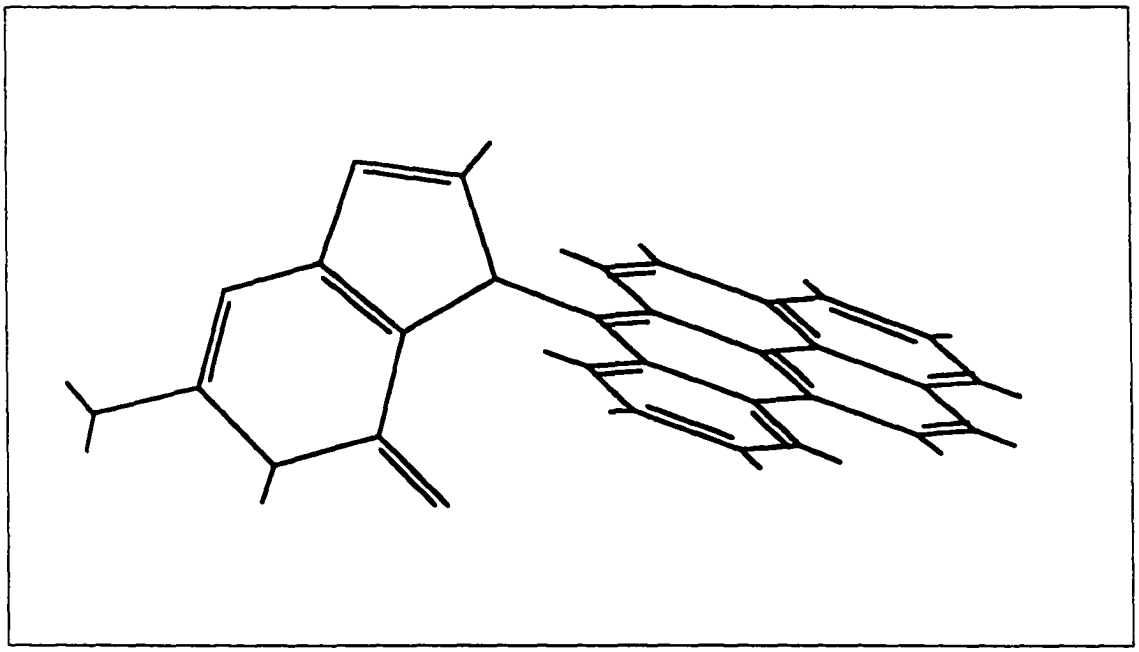

Figure 5-8. Optimized structure of the BP-6-N7Gua adducts. The average value of α is 90.2° at T = 0 K.

value of α over the whole simulation period was ~91° with a root-mean-square (RMS) deviation of ~ 6°. This suggests that, upon cooling to 4.2 K, a distribution of conformations with slightly different α values is possible. As a check on this, fifteen randomly selected and thermally equilibrated (at 400 K) structures of BP-6-N7Gua were subjected to additional quenched dynamics to see whether or not a distribution of α exists at 0 K. The calculations revealed a narrow distribution of dihedral angles with α equal to 91.5° ± 1.4°.

Results of the ZINDO/S calculations on the fifteen structures showed that the mean (0,0)-transition was at 397.0 nm with a RMS of ± 0.5 nm. The experimentally observed (0,0)-band for BP-6-N7Gua in ethanol and CE-buffer glasses was red-shifted by ~ 8 nm and ~9 nm, respectively; this discrepancy is primarily due to the fact that the calculations were performed *in vacuo*. Since we are interested in the relative energy shift rather then absolute values, the calculated RMS deviation of ± 0.5 nm for the selected conformers can be compared with experimental results. The results show that the RMS deviation of the (0,0)-bands is in reasonable agreement with the experimental data where the relative band shifts are ~1.6 nm for the CE buffer (see Fig. 5-7A) and 1.2 nm for an ethanol glass (results not shown), respectively. However, this agreement might be fortuitous since the blue shift could also originate from a matrix-induced change in the relative orientation between the two moieties and/or frequency-dependent permanent dipole moment changes across the inhomogeneously broadened absorption band.

5.5. Conclusions

CE-FLNS was used to prove that the depurinating adduct BP-6-N7Gua is formed in humans. The urine fractions analyzed were isolated by SPE and RP-HPLC. Attomole detection limits with CE-FLNS were demonstrated and quantitative studies revealed that the level of BP-6-N7Gua formed in humans exposed to coal smoke was ~200 pmol per day (~226 pmol per μmol of creatinine). The identification of BP-6-N7Gua in humans provides further support for the hypothesis that the one-electron oxidation metabolic pathway plays an important role in PAH-induced carcinogenesis. It is possible that the formation of apurinic sites and stable BP-diolepoxide type adducts work in concert to prevent error-free repair of DNA. Be that as it may, it is reasonable to assume that there is considerable positive correlation between the levels of apurinic sites and stable adducts formed. Thus, the characterization and determination of depurinating PAH-DNA adducts in urine provides a basis for risk assessment monitoring. This approach is more reliable than one based on the monitoring of PAH metabolites produced by detoxification pathways since it reports DNA damage directly.

5.6. Abbreviations: Ade, adenine; BP, benzo[*a*]pyrene; BP-6-N7Ade, 7-(benzo[*a*]pyren-6-yl)adenine; BP-6-N7Gua, 7-(benzo[*a*]pyren-6-yl)guanine; CE, capillary electrophoresis; CW, continuous wave; DB[*a,l*]PDE, dibenzo[*a,l*]pyrene diol epoxide; FLNS, fluorescence line-narrowing spectroscopy; ICCD, intensified charge-coupled device; LIF, laser-induced fluorescence; NLN, non-line-narrowing; PAH, polycyclic aromatic hydrocarbon; RP-HPLC, reverse-phase high-performance liquid chromatography; SPE, solid phase extraction.

5.7. Acknowledgements

Ames Laboratory is operated for the U.S. Department of Energy by Iowa State University under contract no. W-7405-Eng-82. The Office of Health and Environmental Research supported this research. Support to C.-H. Lin, G. Casale, and M. Singhal was provided by the NCI, grant PO1 CA49210. The authors thank Dr. J. Mumford (US Environmental Protection Agency, National Health and Environmental Effects Research Laboratory; Epidemiology and Biomarker Branch, Research Triangle Park, NC 27711) for urine samples, and Dr. E.L. Cavalieri (Eppley Institute for Research in Cancer, University of Nebraska Medical Center, Omaha, NE) for providing the BP-6-N7Gua and BP-6-N7Ade adduct standards.

References:

1. Yan, C., Dadoo, R., Zhao, H., Zare, R.N., Rakestraw, D.J., *Anal. Chem.*, 1995, *67*, 2026.

2. Milofsky, R. E., Yeung, E.S., *Anal. Chem.*, 1993, *65*, 153.

3. Roberts, K., Lin, C.-H., Jankowiak, R., Small, G.J., *J. Chrom. A*, 1999, *853*, 159.

4. Jankowiak, R., Zamzow, D., Ding, W., Small, G.J., *Anal. Chem.*, 1996, *68*, 2549.

5. Nie, S., Dadoo, R., Zare, R.N., *Anal. Chem.*, 1993, *65*, 3571.

6. Barry, J.P., Norwood, C., Vouros, P., *Anal. Chem.*, 1996, *68*, 1432.

7. Deforce, D,L,D, Ryniers F,P.K., Van den Eeckhout, E.G., Lemiere, F., Esmans, E.L., *Anal. Chem.*, 1996, *68*, 3575.

8. Zamzow, D., Lin, C.-H., Small, G.J., Jankowiak, R, *J. Chrom. A*, 1997, *781*, 73.

9. Zamzow, D., Small, G.J., Jankowiak, R., *Mol. Cryst. Liq. Cryst.*, 1996, *291*, 155.

10. Jankowiak, R., Cooper, R.S., Zamzow, D., Small, G.J., Doskocil, G., Jeffrey, A.M., *IARC Scientific Publications*, 1988, *89*, 372.

11. Jankowiak, R., Small, G.J., *Anal. Chem.*, 1989, *61*, 1023A.

12. Devanesan, P.D., RamaKrishna, N.V.S., Todorovic, R., Rogan, E.G., Cavalieri, E.L., Jeong, H., Jankowiak, R., Small, G.J., *Chem. Res. Toxicol.*, 1992, *5*, 302.

13. Rogan, E.G., Devanesan, P.D., RamaKrishna, N.V.S., Higginbotham, S., Padmavathi, N.S., Chapman, K., Cavalieri, E.L., Jeong, H., Jankowiak, R., Small, G.J., *Chem. Res. Toxicol.*, 1993, *6*, 356.

14. Devanesan, P.D., RamaKrishna, N.V.S., Padmavathi, N.S., Higginbotham, S., Rogan, E.G., Cavalieri, E.L., Marsch, G.A., Jankowiak, R., Small, G.J., *Chem. Res. Toxicol.*, 1993, *6*, 364.

15. Suh, M., Ariese, F., Small, G.J., Jankowiak, R., Hewer, A., Phillips, D.H., *Carcinogenesis*, 1995, *16*, 2561.

16. Jankowiak, R., Small, G.J., *Chem. Res. Toxicol.*, 1991, *4*, 256.

17. Todorowic, R., Ariese, F., Devanesan, P., Jankowiak, R., Small, G.J., Rogan, E.G., Cavlieri, E.L., *Chem. Res. Toxicol.*, 1997, *10*, 941.

18. Cavalieri, E., Rogan, E.L., *The Handbook of Environmental Chemistry*, Chapter 11, 1998, (A.H. Neilson, ed.), Springer-Verlag, Heidelberg, *3J*, 81. (refs. therein)

19. Chakravarti, D., Pelling, J.C., Cavalieri, E.L., Rogan, E.G., *Proc. Natl. Acad. Sci. USA*, 1995, *92*, 10422.

20. Cavalieri, E.L., Rogan, E.G., *Pharm. Ther.*, 1992, *55*, 1083.

21. Rogan, E.G., RamaKrishna, N.V.S., Higginbotham, S., Cavalieri, E.L., Jankowiak, R., Small, G.J., *Chem. Res. Toxicol.*, 1990, *3*, 441.

22. Jankowiak, R., Small, G.J., *The Handbook of Environmental Chemistry*, Chapter 12, 1998, (A.H. Neilson, ed.), Springer-Verlag, Heidelberg, *3J*, 81. (refs. therein)

23. Cavalieri, E.L., Rogan, E.G., *Xenobiotica*, 1995, *25*, 677.

24. Cheng, L., Devanesan, P.D., Higginbotham, S., Ariese, F., Jankowiak, R., Small, G.J., Rogan, E.G., Cavalieri, E.L., *Chem. Res. Toxicol.*, 1996, *9*, 897.

25. Devanesan, P.D., Higginbotham, S., Ariese, F., Jankowiak, R., Suh, M., Small, G.J., Cavalieri, E.L., Rogan, E.G., *Chem. Res. Toxicol.*, 1996, *9*, 1113.

26. Devanesan, P.D., RamaKrishna, N.V.S., Higginbotham, S., Padmavathi, N.S., Chapman, K., Cavalieri, E.L., Jeong, H., Jankowiak, R., Small, G.J., *Chem. Res. Toxicol.*, 1993, *6* 356.

27. Mumford, J.L., Li. X., Hu, F., Lu, X.B., Chuang, J.C., *Carcinogenesis*, 1995, *16*, 3031.

28. Bowman, E.D., Rothman, N., Hackl, C., Santella, R.M., Weston, A., *Biomarkers*, 1997, *2*, 321-327.

29. Terabe, S., Otsuka, K., Ichikawa, K., Tsuchiya, A, Ando, T., *Anal. Chem.*, 1984, *56*, 111.

30. Jongeneelen, F.J., Anzion, R.B.M., Leijdekkers, C.-M., Bos, R.P., Henderson, P.T., *International Archives of Occupational and Environmental Health*, 1985, *57*, 47-55.

31. Geacintov, N.E., Polycyclic Aromatic Hydrocarbon Carcinogenesis, 1985, (Harvey, E.G., ed.), American Chemical Society, Washington, D.C., 107-124.

32. Schaller, K.H., Angerer, J., Hausmann, N., *Proceedings of the 13th International Symposium on Polynuclear Aromatic Hydrocarbons, Bordeaux, France*, 1993, 1023-1030.

33. Lin, C.-H., Zamzow, D., Small, G.J., Jankowiak, R., *Polycyclic Aromatic Compounds*, 1999, in press.

CHAPTER 6. HIGH-PERFORMANCE LIQUID CHROMATOGRAPY INTERFACED WITH FLUORESCENCE LINE-NARROWING SPECTROSCOPY FOR ON-LINE ANALYSIS

A paper published in *Analytical Chemistry*, 2001, *73*, 951.

K. P. Roberts, R. Jankowiak, and G. J. Small

6.1. Abstract

We have demonstrated, for the first time, that high-performance liquid chromatography (HPLC) can be interfaced with fluorescence line-narrowing spectroscopy (FLNS) for on-line identification and characterization of analytes. Interfacing centered primarily on the design and construction of a novel liquid helium cryostat that accommodates variable-sized quartz tubes/capillaries suitable for HPLC as well as capillary electrophoresis/electrochromatography. In addition to the high spectral resolution afforded by FLNS, analyzing the separated components at 4.2 K minimizes photodegradation from the excitation source and provides indefinite detection times for signal averaging. The proof-of-principle for the HPLC-FLNS system is first demonstrated with a mixture of four structurally similar polycyclic aromatic hydrocarbons, then applied to the analysis of DNA adducts from mouse skin exposed to the carcinogen dibenzo[*a,l*]pyrene. With femtomole detection limits, HPLC-FLNS can be used for real-world analyses of complex mixtures.

6.2. Introduction

High-performance liquid chromatography (HPLC) is a powerful, practical, and, hence, common separation technique used for analysis of chemical and biochemical mixtures. The success of HPLC is due to the attention given to developing column technology, establishing rigorous separation protocols, and improving detection methods. Traditionally, analyte identification in HPLC has been based on chromatographic retention times determined with standards that, however, can be expensive to obtain. Such identification, together with quantification, requires the absence of coelution and a high degree of reproducibility. Consequently, there is a need for high-resolution detection/identification methods that can provide unambiguous characterization of separated analytes without depending on standards. Moreover, on-line analysis avoids any post-column degradation associated with off-line analysis of separated fractions. Several on-line methods have shown success either by providing selective information, such as *m/z* ratios when interfacing HPLC with MS [1-3], or by providing structural information when combined with HPLC-NMR [4,5], -FTIR [6,7], and -Raman [8-10].

In this paper, we report the first on-line interfacing of HPLC with fluorescence line-narrowing spectroscopy (FLNS), which utilizes narrow-line excitation at low temperatures (typically 4.2 K) [11-14]. Identification in FLNS is based on comparison of an analyte's vibronically resolved fluorescence spectra to a library of reference spectra generated once from standards, alleviating the need for standards for every identification. The average widths of vibronic bands in FLNS are ~ 5 cm^{-1}. At this temperature photodegradation is minimized and the sensitivity of the laser-induced fluorescence (LIF) increases by a factor of ~10 for many molecules. FLNS can also be used for

conformational analysis [15], and for non-fluorescent molecules upon derivatization with a fluorescent label [16].

Originally, identification of constituents in chemical mixtures by FLNS required separation and isolation of the individual components with preparative chromatography to avoid spectral interference. This off-line approach, however, necessitates ample amounts of material and sample stability. Therefore, to overcome these detriments, FLNS was interfaced semi-on-line with thin-layer chromatography (TLC) [17-21] and polyacrylamide gel electrophoresis (PAGE) [22,23]. It was shown, for example, that by directly depositing (and drying) effuent from an LC column onto a linearly translating TLC plate by a novel spray-jet assembly, FLNS could be performed on the deposited trace, or after an additional TLC separation perpendicular to the trace. This approach was used to identify structurally similar molecules such as tetrols derived from polycyclic aromatic hydrocarbons (PAH) and PAH-DNA adducts [20,21]. Although only minor losses in chromatographic resolution were encountered, spectral interference from the separation media in both TLC- and PAGE-FLNS limit the sensitivity of these approaches. Recently, FLNS was coupled on-line with capillary electrophoresis/electrochromatography (CE/CEC) [24-28]. In comparison to TLC- and PAGE-FLNS, the CE-FLNS methodology provided: *i*) reduced background luminescence, *ii*) elimination of the post-separation extraction step often needed in TLC and PAGE; *iii*) high separation efficiency of CE; and *iv*) small sample volume compatibility of CE with bioanalysis. It was shown with the CE-FLN system that complex mixtures of PAHs, stable PAH-DNA adducts, and depurinating PAH-DNA adducts can be unambiguously identified on-line [24]. With low attomole detection

limits, CE-FLNS showed, for the first time, that depurinating benzo[*a*]pyrene-guanine adducts are formed in humans and excreted into urine [28].

In this study, the construction and feasibility of an on-line HPLC-FLNS system are demonstrated with a mixture of four structurally similar PAHs. In addition, the first real-world application of the system is shown for the analysis of a PAH-DNA adduct formed from dibenzo[*a,l*]pyrene (DB[*a,l*]P) treated mouse-skin. We believe that interfacing FLNS with HPLC will further expand the applicability of FLNS and provide a complementary technique to CE-FLNS.

6.3. Experimental Section

Caution. Benzo[*a*]pyrene, *trans*-7,8-dihydrodiol-benzo[*a*]pyrene, and *trans*-9,10-dihydrodiol-benzo[*a*]pyrene are extremely hazardous chemicals and should be handled carefully in accordance with NIH guidelines.

6.3.1. Reagents and Chemicals

Ethanol (EtOH) and water were of HPLC grade and purchased from Aldrich (Milwaukee, WI). Both solvents were filtered through 0.22 μm filters (Costar, Corning, NY), sonicated, and purged with dry helium gas prior to use. Benzo[*a*]pyrene (B[*a*]P), benzo[*e*]pyrene (B[*e*]P), *trans*-7,8-dihydrodiol-benzo[*a*]pyrene (*trans*-7,8-B[*a*]P-diol), and *trans*-9,10-dihydrodiol-benzo[*a*]pyrene (*trans*-9,10-B[*a*]P-diol) were purchased from Midwest Research Institute (Kansas City, MO), stored at -70°C, and kept from contact with water and light during handling. Stock solutions (1×10^{-5} M) were prepared in EtOH and subsequent dilutions were made with the HPLC mobile phase.

6.3.2. Mouse Skin Treated with DB[*a,l*]P

Female Swiss mice were treated with 200 nmol of DB[*a,l*]P in 50 mL of acetone. Four hours later, the mouse skin was excised, minced, and grounded in liquid nitrogen. The ground mouse skin was soxilated with a solvent mixture ($CHCl_3$: MeOH (1:1 v/v)) for 48 hours to extract any depurinating DNA adducts. After evaporating the soxilate extract to dryness, the residue was dissolved in DMSO/MeOH for preparative HPLC fractionation. The sample was first ran through an acetonitrile (ACN)/H_2O gradient using a YMC ODS-AQ 6.0 x 250 mm column (YMC, Wilmington, NC), a Waters 600E solvent delivery system and 996 PDA UV absorbance (254 nm) detector. An 80-min linear gradient from 20 to 100% ACN, at a constant flow rate of 1.0 mL/min was performed followed by re-fractionation with a MeOH/H_2O gradient over 70-min from 30-100% MeOH. This HPLC separation used a Jasco FP-920 (Jasco Inc., Easton, MD) fluorescence detector. Broad fractions were collected according to retention times established by standards of DB[*a,l*]P adducts, dried, and then immediately stored in the freezer to prevent decomposition prior to HPLC-FLNS analysis.

6.3.3. FLN Chromatographic System

Micro-HPLC separations of the mixture of the four PAHs were performed by interfacing a standard quaternary Hewlett-Packard (HP) series 1050 (Hewlett-Packard Co., Palo Alto, CA) HPLC system with a microflow processor (Acurate, LC Packings, San Francisco, CA). Separations were achieved by setting the HPLC pump to a flow rate of 250 μL per minute and reducing the flow through a 1-mm calibrator (CAL-400-1.0) of the microflow processor. The microflow processor split the mobile phase to give a column flow rate of 30 μL per minute. An HP-1050 autosampler was used to inject 2 –

50 μL sample volumes onto an Advantage 100, 1.0 x 250 mm C18 5-μm column (Thomson Instrument Co., Clear Brooke, VA). The column was directly connected to a 0.460 mm i.d. x 2 mm o.d. x 30 cm quartz tube (InnovaQuartz Inc., Phoenix, AZ). The quartz tube was positioned in the center of the on-line FLN cryostat and served as the detection cell for all LIF experiments discussed in the Results and Discussion Section, excluding Section 6.5.4, which utilized a smaller i.d. tube. Effluent flow rate was measured at the end of the quartz tube. Separations were carried out in an isocratic mode with an 85% EtOH and 15% H_2O (v/v) mobile phase composition.

HPLC-FLNS analyses of the mouse-skin preparative HPLC fractions utilized a narrow-bore (2.1 x 150 mm) Waters Symmetry-C8 column connected to the 0.360 mm i.d. detection tube. A 30-min linear EtOH/H_2O gradient, starting at 30% EtOH and ending at 100% EtOH at a constant flow rate of 0.20 mL/min was utilized. Elution of DB[*a,l*]P-N3Ade was monitored by room-temperature fluorescence emission spectra of the standard (see below). The same HPLC system was used as described above; excluding the micro-flow processor since the HP-1050 pumping system could adequately operate at this flow rate. Injection volumes of 5 μL were used in the mouse-skin experiments. Each day the separation column was equilibrated for 30 minutes or until the baseline was stabilized prior to sample injection. When the analytes of interest were detected in the quartz detection cell, liquid helium was introduced into the cryostat to freeze the separation and the HPLC pump was turned off.

6.3.4. Laser Systems and Fluorescence Instrumentation

The excitation source used for room-temperature HPLC separations was a model Innova 90C (Coherent, Santa Clara, CA) CW argon-ion laser excitation source operating

at 351.1 nm (100 mW output power). The excitation source for FLNS studies was a Lambda Physik FL-2002 pulsed dye laser (line-width of ~ 0.2 cm^{-1}), pumped by a Lambda Physik Lextra 100 XeCl excimer laser (Lambda Physik, Ft. Lauderdale, FL) at a repetition rate of 10-30 Hz. Fluorescence emission for on-line HPLC-FLNS was collected at a 90-degree angle to the excitation beam with a reflecting objective (25-0506 X 15, Ealing, Holliston, MA), focused into a 0.3-m monochromator (Model 218, McPherson, Acton, MA), and detected with an intensified charge-coupled device (Model ICCD-1024MLG-E/1, Roper Scientific, Trenton, NJ).

Off-line FLN reference spectra for the studied analytes were acquired to serve as a library for spectral identification in the on-line analyses. Samples of the four PAH standards were diluted to 1 X 10^{-6} M in the HPLC mobile phase (85/15 : EtOH/H_2O v/v%), while the mouse-skin sample and DB[*a,l*]P-N3Ade standard were dissolved in a 50/50 (v/v%) solution of the EtOH and H_2O mobile phase constituents with a drop of DMSO to enhance solubility. Standard solutions were placed in 2 mm i.d. quartz tubes and submerged in a double-nested glass liquid helium dewar equipped with quartz windows (H.S. Martin Inc., Vineland, NJ). Approximately 30 μL sample volumes were sufficient for off-line FLN analyses. Fluorescence emission was collected with a 2-inch lens at a 90-degree angle to the excitation beam, focused into a 1-m monochromator (McPherson Model 2061, Acton, MA), and detected with an intensified linear photodiode array (Model IRY-1024/GRB, Roper Scientific, Trenton, NJ). A series of reference spectra were taken for each standard with various delay times and excitation wavelengths. Gate widths and delay times are specified in the figure captions. The spectral resolution for this FLN setup was 0.03 nm.

6.5. Results and Discussion

6.5.1. On-line Cryostat

The first step in developing an HPLC system with low temperature FLN detection was the design of a cryostat that would be compact, robust, and amendable to either large diameter (0.5-3 mm o.d.) quartz tubing or capillaries (< 0.5 mm o.d.). As shown in Figure 6-1, the cryostat consists of a double-walled quartz observation window (15 cm in length) and inlet/return lines for introducing a continuous flow of liquid nitrogen or liquid helium; the outer portion of the cryostat is evacuated. In some cases, liquid nitrogen temperatures may provide sufficient spectral information for analyte identification [25]. The cryostat shown in Figure 6-1 is a modification of a previous capillary cryostat, which had a shorter observation window and longer inlet/return lines [24-28]. Automated translation of the cryostat was accomplished by mounting the cryostat to a micron step-size translation stage (Model 310-M, New England Affiliated Technologies, Lawrence, MA). Laser excitation was performed perpendicular to the length of the observation window and at a 90-degree angle to the fluorescence collection objective. This allowed FLNS to be performed along the entire length of the quartz observation window of the cryostat. To discriminate against scattered and reflected laser light, the cryostat was tilted 20° with respect to the laser beam. The cryostat is now commercially available from Janis Research Co. Inc., Wilmington, MA.

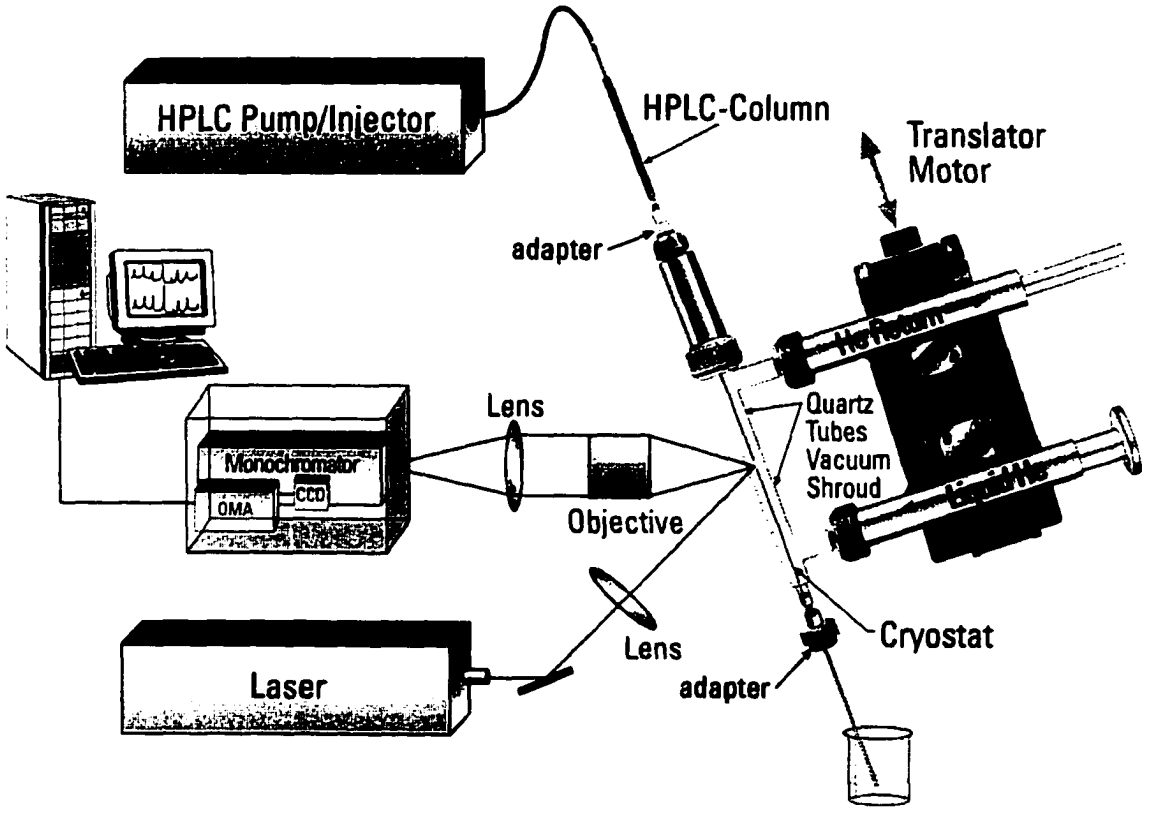

Figure 6-1. Schematic diagram of the HPLC-FLNS system. The instrumentation consists of a micro-HPLC apparatus with a quartz tube connected to the outlet of a separation column, HPLC cryostat, translation stage, and FLNS detection system. The quartz tube is positioned axially in the cryostat (see text for details).

6.5.2. Cooling efficiency

A fast cooling rate is desirable to lessen the diffusion of the separated analyte zone and to minimize analysis time. The performance of the cryostat was tested by measuring the cooling rate from 300 to 4.2 K as described in Ref. [26]. In brief, a 0.460 mm i.d. quartz detection tube was placed in the cryostat and filled with a micromolar solution of B[*a*]P. With an excitation wavelength of 395.7 nm, the room-temperature fluorescence of B[*a*]P was broad and featureless, with an origin-band width of ~ 500 cm^{-1}. However, less than 2 minutes after opening the helium inlet valve, 4.2 K was achieved as revealed by a fluorescence intensity increase of ~ 10 and vibronic band-widths of ~ 5 cm^{-1} (results not shown). Reaching 4.2 K can also be visualized by the presence of liquid helium in the cryostat observation window. However, it is worthy to note that the time needed to reach the freezing point of the mobile phase is all that is necessary to "trap" the separated components in the cryostat. By relieving the pressure on the HPLC prior to opening the liquid helium inlet valve diffusion of the analyte zone diffusion was not significant within the time needed to freeze the mobile phase. In most cases, the mobile phase was frozen in approximately 30 seconds.

6.5.3. HPLC-FLNS analysis of four closely related analytes

Four structurally similar test molecules (B[*e*]P, B[*a*]P, and two metabolite isomers of B[*a*]P, *trans*-7,8-B[*a*]P-diol and *trans*-9,10-B[*a*]P-diol) were used in this study to demonstrate the potential of on-line HPLC-FLNS. As a mixture, off-line FLNS could not be used to identify the four test components due to spectral overlap. This problem often rises when attempting to identify analytes susceptible to partial decomposition, or when attempting to identify geometric/positional isomers. Therefore, the mixture of the above

four test molecules provided a case in point of where on-line HPLC-FLNS could be used and off-line FLNS could not. The result of injecting 2 μL of a mixture of the four components (1 x 10^{-6} M each) is shown in the fluorescence HPLC chromatogram in Figure 6-2. It can be seen in the chromatogram that, under isocratic separation conditions (see Experimental Section), all four components are not resolved. Specifically, the first major peak in the chromatogram shows a fronting shoulder (marked with an arrow), suggesting coelution of two of the four components. Standard-addition experiments indicated that the shouldering peak at 11 minutes was a mixture of *trans*-7,8- and *trans*-9,10-B[*a*]P-diol and that the more clearly resolved peaks at 25 and 27 minutes were B[*e*]P and B[*a*]P, respectively. However, with the poor resolution exhibited in the 11-minute peak, absolute identification of the peak's constituents based on retention time or spiking with standards creates a degree of uncertainty. This scenario provided a good example of how on-line FLNS detection could be employed to test peak purity and selectively identify coeluting components.

On-line FLN analysis began by freezing the analyte zone corresponding to the unresolved peak at 11 minutes as it traversed into the detection window of the cryostat. The cryostat was then automatically translated to the lower portion of the observation window, which corresponded to the peak's shoulder. This process was monitored by non-selective excitation at 351.1 nm (data not shown). Selectively tuning the laser through the S_1 vibronic bands of the two suspected B[*a*]P-diol isomers was then performed to determine which isomer corresponds to the peak's shoulder. At an excitation wavelength of 394.2 nm (Figure 6-3), for example, the on-line FLN spectrum (solid line) shows characteristic peaks at 328, 342, 404, 453, 467, 492, 517, and 585 cm^{-1}

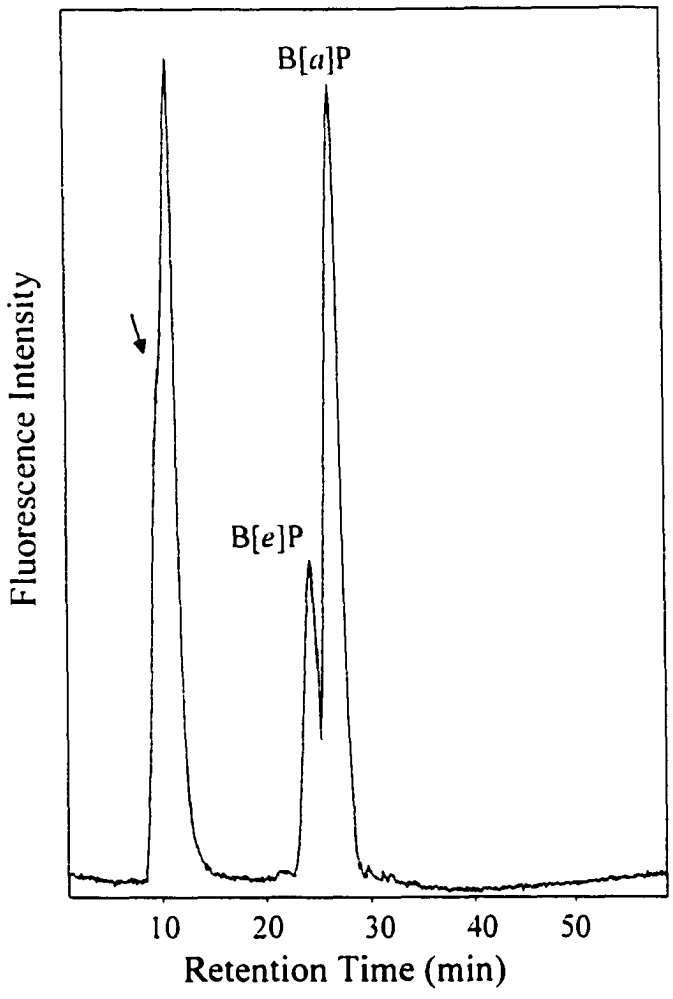

Figure 6-2. Room-temperature fluorescence chromatogram acquired during the HPLC separation of the four components in the test mixture. B[*e*]P and B[*a*]P are fairly-well resolved, while the peak at ~ 11 minutes appears to be coelution of the B[*a*]P-diols, as suggested by the shoulder on the front of the peak. Column, 1 mm X 25 cm, C18; mobile phase, EtOH/H_2O (85/15, v/v%); λ_{ex} = 351.1 nm.

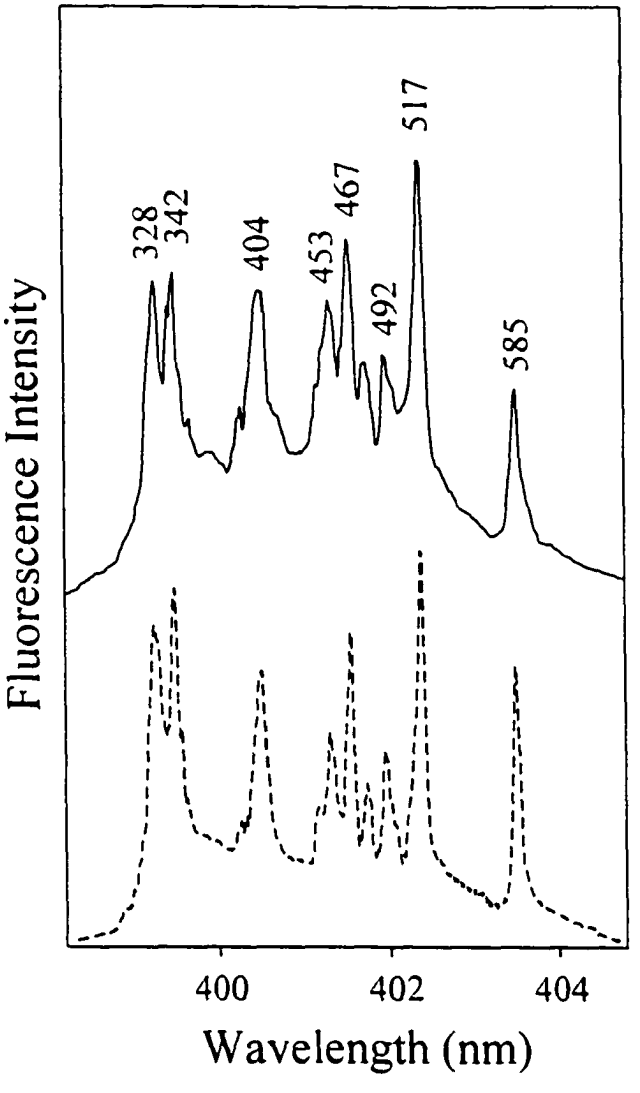

Figure 6-3. Comparison of an on-line HPLC-FLN spectrum for the front shoulder of the peak at ~ 11 minutes (solid line) in the chromatogram of Figure 6-2 with the off-line reference spectrum for the *trans*-9,10-B[*a*]P-diol standard (dashed line). Conditions: T = 4.2 K, λ_{ex} = 394.2 nm, 200 ns gate-width with a 40 ns delay. Peaks are labeled with their excited state vibrational frequencies, in cm^{-1}. Delaying the detection gate by 40 ns significantly reduced scattering incident laser light, providing a much cleaner FLN spectrum.

identical to that of the off-line reference spectrum obtained for *trans*-9,10-B[*a*]P-diol (dashed line), thus identifying the 11-min peak's shoulder in Figure 6-2.

Next, the cryostat was translated up to the portion of the observation window corresponding to the second half of the 11-minute peak for FLN analysis. Comparison of the on-line FLN spectrum to the off-line FLN reference spectrum (λ_{ex} = 381.9 nm) identified the second half of the 11-minute peak as *trans*-7,8-B[*a*]P-diol (results not shown). A second level/method of FLNS identification was accomplished by mapping out all excited-state vibrational modes of the molecule; typically, 6-8 excitation wavelengths are used in this process. For simplicity, an example of FLN spectra obtained at two different excitation wavelengths is shown in Figure 6-4. Selective excitation into the vibrational levels of S_1 produce FLN spectra where the position of the peaks reflects the analyte's excited-state vibrational frequencies, as measured relative to the laser-excitation frequency. Utilizing multiple excitation wavelengths ensures that the FLN spectra correspond to the molecule of interest and not to an impurity with similar vibrational frequencies. For example, distinctive modes at 743, 776, 794, and 832 cm^{-1} are revealed at the excitation wavelength of 381.9 nm as shown in spectrum a of Figure 6-4. In spectrum b it can be seen that at excitation wavelength of 383.1 nm, in addition to the modes observed in spectrum a (e.g., 743, 776, 794, and 832 cm^{-1}), new modes at 560 and 651 cm^{-1} are also revealed. The variations in intensity reflect the difference in selectivity for certain S_1 vibrational modes at the two excitation wavelengths. The concentration limit of detection was determined, from room-temperature HPLC-LIF experiments, to be 5×10^{-10} M with a 2 μL injection of *trans*-7,8-B[*a*]P-diol.

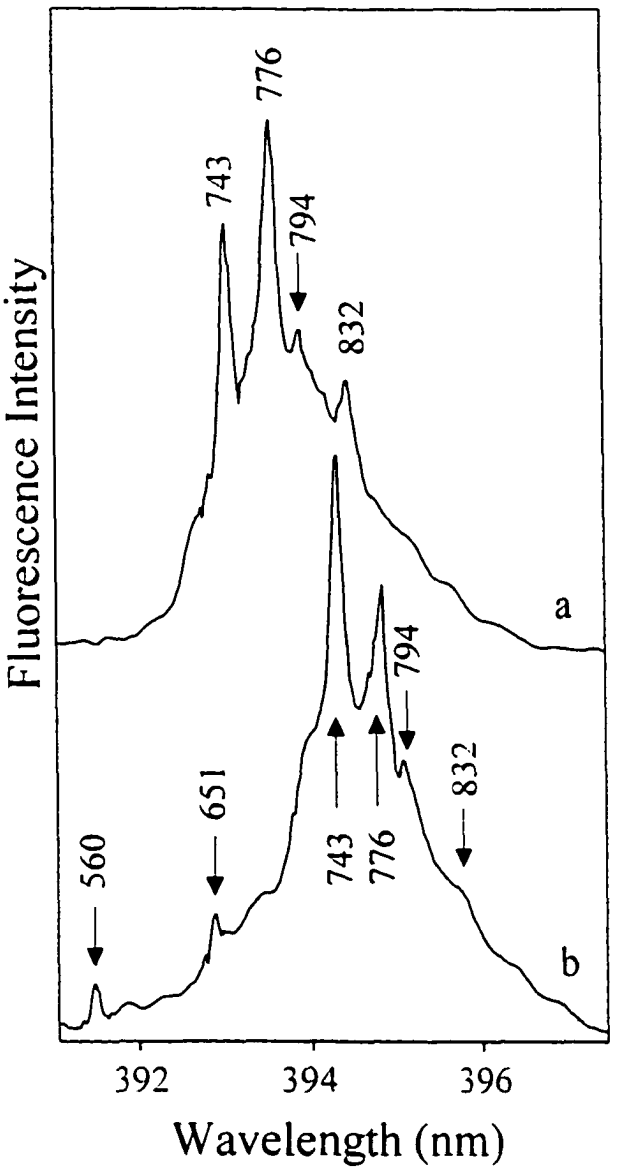

Figure 6-4. On-line FLN spectra obtained at two different excitation wavelengths for the second half of the 11-minute peak in the HPLC chromatogram of Figure 6-2. Spectra a and b were obtained with an excitation wavelength of 381.9 and 383.1 nm, respectively. Both spectra were taken with a 200 ns gate width and a 60 ns delay time. Peaks are labeled with their excited-state vibrational frequencies, in cm^{-1}.

The peak at 25 minutes in Figure 6-2 was assumed, based on retention time, to be B[*e*]P. As shown in Figure 6-5A, on-line FLNS of this analyte zone by selectively exciting 500 cm^{-1} above the origin band of B[*e*]P at 368.9 nm revealed characteristic vibronic modes of B[*e*]P at 453, 497, 534, and 563 cm^{-1}. As expected, these modes perfectly match those in the off-line reference library (data not shown for simplicity). Likewise, with an excitation wavelength of 395.7 nm, the peak at 27 minutes in the chromatogram was confirmed by FLNS to be B[*a*]P, with distinct modes at 326, 374, 450, 471, 512, and 580 cm^{-1} (see Figure 6-5B).

6.5.4. HPLC-FLNS of mouse skin treated with DB[*a,l*]P

Attempts to identify depurinating DB[*a,l*]P-derived DNA adducts in an HPLC fraction from mouse skin by off-line FLNS were impossible due to spectral interference from impurities, as shown in Figure 6-6 (solid line spectrum). Although a few partially-resolved vibronic modes (300, 352, 385, and 446 cm^{-1}) line up with those in the off-line FLNS reference standard spectrum for the expected DB[*a,l*]P-10-N3Ade adduct (dashed line), impurities in the mouse-skin fractions prevent absolute identification of the DNA adduct. Identification of DB[*a,l*]P adducts by FLNS has been previously shown for synthetic DB[*a,l*]P-type standards, but not for real-world samples [26,29]. Frame A of Figure 6-7 shows the result of a narrow-bore HPLC-LIF separation of the mouse-skin fraction. Based upon retention times established with standards (data not shown) and monitoring the position of the room-temperature fluorescence spectra, the peak at ~ 23 minutes in the chromatogram (marked with an asterisk) was tentatively assigned as the depurinating DB[*a,l*]P-10-N3Ade adduct. However, room-temperature spectral resolution was not sufficient for unambiguous identification, since many isomeric

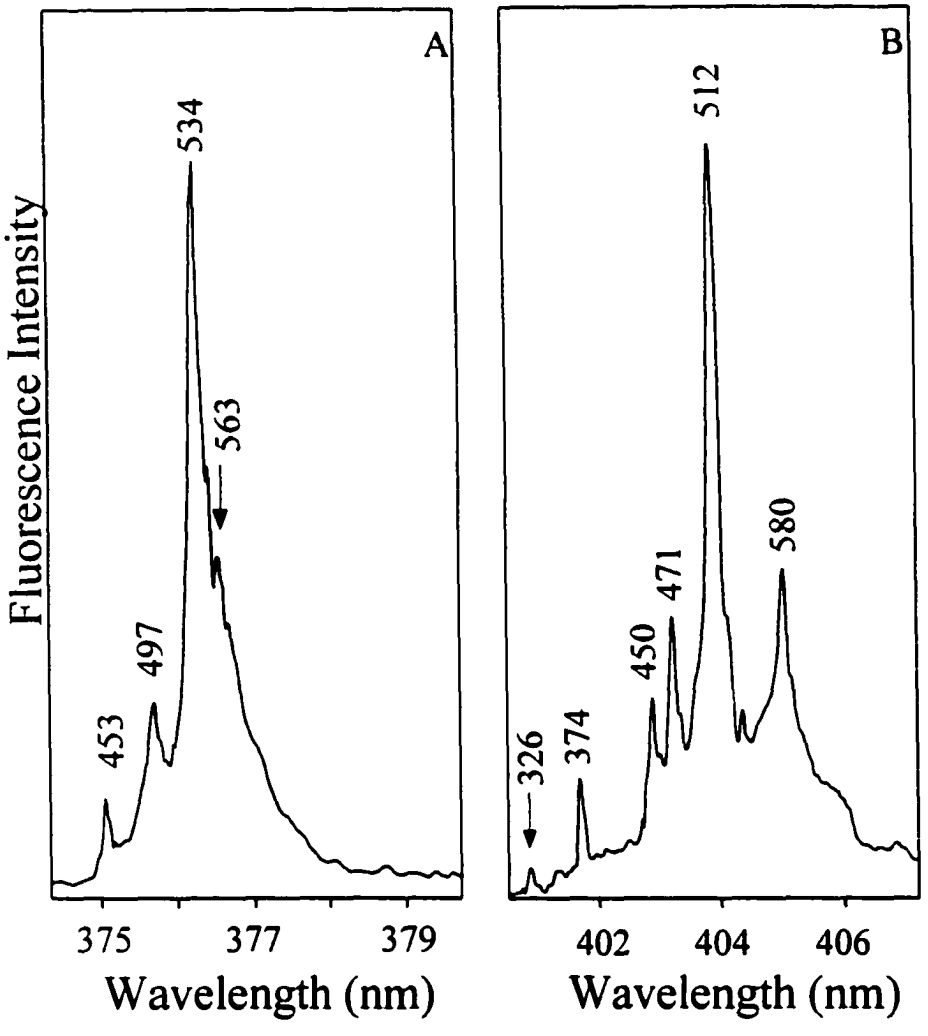

Figure 6-5. Frame A; On-line FLN spectrum of the peak at ~ 25 minutes in the chromatogram of Figure 6-2. The vibrational frequencies (λ_{ex} = 368.9 nm) identify the peak at 25 minutes as B[*e*]P. The spectrum was taken at with a gate-width of 200 ns and a 0 ns delay time. Frame B; FLN spectrum of the peak at ~ 27 minutes in the chromatogram. The vibronic modes (λ_{ex} = 395.7 nm) identify the 27-min peak as B[*a*]P; 200 ns gate-width, 20 ns delay. The vibronic modes are labeled with their excited-state frequencies, in cm^{-1}.

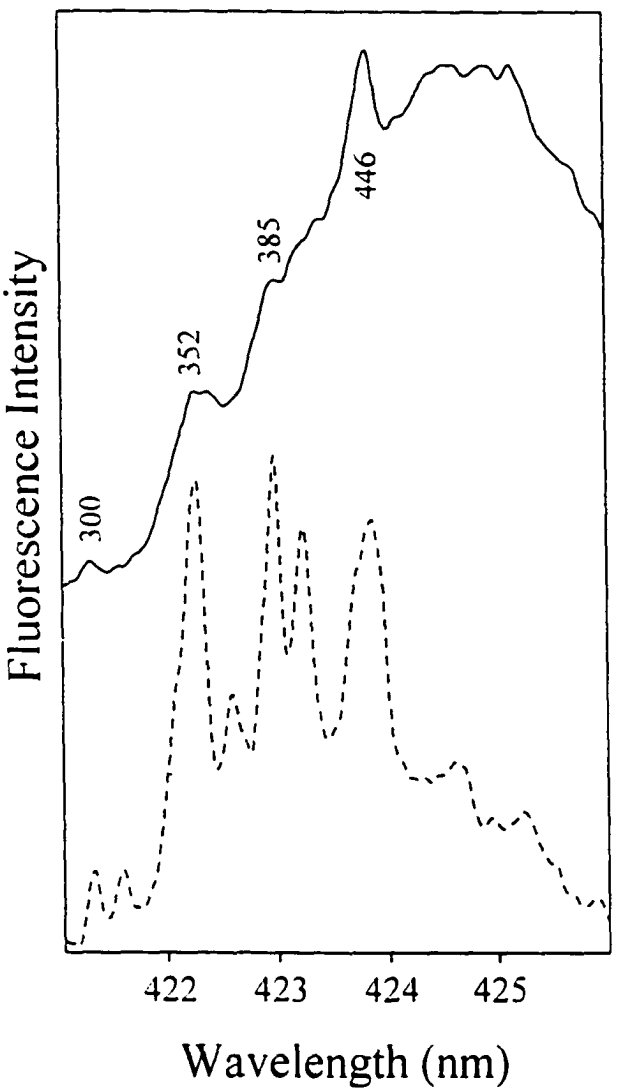

Figure 6-6. Comparison of off-line spectrum from a mouse-skin fraction (solid line) expected to contain the depurinating DB[*a,l*]P-10-N3Ade adduct, to the FLN reference spectrum of the adduct standard (dashed line). Spectral interference prevents certain identification of DB[*a,l*]P-10-N3Ade from mouse skin treated with DB[*a,l*]P. Both spectra were taken with an excitation wavelength of 416 nm, 200 ns gate width, and a 40 ns delay time. The solutes were dissolved in a 50/50 (v/v%) EtOH/H_2O mixture.

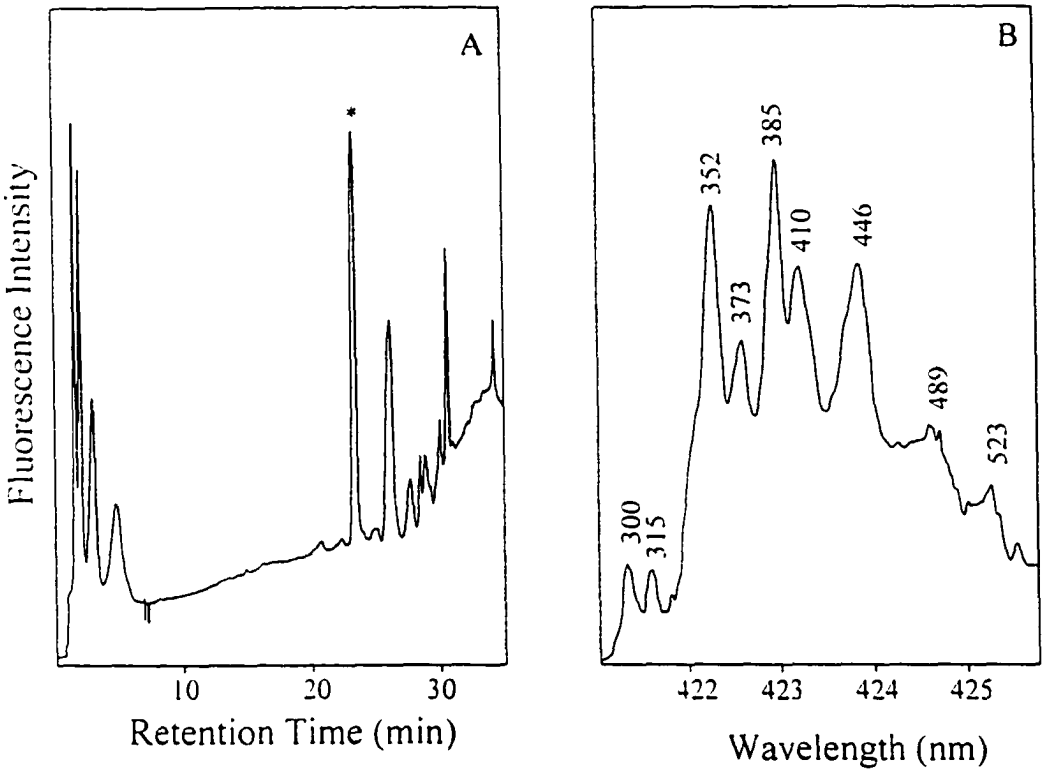

Figure 6-7. On-line identification of the depurinating DB[*a,l*]P-N3Ade adduct by HPLC-FLNS. Frame A shows the room-temperature, narrow-bore HPLC-LIF chromatogram of the mouse-skin fraction; λ_{ex} = 351.1 nm. The peak at ~ 23 minutes is suspected to correspond to the depurinated DB[*a,l*]P-10-N3Ade adduct, as established by retention time. The ~ 23-min peak of the chromatogram was trapped in the cryostat and frozen to 4.2 K for on-line FLNS. Frame B shows the result of selective excitation of the 23-min peak with 416 nm and a 200 ns gate width, 40 ns delay. The spectrum is identical to the reference spectrum of the DB[*a,l*]P-10-N3Ade adduct standard shown in Figure 6-6 (dashed line). Peaks are labeled with their excited state vibrational frequencies, in cm^{-1}.

adducts or decomposition products could show similar retention times and/or spectra. Therefore, absolute identification was accomplished by chromatographically displacing the spectrally interfering components and analyzing the 23-minute peak with on-line FLNS.

As the 23-minute peak made its way into the cryostat observation window, the analyte zone was frozen to 4.2 K. As shown in Frame B of Figure 6-7, selective laser excitation of 416 nm revealed distinct vibronic modes at 300, 315, 352, 373, 385, 410, 446, 489, and 523 cm^{-1} in the spectrum of the separated analyte. When compared to the library of reference spectra of DB[*a,l*]P-derived DNA adducts, these modes match identically to those of the off-line spectra for DB[*a,l*]P-10-N3Ade (dashed line spectrum of Figure 6-6). By identifying the above adduct in mice, these results further substantiate the formation of depurinating DNA adducts from the most potent chemical carcinogen DB[*a,l*]P via the one-electron oxidation metabolic pathway [29]. Since the adduct of interest was identified, no attempt was made to characterize the other peaks in the chromatogram. The quantity of the –N3Ade adduct was determined with room-temperature HPLC-LIF to be ~ 2 X 10^{-7} M, using DB[*a,l*]P as an external standard and 5 μL injection volumes. More detailed studies of DB[*a,l*]P-10-N3Ade and other DNA adducts possibly formed on mouse-skin treated with DB[*a,l*]P are the subject of future investigations with on-line HPLC-FLNS.

6.6. Conclusions and Future Prospects

We have demonstrated that on-line HPLC-FLNS can be used for on-line identification of closely related molecular analytes. The HPLC/CE cryostat provides a

fast cooling rate, has a longer detection window, and accommodates variable-size quartz tubes and capillaries for HPLC and CE, respectively. The separation shown in Figure 6-2 was obtained with a 1-mm i.d. column directly connected to 0.46 mm i.d. detection tubing, whereas the separation shown in Figure 6-7A utilized a new 2.1-mm i.d. column connected to 0.36 mm detection tubing. The former was available in the early stages of developing HPLC-FLNS. Although improvements were made in the latter chromatographic set-up, the separation shown in Figure 6-2 provided a demonstrative example of how HPLC-FLNS can be used to identify/resolve analytes not clearly resolved by HPLC alone, as shown with the coelution of the *trans*-7,8- and *trans*-9,10-B[*a*]P-diols (see Figures 6-2, -3, and -4).

It is anticipated that HPLC-FLNS will be a useful tool in the analysis of complex mixtures where structurally similar analytes are commonly encountered. Situations such as these often arise in analyzing biological mixtures (e.g., depurinating PAH-DNA adducts formed *in vivo*) where absolute, unambiguous identification is of vital importance, and identification based solely on retention time may not be sufficient. Moreover, with femtomole detection limits, this system should be adequate for many real-world applications.

Future plans are to utilize the HPLC-FLNS system to study estrogen quinone derived DNA adducts, urinary porphyrins, and various intact (and/or partly denatured) photosynthetic protein-antenna complexes. In each case, the availability of standards and sample stability often compromises (or negates) identification. It is also anticipated that FLNS detection can be used in combination with nano- and capillary-HPLC (research in progress), which provide high separation efficiencies and detection sensitivities.

Moreover, detection of non-line-narrowed fluorescence spectra at liquid nitrogen temperatures may be adequate in many situations [26].

6.7. Acknowledgements

Ames Laboratory is operated for the U.S. Department of Energy by Iowa State University under contract No. W-7405-Eng-82. This work was supported by the Office of Health and Environmental Research, Office of Energy Research. The authors would like to thank Peter Shields (Janis Research Co. Inc.) for his dedication and assistance in developing the cryostat and Dr. E.L. Cavalieri (Eppley Institute for Research in Cancer, University of Nebraska Medical Center, Omaha, NE) for providing the mouse skin samples.

References

1. Andrews, C. L.; Vouros, P.; Harsch, A. *J. Chromatogr. A* **1999**, *856*, 515-526.
2. Lagerwerf, F. M.; van Dongen, W. D.; Steenvoorden, R. J. J. M.; Honing, M.; Jonkman, J. H. G, *Trends in Anal. Chem.* **2000**, *19(7)*, 418-427.
3. Apruzzese, W. A.; Vouros, P. *J. Chromatogr.* A **1998**, *794*, 97-108.
4. Olson, D. L.; Lacey, M. E.; Sweedler, J. V. *Anal. Chem.* **1998**, *70*, 257A-264A.
5. Mistry, N.; Roberts, A. D.; Tranter, G. E.; Francis, P.; Barylski, I.; Ismail, I. M.; Nicholson, J. K.; Lindon, J. C. *Anal. Chem.* **1999**, *71*, 2838-2843.
6. Fujimoto, C.; Jinno, K. *Trends in Anal. Chem.* **1989**, *8*, 90-96.
7. Somsen, G. W.; Jooijschuur, E. W. J.; Gooijer, C.; Brinkman, U. A. Th.; Velthorst, N. H. *Anal. Chem.* **1996** *68*, 746-752.

8. Mulvaney, S. P.; Keating, C. D. *Anal. Chem.* **2000**, *72*, 145R-157R.

9. Cooper, S. D.; Robson, M. M.; Batchelder, D. N.; Bartle, K. D. *Chromatographia* **1997**, *44*, 257-262.

10. Kennedy, B. J.; Milofsky, R.; Carron, K. T. *Anal. Chem.* **1997**, *69*, 4708-4715.

11. Personov, R. I.; Agranovich, V. M.; Hochstrasser, R.M. (Eds.), *Spectroscopy and Excitation Dynamics of Condensed Molecular Systems*, North-Holland, Amsterdam, Vol. 4, 1983; pp. 555-619.;

12. Jankowiak, R.; Small, G. J.; *Anal. Chem.* **1989**, *61*, 1023A-1032A.;

13. Jankowiak, R.; Small, G. J. *Chem. Res. Toxicol.* **1991**, *4*, 256-269.;

14. Jankowiak, R.; *Fundamental Aspects of Fluorescence Line-narrowing in Shpol'skii Spectroscopy and Related Site Selective Methods: Applications in Environmental Analysis, Bioanalytical Chemistry, and Chemical Physics* Gooijer, C.; Ariese, F.; Hofstraat, J. W. (Eds.); John Wiley and Sons, Inc., New York, 2000; Chapter 8.

15. Jankowiak, R.; Lin, C. –H.; Zamzow, D.; Roberts, K. P.; Li, K. –M.; Small, G. J. *Chem. Res. Toxicol.* **1999**, *12*, 768-777.

16. Jankowiak, R.; Zamzow, D.; Stack, D.E.; Todorovic, R.; Cavalieri, E. L; Small, G. J. *Chem. Res. Toxicol.* **1998**, *11*, 1339-1345.

17. Hofstraat, J. W.; Jansen, H. J. M.; Hoornweg, G. Ph.; Gooijer, C.; Velthorst, N. H. *Anal. Chim. Acta* **1985**, *170*, 61-71.

18. Hofstraat, J. W.; Gooijer, C.; Velthorst, N. H. *App. Spectrosc.* **1988**, *42*, 614-619.

19. Cooper, R. S.; Jankowiak, R.; Hayes, J. M.; Lu, P.; Small, G. J. *Anal. Chem.* **1988**, *60*, 2692-2694.

20. Kok, S. J.; Posthumus, R.; Bakker, I.; Gooijer, C.; Brinikman, U. A. Th.; Velthorst, N. H. *Anal. Chim. Acta* **1995**, *303*, 3-10.

21. Kok, S. J.; Evertsen, R.; Velthorst, N. H.; Brinkman, U. A. Th.; Gooijer, C. *Anal. Chim. Acta*, **2000**, *405*, 1-7.

22. Marsch, G. A.; Jankowiak, R.; Suh, M.; Small, G. J. *Chem. Res. Toxicol.* **1994**, *7*, 98-109.

23. Marsch, G. A.; Jankowiak, R.; Farhat, J. H.; Small, G. J. *Anal. Chem.* **1992**, *64*, 3038-3044.

24. Jankowiak, R.; Roberts, K. P.; Small, G. J. *Electrophoresis* **2000**, *21*, 1251-1266.

25. Jankowiak, R.; Zamzow, D.; Ding, W.; Small, G. J. *Anal. Chem.* **1996**, *68*, 2549-2553.

26. Zamzow, D.; Lin, C.-H.; Small, G. J.; Jankowiak, R. *J. Chromatogr. A* **1997**, *781*,73-80.

27. Roberts, K. P.; Lin, C.-H.; Jankowiak, R.; Small, G.J. *J. Chromatogr. A* **1999**, *853*, 159-170.

28. Roberts, K. P.; Lin, C.-H.; Singhal, M.; Casale, G. P.; Small, G. J.; Jankowiak, R. *Electrophoresis* **2000**, *21*, 799-806.

29. Li, K. M.; Todorovic, R.; Rogan, E. G.; Cavalieri, E. L.; Ariese, F.; Suh, M.; Jankowiak, R.; Small, G. J.*Biochemistry* **1995**, *34*, 8043-8049.

CHAPTER 7. CONCLUDING REMARKS

It has been shown in this thesis that combining the highly efficient separation processes of HPLC and CE with highly selective and sensitive FLNS detection can be powerful combinations used for real-world applications. By providing a detection method that can alleviate the dependence on highly expensive (and/or difficult to attain) working standards, many more application can be envisioned. Techniques such as these are clearly in high demand, and by combining information-rich detection with new and improving separation methodologies, many advances in characterizing complex biochemical and biomedical are anticipated.

In comparison to off-line FLNS detection, operating in an on-line mode of detection is fast and reduces interferences from decomposition and losses associated with sample handling. In comparison to TLC- and PAGE-FLNS, CE- and HPLC-FLNS provided higher separation power, a reduction in background luminescence, eliminated the post-separation extraction step often needed in TLC and PAGE, and can easily accommodate the small sample volume often encountered in bioanalysis. The HPLC-/CE-FLNS systems have proven useful in the analyses of structurally similar molecules such as PAHs and PAH-DNA adducts. In particular, a highly important bioanalytical application of CE-FLNS showed, for the first time, that depurinating adducts are formed in humans, leading to further understanding of the initial events in chemical carcinogeneis. With low detection limits, the ability to utilize well-established separation protocols, and the need in modern analytical sciences for detection methods that can provide unambiguous identification, CE- and HPLC-FLNS will be valuable contributors. Further expansion of these systems to applications in photosynthetic complexes (see

Appendix C), porphyrins, and DNA adducts formed from the anti-estrogen drug, tamoxifen (see Appendix B) are underway and preliminary results are encouraging. Finally, with the growing trend in miniaturized separation techniques such as nano-, capillary-HPLC, lab-on-a-chip, etc, the highly informative and sensitive fluorescence detection method of FLNS will continue to diversify to many more bioanalytical applications.

APPENDIX A. SPECTRAL AND CONFORMATIONAL ANALYSIS OF DEOXYADENOSINE ADDUCTS DERIVED FROM *SYN-* AND *ANTI-* DIBENZO[*a,l*]PYRENE DIOLEPOXIDES: FLUORESCENCE STUDIES

A paper published in *Chemical Research and Toxicology*, 1999, *12*, 768.

R. Jankowiak, C.-H. Lin, D. Zamzow, K. P. Roberts, K.-M. Li, and G. J. Small

A.1. Abstract

Low-temperature fluorescence spectra and results of conformational studies on *trans-syn-*, *cis-syn-*, *trans-anti-*, and *cis-anti*-dibenzo[*a,l*]pyrene diol epoxide (DB[*a,l*]PDE) derived deoxyadenosine (dA) adducts are presented and compared with those previously obtained for the stereoisomeric DB[*a,l*]P-tetrols (Jankowiak et al., *Chem. Res. Toxicol.* 1997, **10**, 677-686). In contrast to DB[*a,l*]P-tetrols, for which only *trans*-isomers showed two conformers, all stereoisomeric dA adducts adopt two different conformations with either half-chair or half-boat structures for the cyclohexenyl ring, and an 'open'- or 'folded'-type configuration between dA and the DB[*a,l*]P moiety. The major conformations observed for *trans-syn-*, *cis-syn-*, and *cis-anti*-DB[*a,l*]PDE-14-N^{6}dA could be assigned based on the previous calculations for the DB[*a,l*]P-tetrols. The major conformers of the *trans-syn-* and *cis-syn*-DB[*a,l*]PDE-14-N^{6}dA adducts exist in conformations I and II, with their fluorescence origin bands at ~382 and ~389 nm, respectively. In conformation I the cyclohexenyl ring adopts a half-boat structure with dA in a pseudoaxial position (an open configuration), whereas the cyclohexenyl ring in conformation II adopts a half-chair structure with dA in pseudoequatorial position (a folded configuration). The major conformation of *cis-anti*-DB[*a,l*]PDE-14-N^{6}dA, with

its origin band at ~389 nm, was also assigned as a folded-type configuration with a half-chair structure in the cyclohexenyl ring. Molecular mechanics and dynamical simulations were performed for interpretation of the low-temperature fluorescence spectra and ^{1}H NMR coupling constants observed for the *trans-anti*-DB[*a,l*]PDE-14-N^{6}dA adduct. The major conformer of this adduct has a half-chair structure in the cyclohexenyl ring, but different deviation from planarity in the fjord-region than conformer II of *cis-anti*-DB[*a,l*]PDE-N^{6}dA. This new structure is labeled as conformer II'. Its (0,0) - fluorescence band is at 388.1 and 388.3 nm in ethanol and glycerol/water glasses, respectively, consistent with the folded-type configuration revealed by the calculations. The fluorescence line narrowed spectra reveal that the *trans-syn-*, *cis-syn-*, *trans-anti-*, and *cis-anti*-DB[*a,l*]PDE-14-N^{6}dA adducts can be distinguished. Thus, their spectra should prove useful for identification of DB[*a,l*]P-DNA adducts formed at low levels in biological samples.

A.2. Introduction

Dibenzo[*a,l*]pyrene (DB[*a,l*]P)[1] is the most potent carcinogen among the polycyclic aromatic hydrocarbons (PAHs) [1,2]. It has been found in river sediment [3]

---

[1] **Abbreviations:** CE, capillary electrophoresis; dAMP, deoxyadenosine monophosphate; DB[*a,l*]P, dibenzo[*a,l*]pyrene; DB[*a,l*]PDE, dibenzo[*a,l*]pyrene diol epoxide; DB[*a,l*]PDE-14-N^2-dG, dibenzo[*a,l*]pyrene diol epoxide-N^2-deoxyguanosine; *syn*-DB[*a,l*]PDE-14-N^{6}dA, *syn*-dibenzo[*a,l*]pyrene diol epoxide-14-N^{6}deoxyadenosine; *anti*-DB[*a,l*]PDE-N^{6}dA, *anti*-dibenzo[*a,l*]pyrene diol epoxide-14-N^{6}deoxyadenosine; DB[*a,l*]PDE-14-N7Ade, 14-(adenin-7-yl)-11,12,13-trihydroxy-11,12,13,14 tetrahydrodibenzo[*a,l*]-pyrene; DB[*a,l*]PDE-14-N7Gua, 14-(guanin-7-yl)-11,12,13-trihydroxy-11,12,13,14-tetrahydrodibenzo[*a,l*]pyrene; DB[*a,l*]P tetrol, 11,12,13,14-tetrahydroxy-11,12,13,14-tetrahydrodibenzo[*a,l*]pyrene; DE, diolepoxide; FLNS, fluorescence line-narrowing spectroscopy; g/w, glycerol/water, MD, molecular dynamics; Me_2SO, dimethyl sulfoxide; MM, molecular mechanics; PAH, polycyclic aromatic hydrocarbon; S_0 state, electronic ground state; S_1 state, lowest excited singlet state; ZPL, zero-phonon lines.

and indoor [4] and outdoor [5] samples, suggesting potential (eco)toxicological hazards. DB[*a,l*]P can be enzymatically activated by two main pathways: one-electron oxidation to yield radical cations [6-9] and monooxygenation to produce bay region diol epoxides [10-15]. Numerous DB[*a,l*]P-DNA adducts have been reported [6-16].

Low-temperature fluorescence spectroscopy has proven to be a valuable tool for DNA-adduct characterization. In particular, fluorescence line-narrowing spectroscopy (FLNS) [8,17] has been used for definitive identification [6,8-24] of adducts. Furthermore, the combination of FLNS and non-line-narrowing (NLN) fluorescence spectroscopy can provide adduct conformational information [23-25], i.e., whether the adduct is external, base-stacked, or intercalated. This methodology has recently been used to characterize DB[*a,l*]P diol epoxide (DB[*a,l*]PDE) derived DNA adducts and conformation dependent DNA repair [16]. These studies were performed using polynucleotides and calf thymus DNA reacted *in vitro* with DB[*a,l*]PDE and native DNA from mouse skin epidermis exposed to DB[*a,l*]P. It was shown that DB[*a,l*]PDE-DNA adducts possess stereochemically different structures and can adopt different conformations [16]. The results indicated a need for spectral characterization of all DB[*a,l*]PDE derived deoxyadenosine (dA) adduct standards at the nucleoside level.

Fluorescence and computational studies have shown that *trans-syn*-DB[*a,l*]P-tetrol [26] and the depurinating adduct *trans-syn*-DB[*a,l*]PDE-14-N7Ade [24] possess two distinct fluorescence (0,0)-bands having different excited-state vibrational frequencies. Molecular dynamics simulations (*in vacuo*) identified two conformers for the DB[*a,l*]P-tetrols and *trans-syn*-DB[*a,l*]PDE-14-N7Ade. The aromatic portion of DB[*a,l*]P was severely distorted, and half-chair or half-boat structures for the

cyclohexenyl ring were observed [24,26]. An example, relevant to the results of this paper, is shown in Fig. A-1. Two unique structures (conformers I and II) are shown for *trans-syn*-DB[*a,l*]PDE-14-N7Ade. In the open-type adduct structure (frame A), the cyclohexenyl ring adopts a half-boat structure where no significant interaction between the adenine (Ade) and the aromatic system is possible. In the folded-type conformation II (frame B), Ade is in a pseudoequatorial position and the cyclohexenyl ring adopts a half-chair structure. Similar conformations were observed for *trans-syn*-DB[*a,l*]P-tetrol [26]. The calculated and observed fluorescence origin bands established for various conformations of the *trans-syn-*, *cis-syn-*, *trans-anti-*, and *cis-anti*-DB[*a,l*]P-tetrols, as well as the calculated dihedral angles and the estimated ^{1}H NMR coupling constants for the proton pairs of the cyclohexenyl ring, are summarized in Table A-1. For stereoisomeric DB[*a,l*]P-tetrols, the agreement between the measured and theoretically estimated NMR coupling constants suggests that the results shown in Table 1 may be useful for interpretation of the spectroscopic data obtained for DB[*a,l*]PDE-dA adducts.

In this work, DB[*a,l*]PDE-dA adducts, for which eight stereochemical configurations are shown in Fig. A-2, were studied by low-temperature fluorescence spectroscopy and molecular modeling. The NLN and FLN spectra of *trans-anti*, *cis-anti*, *trans-cis*, and *cis-syn*- DB[*a,l*]PDE-14-N^{6}dA adducts presented below provide the necessary spectral information for investigating the nature of DB[*a,l*]PDE-DNA adducts formed at low levels in *in vitro* and *in vivo* studies. The structural characterization of these adducts by NMR, circular dichroism, and fast atom bombardment mass

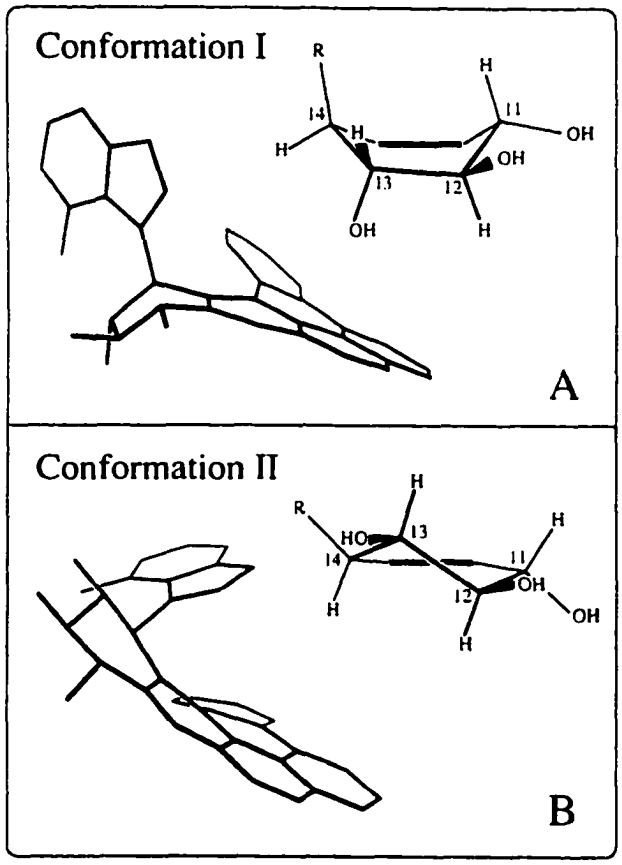

Figure A-1. Optimized 0 K ground state structures of *trans-syn*-DB[*a,l*]PDE-14-N7Ade obtained after simulated annealing. Conformers I and II are shown in frames A and B, respectively. The insets show the conformation of the cyclohexenyl ring (half-boat vs. half-chair); R = adenine. Hydrogens and double bonds are omitted for clarity. Results from Ref. 24.

Table A-1. Calculated and observed (0,0) transition energies, dihedral angles α and β with the estimated coupling constants for the (i,j) proton pairs, and structure assignment for various conformations of *syn*- and *anti*-DB[*a,l*]P-tetrols. Data from reference 26.

DB[*a,l*]P-tetrols	Conf.	λ_{calc} (0,0) (nm)	λ_{obs}[a] (0,0) (nm)	α[b] (deg)	β[b] (deg)	Structure assignment[d]	Coupling constants[e]
trans-syn-	I*	381.4	382.2 (EtOH), 382.7 (g/w)	25	8	half-boat, pseudoaxial	vL/S/S
	II	384.0	387.0 (g/w)	–26	64	half-chair, pseudoequatorial	L/vL/vL
cis-syn-	I*	382.2	--	–24	62	half-chair, pseudoaxial	L/vL/S
	II	384.5	385.2 (EtOH), 385.5 (g/w)	26	–60	half-chair, pseudoequatorial	S/S/S
trans-anti-	I*	383.2	383.6 (EtOH)	–24	60	half-chair, pseudoaxial	L/S/S
	II	384.4	385.4 (g/w)	27	–63	half-chair, pseudoequatorial	S/S/vL
cis-anti-	I	382.0	382.8[c] (EtOH), 383.2 (g/w)	24	–59	half-chair, pseudoaxial	S/S/S
	I'*	382.8	---	24	–25	flattened, pseudoaxial	M/M/S
	II	384.3	---	-24	63	half-chair, pseudoequatorial	L/S/S

---

* The conformations denoted by an asterisk were the most consistent with the room-temperature ^{1}H NMR data.

a) Spectroscopically-observed (0,0) transition energies in ethanol (EtOH) or glycerol/water (g/w) at 77 K.

b) α describes the deviation from planarity in the fjord region and β describes the conformation of the cyclohexenyl ring; see Fig. A-1.

c) The observed fluorescence (0,0)-bands may correspond to either the I or the I' conformation.

d) Conformation of the cyclohexenyl ring and orientation of the hydroxyl group at the C^{14} position.

e) Estimated coupling constants for the (11,12), (12,13) and (13,14) proton pairs; L ≡ large, vL ≡ very large, M ≡ medium, S ≡ small; for details see ref. 26.

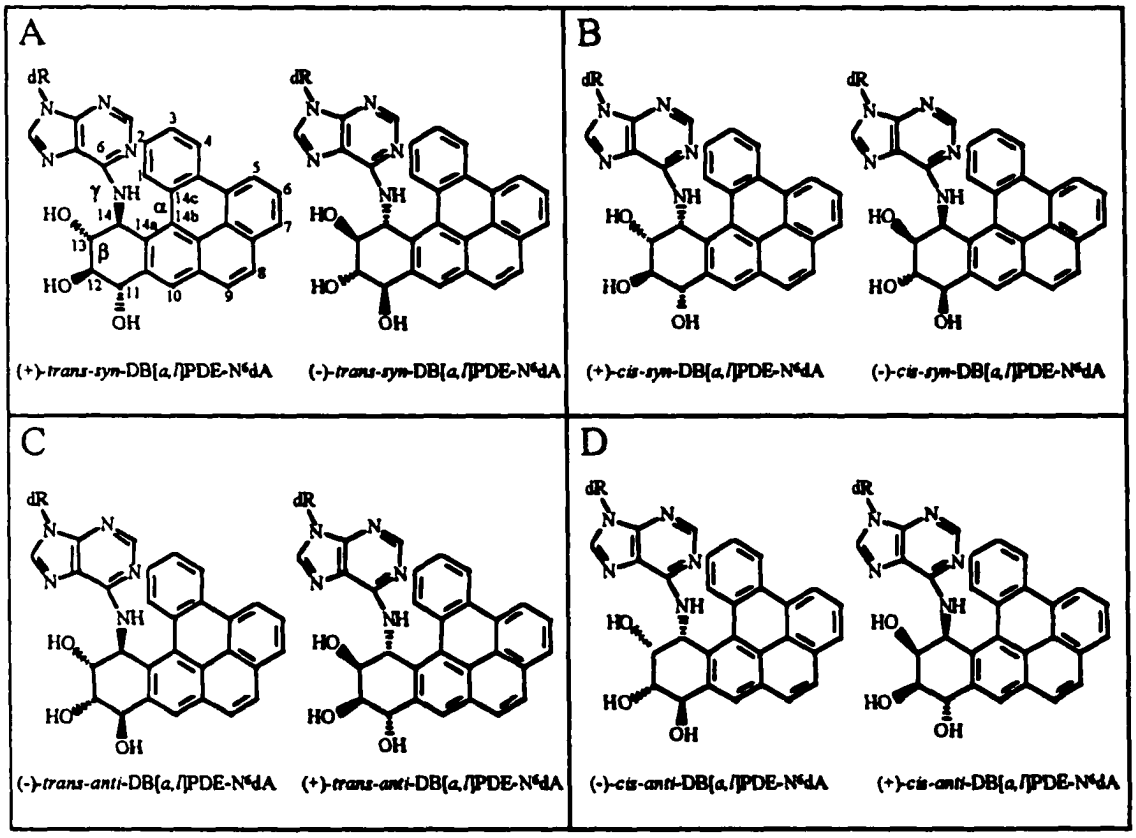

Figure A-2. Molecular structures of the eight DB[*a,l*]PDE-14-N^{6}dA adducts investigated:A) (+/–)-*trans-syn*-DB[*a,l*]PDE-14-N^{6}dA; B) (+/–)-*cis-syn*-DB[*a,l*]PDE-14-N^{6}dA; C): (+/–)-*trans*-anti-DB[*a,l*]PDE-14-N^{6}dA; and D): (+/–)-*cis*-anti-DB[*a,l*] PDE-14-N^{6}dA. The dihedral angles α, β, and γ will be used to describe the deviation from planarity in the fjord region, the conformation of the cyclohexenyl ring, and the orientation of the dA moiety, respectively. dR corresponds to deoxyribose.

spectrometry is presented elsewhere.[2]

A.3. Materials and Methods

A.3.1. Caution: *Anti- and syn-DB[a,l]P diolepoxides are extremely hazardous chemicals and should be handled carefully in accordance with NIH guidelines.*

A.3.2. Sample Preparation

The DB[*a,l*]PDE derived adducts *trans-anti-*, *cis-anti-*, *trans-syn-*, and *cis-syn-*DB[*a,l*]PDE-14-N^{6}dA were synthesized by the reaction of *anti-* and *syn-*DB[*a,l*]PDE with dA. The (+/–)-*anti-*DB[*a,l*]PDE was reacted with dA in dimethylformamide at 100°C for 30 minutes to give four *anti-*DB[*a,l*]PDE-14-N^{6}dA adducts. The (+/–)-*syn-*DB[*a,l*]PDE was reacted with dA under the same conditions, to yield the four *syn-*DB[*a,l*]PDE-14-N^{6}dA adducts. For details on the synthesis and structural characterization, see the paper by K.-M. Li et al.[2]

A.3.3. Adduct Purity.

The purity of -dA standards separated by HPLC was checked by capillary electrophoresis (CE), which possesses higher separation power (i.e. higher efficiency) than HPLC. A mixture of 85% of A (40 mM dioctylsulfosuccinate and 8 mM sodium borate in 30% (by volume) acetonitrile – 70% water; pH= 9) and 15% of B (50mM Brij S)) was used as the CE buffer. These conditions allowed for separation of all eight

[2] K.-M. Li, E.L.Cavalieri, E.G. Rogan, M. George, M.L. Gross, and A. Seidel, Structure elucidation of the adducts formed by dibenzo[a,l]pyrene diol epoxides with deoxyadenosine. *Chem. Res.Toxicol.*, accompanying paper.

diastereomers.[3] Figure A-3 shows room-temperature absorbance electropherograms of the HPLC separated (–)-*trans-anti-* (a), (–)-*cis-anti-* (b), (+)-*trans-syn-* (c), and (+)-*cis-syn*-DB[*a,l*]PDE-14-N^6dA (d). The results establish that the purity levels are very high and, thus, one can be confident that the library of NLN and FLN spectra obtained is reliable.

A.3.4. Low-Temperature Fluorescence Spectroscopy

NLN fluorescence spectra at T = 77 K and FLN spectra ($S_1 \leftarrow S_0$ excitation) at T = 4.2 K were obtained using a Lambda Physik FL-2002 dye laser pumped by a Lambda Physik Lextra 100 XeCl excimer laser as the excitation source. For FLN spectroscopy several excitation wavelengths were used, each of which reveals a portion of the S_1 excited-state vibrational frequencies of the analyte (only selected spectra are presented). NLN spectra were obtained using non-selective excitation at 308 nm from the excimer laser. Samples were cooled in a glass cryostat with quartz optical windows. Fluorescence was dispersed by a McPherson 2061 1-m focal-length monochromator and detected by a Princeton Instruments IRY 1024/G/B intensified photodiode array. For time-resolved spectroscopy, a Princeton Instruments FG-100 pulse generator was employed; different detector delay times (0-60 ns) with a gate width of 200 ns were used. Resolution for FLN and NLN spectra was 0.03 nm and 0.8-nm, respectively. Two solvent matrices of different polarity were used: ethanol and a mixture of glycerol/water (50/50 v/v). Ethanol was spectrophotometric grade from Aldrich. Ultra pure grade glycerol was purchased from Spectrum Chemical (Gardena, CA). Samples (ca. 20 μL)

---

[3] K. P. Roberts, C-H. Lin, R. Jankowiak, and G. J. Small "On-line Identification of Diastereomeric Dibenzo[*a,l*]pyrene Diolepoxide-Derived Deoxyadenosine Adducts by Capillary Electrophoresis – Fluorescence Line-Narrowing and Non-Line Narrowing Spectroscopy". *J. Chrom. A*, (in press).

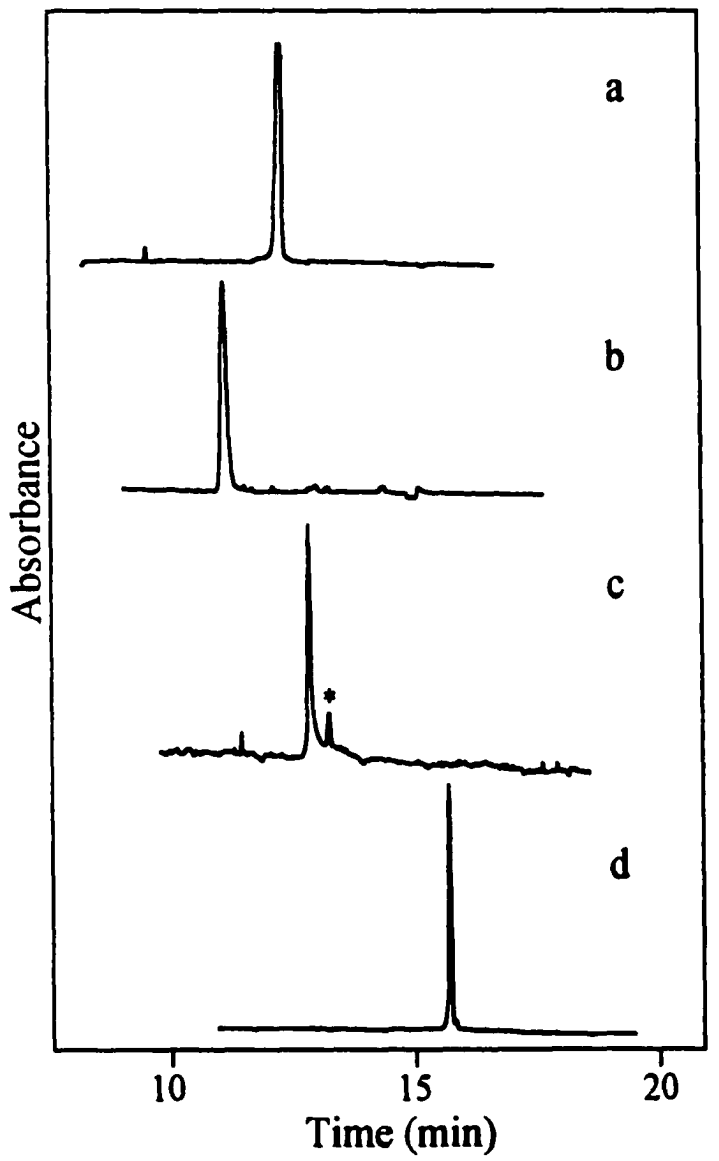

Figure A-3. Room-temperature absorbance electropherograms acquired during CE-separation of the HPLC preseparated DB[*a,l*]PDE-derived adduct standards: a) (+)-*trans-syn*-DB[*a,l*]PDE-N^6dA; b) (+)-*cis-syn*-DB[*a,l*]PDE-N^6dA; c) (−)-*trans-anti*-DB[*a,l*]PDE-N^6dA; and d) (−)-*cis-anti*-DB[*a,l*]PDE-N^6dA. The asterisk marks an impurity in the *trans-anti*-dA adduct.

were transferred to quartz tubes (2-mm i.d.) and sealed with a rubber septum. Adduct concentrations were in the ~10^{-6} M range.

A.3.5. Molecular Mechanics

Conformational analyses were carried out utilizing methods of molecular mechanics (MM), wherein energy calculations were performed with HyperChem's molecular modeling program (Release 5.1 for Windows™ Hypercube Inc.). HyperChem's force field (MM+) developed for organic molecules [27,28] was employed utilizing default parameters. As starting structures for the *trans-anti*-DB[*a,l*]PDE-14-N^6dA adduct, different model-built configurations in which the saturated ring was either in a half-chair or half-boat conformation were used. The Polak-Ribiere algorithm (*in vacuo*) was used for molecular mechanics optimization; the structures were refined until the r.m.s. gradient was less than 0.001 kcal/mol. Electrostatic contributions were evaluated by defining a set of bond dipole moments for polar bonds.

A.3.6. Molecular Dynamics (MD)

To calculate thermodynamically favored conformations of the *trans-anti*-DB[*a,l*]PDE-14-N^6dA adduct, separated from MM structures by energy barriers, quenched dynamics (simulated annealing) was used to explore the conformational space. No constraints were used during high-temperature searches of the conformational space. The starting half-chair and half-boat structures were minimized and then subjected to 50 ps of molecular dynamics at various temperatures between 300 and 400 K. Starting and final temperatures in a dynamic run were set to 0 K, and the heating and cooling times were set to 5 ps; the step size was 0.0005 ps. At various time points during the simulation approximately 30 randomly selected structures were also annealed to 0 K and

optimized. These optimized structures were subsequently used as starting points for further calculations. The two dihedral angles α and β, which define the distortion in the fjord region and the conformation of the cyclohexenyl ring, Figure A-2, were used as variables during exploration of the conformational space. All simulations were performed *in vacuo*.

A.4. Results and Discussion

DB[*a,l*]PDE derived -dA adducts, which were isolated from reaction mixtures in which both the racemic mixture and the optically pure *syn*- and *anti*-DB[*a,l*]PDE were reacted with Ade, were studied. The NLN and FLN spectra obtained for adducts formed with the racemic mixtures of the respective diol epoxides gave four pairs of identical spectra (not shown) with the pairs corresponding to (+)- and (–)- enantiomers of *trans-syn*-, *cis-syn*-, *trans-anti*-, and *cis-anti*-DB[*a,l*]PDE-14-N^6dA adducts. These identical fluorescence spectra for (+)- and (–)- enantiomers, for a given adduct, was expected since we have previously reported for benzo[*a*]pyrene diol epoxide derived adducts that the (+)- and (–)-*trans* or (+)- and (–)-*cis* nucleoside enantiomers cannot be distinguished from one another by fluorescence methods [23]. True (+)- and (–)-enatiomers can not be distinguished since they are related by reflection (mirror) symmetry. Apparently, in the case of these DB[*a,l*]PDE-dA nucleotide adducts, the influence of the sugar moiety on the fluorescence characteristics is negligible. It is worthy to note that, due to the deoxyribose ring, these (+)- and (–)-dA adducts are not true enantiomers, but rather diastereomers.[2] In what follows, detailed characterization of -dA adducts obtained with

the optically pure (–)-*anti*-DB[*a,l*]PDE and (+)-*syn*-DB[*a,l*]PDE enantiomers will be discussed for both *trans*- and *cis*- opening dA adducts. Identical data for (+)-*anti*-DB[*a,l*]PDE and (–)-*syn*-DB[*a,l*]PDE enantiomers were also obtained (not shown).

NLN spectra of *trans-syn*-, *cis-syn*-, *trans-anti*-, and *cis-anti*-DB[*a,l*]PDE-14-N^6dA adducts are shown in frames A-D of Fig. A-4, respectively. The major differences between the spectra in Fig. A-4 are revealed by the spectral position of the (0,0)-bands, the intensity distribution of the vibronic bands, and the relative distribution of adduct conformations. The origin bands labeled as $(0,0)_I$ or $(0,0)_{II}$ indicate that they belong to different molecular conformations, *vide infra*. As was the case for *trans-anti*- and *trans-syn*-DB[*a,l*]P-tetrol isomers (see Table A-1), the NLN spectra of the -dA adducts are also solvent dependent. As a result, each of these adducts may exist in a conformation having its origin band at 382-385 nm (labeled as conformation I) and/or in a conformation having its origin band at ~388-390 nm (denoted as conformation II) with the ratio of I/II being solvent dependent. Additionally, variations in the vibronic intensity distribution and the S_0 vibrational frequencies (Fig. A-4) are not surprising given that the parent fluorophore B[*e*]P has C_{2v} symmetry, and the out-of-plane deformation, as well as conformation of the cyclohexenyl ring should depend on adduct stereochemistry as observed in the case of the stereoisomeric DB[*a,l*]P-tetrols [26].

A.4.1. *syn*-DB[*a,l*]PDE–dA Adducts.

The NLN spectra of the (+)-*trans-syn*-DB[*a,l*]PDE-dA adduct, in ethanol (a) and glycerol/water (b) glass, are shown in Fig. A-4A. The spectra brought to light two fluorescence (0,0)-bands at 382.0 nm and 389.0 nm with relative intensity distributions dependent on the solvent (see Table A-2). Comparison with results obtained for the

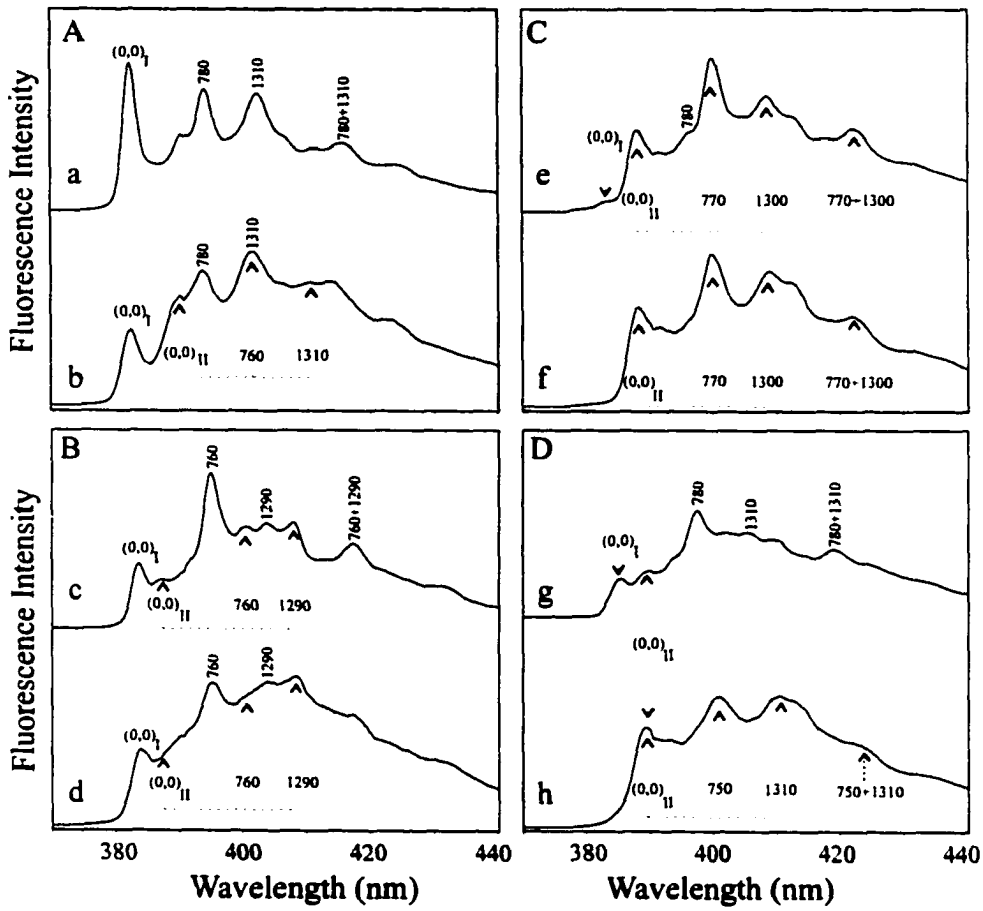

Figure A-4. NLN fluorescence spectra obtained for (+)-*trans-syn*-DB[*a,l*]PDE-N^{6}dA (Frame A), (+)-*cis-syn*- DB[*a,l*]PDE-N^{6}dA (Frame B), (–)-*trans-anti*-DB[*a,l*]PDE-N^{6}dA (Frame C), and (–)-*cis-anti*- DB[*a,l*]PDE-N^{6}dA (Frame D) adducts in ethanol (spectra a, c,e and g) and glycerol/water (spectra b,d,f and h). T = 77 K, λ_{ex} = 308 nm, delay time = 20 ns, and gate width = 200 ns. The numbers correspond to the ground-state (S_0) vibrational frequencies.

Table A-2. Fluorescence characterization and conformational analysis of *syn-* and *anti*-DB[*a,l*]PDE-14-N^{6}dA adducts.

Stereoisomeric -dA Adducts	**Matrix**				**Assignment**			
	Ethanol		**Glycerol/Water**					
	(0,0) nm	**Conf.**	**(0,0) nm**	**Conf.**	**α deg.**	**β deg.**	**Conf. Observed by ^{1}H NMR**	**Cyclohexenyl ring, -dA moiety[b]**
(+)-*trans-syn-*	382.0	**I**[a]	382.0	**I**	Pos.[c]	~0		Half-boat, pseudoaxial
	389.0	**II**	389.0	**II**	Neg.	Pos.	**II**	Half-chair, pseudoequatorial
(+)-*cis-syn-*	383.6	**I**	384.0	**I**	Neg.	Pos.	**I**	Half-chair, pseudoaxial
	388.0	**II**	388.0	**II**	Pos.	Neg.		Half-chair, pseudoequatorial
(−)-*trans-anti-*	383.0[d]	**I′**	------	**I′**	28.5	−63.8		Half-chair, pseudoaxial ($\gamma = -158.4°$)
	388.1	**II′**	388.3	**II′**	30.9	59.0	**II′**	Half-chair, pseudoequatorial ($\gamma = -61.0°$)
(−)-*cis-anti-*	385.0	**I**	385.0[e]	**I**	Pos.	Neg.		Half-chair, pseudoaxial
	389.0	**II**	389.0	**II**	Neg.	Pos.	**II**	Half-chair, pseudoequatorial

a) The bold Roman numerals indicate the major conformations observed by low-temperature fluorescence.
b) Conformation of the cyclohexenyl (non-aromatic benzylic) ring and the orientation for the dA moiety; α, β, and γ are defined in Fig A-1.
c) Pos., neg. = positive, negative.
d) Minor conformation at the nucleoside level, but major conformation in single-stranded DNA [16] and in CE buffer solution.[3] In double stranded DNA this adduct adopts an intercalated Conf. II [16] (see text for details)
e) Very weak, so *cis-anti-* DB[*a,l*]PDE-14-N^{6}dA in glycerol/water glass exists mostly in conformer II (see Figs. A-4D and A-10).

DB[*a,l*]P-tetrols (see Table A-1) and *trans-syn*-DB[*a,l*]PDE-14-N7Ade adducts [24] suggests that the main conformation of this adduct, with a characteristic origin band at 382.0 nm, has an open-like structure (conformer I) with the cyclohexenyl ring in a half-boat conformation. In the open-type structure, no strong interaction between dA and the aromatic system is possible. This is the dominant conformation observed in the ethanol matrix. In contrast, two distinct origin bands are observed in the glycerol/water matrix, which are assigned to conformer I ((0,0)-band at 382.0 nm) and conformer II, respectively. The latter conformer has its origin band at 389.0 nm and an intense Herzberg-Teller origin band [29-31] at ~760 cm^{-1}. Based on the results for the DB[*a,l*]P-tetrols (see Table A-1) and conformer II of *trans-syn*-DB[*a,l*]PDE-14-N7Ade [24], conformation II of *trans-syn*-DB[*a,l*]PDE-N^6dA can be assigned as a half-chair with dA partially stacked over the distal ring in a folded-type configuration. This conformation is characterized by significant π-π interaction between dA and the DB[*a,l*]P moiety, resulting in the red-shifted origin band. The NMR coupling constants obtained for the *trans-syn*-DB[*a,l*]PDE-dA adduct ($J_{11,12}$ = ~7 Hz, $J_{12,13}$ = 9.0 Hz, $J_{13,14}$ = 8.0 Hz)[2] are consistent with the above half-chair assignment predicted by dynamical simulation for *trans-syn*-DB[*a,l*]P-tetrol, for which the estimated coupling constants of the (11,12), (12,13) and (13,14) proton pairs were large, very large and very large, respectively. We conclude therefore, that *trans-syn*-DB[*a,l*]PDE-N^6dA, as observed in room-temperature NMR spectra (in Me_2SO solvent)[2] exists in the folded-type conformation II.

The existence of the above-discussed conformers is confirmed by FLN spectra. Multiplet origin structures for the *trans-syn*-DB[*a,l*]PDE-14-N^6dA adduct in ethanol (spectra a and c) and in glycerol/water glass (spectra b and d) are shown in Fig. A-5.

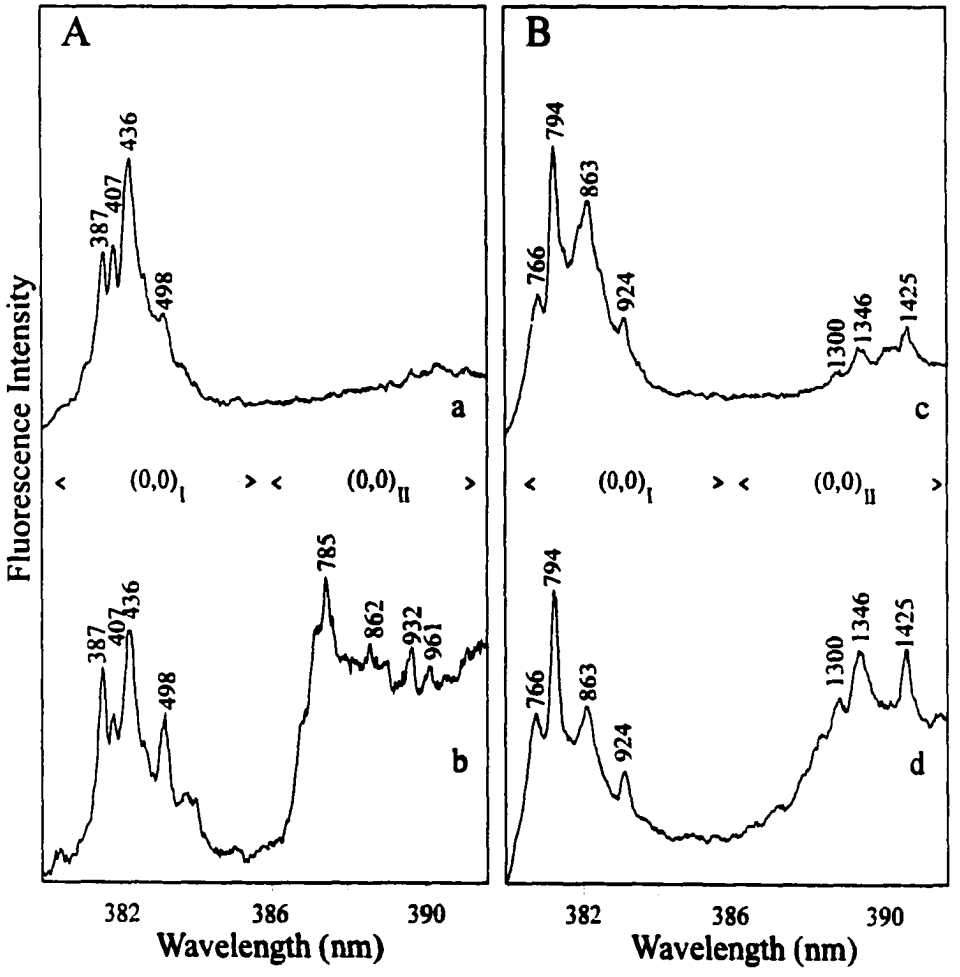

Figure A-5. FLN spectra for (+)-*trans-syn*-DB[*a,l*]PDE-N^6dA adducts in ethanol (spectra a and c) and 50/50 glycerol/water glass (spectra b and d) obtained for excitation wavelengths of 376.0 nm (Frame A) and 370.0 nm (Frame B), respectively. T = 4.2 K. The FLN peaks are labeled with their excited-state vibrational frequencies, in cm^{-1}. The spectral range shown covers the fluorescence origin bands of conformations I and II (see text).

Frames A and B, which reveal different regions of the vibronic spectrum, show FLN spectra obtained for two different excitation wavelengths, 376.0 nm and 370.0 nm, respectively. The FLN bands (zero-phonon lines (ZPL)) are labeled with their S_1 vibrational frequencies in cm^{-1}. The vibrational frequencies of conformer I ($(0,0)_I \sim 382$ nm) are the same in both glasses, with minor differences in the intensity distribution due to larger inhomogeneous broadening commonly observed in a glycerol/water glass [24,26]. However, comparison of the ZPL in spectra c and b of Fig. A-5 reveals significant differences in the vibrational frequencies between conformer I and II. For example, the excited state mode frequencies at 766, 794, 863 and 924 cm^{-1} are typical for conformer I, while modes at 785, 862, 932, and 961 cm^{-1} are observed for conformer II. These results suggest that the molecular conformations of conformer I and II are different. The same conclusion was reached based on results presented in Fig. A-4A and calculations performed for *trans-syn*-DB[*a,l*]P-tetrol [26], which indicate that the major conformation (conformer I) of the *trans-syn*-dA adduct has the cyclohexenyl ring in a half-boat structure. However, at room temperature the major conformation observed, as shown by ^1H NMR spectroscopy,[2] is conformation II with a half-chair structure for the cyclohexenyl ring, and a folded-type structure with dA in a pseudoequatorial position. The latter is consistent with the large experimentally observed red-shift (~ 470 cm^{-1}) of the $(0,0)_{II}$ band.

Frame B of Fig. A-4 shows NLN spectra of the (+)-*cis-syn*-DB[*a,l*]PDE-dA adduct in ethanol (curve c) and glycerol/water (curve d), respectively. In ethanol the (0,0) band is located at 383.6 nm, while in glycerol/water it is at 384 nm. The small spectral shift of 0.4 nm is due to the solvent effect. However, a small contribution from

the red-shifted conformer II, with its origin band at ~388 nm, is also revealed in both solvents. Unlike conformer I of *trans-syn*-DB[*a,l*]PDE-dA in ethanol, both conformations of the *cis*-isomer have a weak (0,0) band and very intense Herzberg-Teller origin band at ~760 cm^{-1}. The significant intensity of this band is owing to electronic vibrational coupling between the S_1 and higher energy dipole-allowed states, and is a consequence of the $S_1 \leftarrow S_0$ absorption transition being only weakly allowed [31].

For *cis-syn*-DB[*a,l*]P-tetrol, only conformer I [26] was observed experimentally. However, modeling studies suggested that *in vacuo cis-syn*-DB[*a,l*]P-tetrol may exist in two different half-chair conformations [26]. Thus, based on Ref [26] and Table A-1, the minor conformation of *cis-syn*-dA (conformer II having its (0,0)-band at 388 nm) is tentatively assigned as a half-chair structure for the cyclohexenyl ring (negative β value) with dA in a folded-type geometry. The main conformation (conformer I with its (0,0)-band at 384 nm) is assigned as a different half-chair (with a positive β value) and dA in an open-type configuration. The latter assignment is in good agreement with the ^1H NMR coupling constants for the proton pairs of the cyclohexenyl ring with $J_{11,12}$, $J_{12,13}$, $J_{13,14}$ being ~7 Hz (large), 7.5 Hz (large), and ~3 Hz (small), respectively.[2]

In Fig. A-6, FLN spectra for the *cis-syn*-dA adduct, obtained for 378.0 nm excitation, are presented. Spectra a and b were obtained in ethanol and glycerol/water glasses, respectively. Again, comparison of these spectra shows no differences in vibrational frequencies for conformer I (within the $(0,0)_I$ spectral range), proving that this conformation is the same in both glasses. The higher relative intensities of the 270 and 428 cm^{-1} modes in glycerol/water glass are, as in the case of the *trans-syn*-isomer, due to larger inhomogeneous broadening observed in glycerol/water glass. However, in

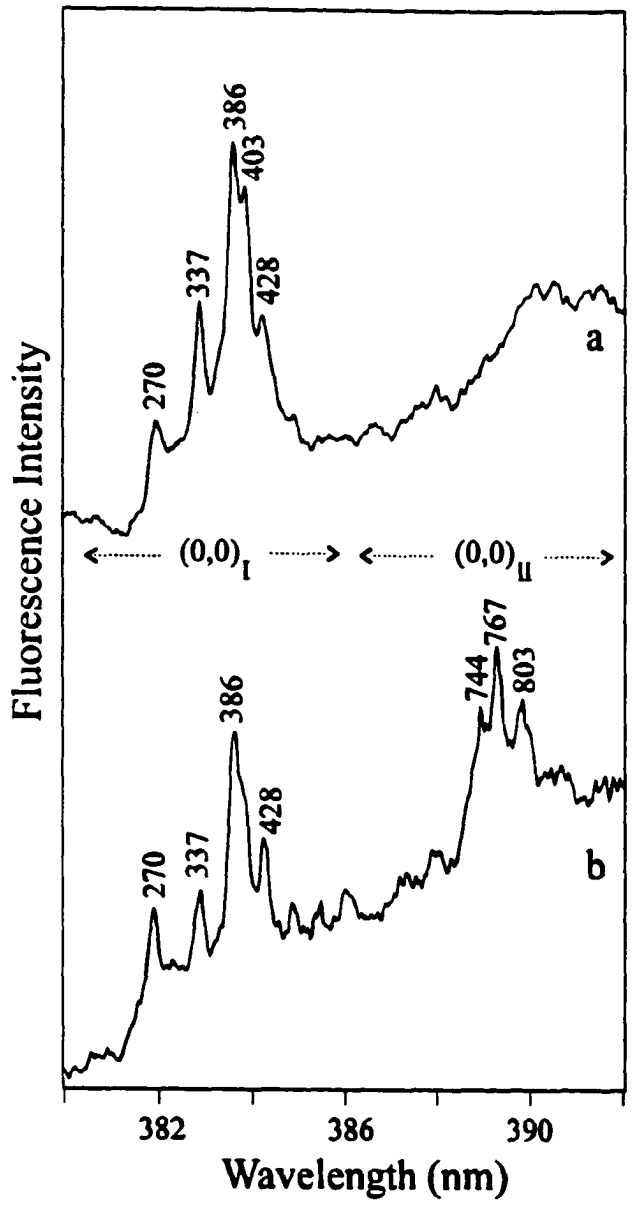

Figure A-6. FLN spectra for (+)-*cis-syn*-DB[*a,l*]PDE-N^{6}dA adducts in ethanol (spectrum a) and 50/50 glycerol/water glass (spectrum b) obtained for an excitation wavelength of 378.0 nm. Delay time 40 ns, T = 4.2 K. The $(0,0)_I$ and $(0,0)_{II}$ indicate the origin bands of conformation I and II, respectively. The FLN peaks are labeled with their excited-state vibrational frequencies, in cm^{-1}.

glycerol/water, a relatively large contribution from adduct conformation II, having its origin band red-shifted to ~ 389 nm, is also observed. This is in agreement with data presented in Fig. A-4B (spectrum d).

A.4.2. *anti*-DB[a,l]PDE–dA Adducts.

Frames C and D of Fig. A-4 show NLN fluorescence spectra for *trans-anti-* and *cis-anti*-DB[*a,l*]PDE-dA adducts. Spectra e,g and f,h were obtained in ethanol and glycerol/water glasses, respectively. In contrast to the *syn*-DB[*a,l*]PDE derived adducts, the red-shifted conformation is clearly observed for both *trans-anti-* and *cis-anti*-dA adducts. Fig. A-4C shows that the major conformer for *trans-anti*-DB[*a,l*]PDE-dA, in both solvents, has its origin band at ~ 389 nm. Also, in this case, the Herzberg-Teller origin band at ~770 cm^{-1} is the most intense. The coupling constants previously calculated for conformer I (with $J_{11,12}$ = large, $J_{12,13}$ = small, and $J_{13,14}$ = small) and conformer II (with $J_{11,12}$ = small, $J_{12,13}$ = small, and $J_{13,14}$ = large) of *trans-anti*-DB[*a,l*]P-tetrol [26] cannot explain the proton NMR coupling constants measured for the (+)-*trans-anti*-dA adduct, which are $J_{11,12}$ = 8.0 Hz (large), $J_{12,13}$ = 6.0 Hz (medium), and $J_{13,14}$ = 5.0 Hz (medium).[2] The $J_{12,13}$ and $J_{13,14}$ coupling constants for the (–)-*trans-anti*-dA adduct were not well resolved in Me_2SO, and thus can not be directly compared with those of (+)-*trans-anti*-dA. Nonetheless, we emphasize that circular dichroism, NLN, and FLN spectra for (+)- and (–)- diastereomers were identical (data not shown), proving that the (+)- and (–)-*trans-anti*-DB[*a,l*]PDE-14-N7Ade adducts do exist in the same conformation.

To interpret the above data on *trans-anti*-DB[*a,l*]PDE-14-N7Ade adducts, a theoretical investigation was initiated using MM and MD simulations. The minimum

energy of the major conformation observed in MD simulations was 33.4 kcal/mol. Its structure is shown in Fig. A-7, which indicates that this adduct exists in a folded-type conformation. The dihedral angles α and β are both positive, with values of 30.9° and 59 °, respectively. Angle α, defined as (C^{14a}-C^{14b}-C^{14c}-C^{l}), describes a propeller-like distortion of the DB[*a,l*]P moiety that relieves the strain of the sterically hindered fjord region of the DB[*a,l*]P residue by minimizing the steric repulsion between the H1 and H14 protons. Similar values of α were observed for *trans-syn*-DB[*a,l*]PDE-14-N7Ade [24] and benzo[*c*]phenanthrene diol epoxide adducts [32]. On the other hand, the α and β values for *trans-anti*-DB[*a,l*]P-tetrol, as shown in Table A-1, are (–24°, 60°) and (27°, –63°) for conformers I and II, respectively [26]. The torsion angle γ (C^{6}-N-C^{14}-C^{14a}), which defines the relative orientation of the dA moiety, is equal to –61°. The half-chair structure of the cyclohexenyl ring, with dA at C14 in a semiaxial position, allows formation of a folded-type configuration with strong π-π interaction between dA and the distal ring of DB[*a,l*]P (in the fjord region). This interaction is responsible for the spectroscopically observed red-shift of the (0,0) band to ~389 nm. The calculated coupling constants for the proton pairs $J_{11,12}$, $J_{12,13}$, and $J_{13,14}$ are large, medium, and medium, consistent with the ^{1}H NMR data.[2] Thus the major conformation of the *trans-anti*-DB[*a,l*]PDE-dA adduct, due to specific steric hindrance created by the fjord region of DB[*a,l*]P, exists in a conformation with positive α and β values, and is referred to as conformer II′ (Table A-2).

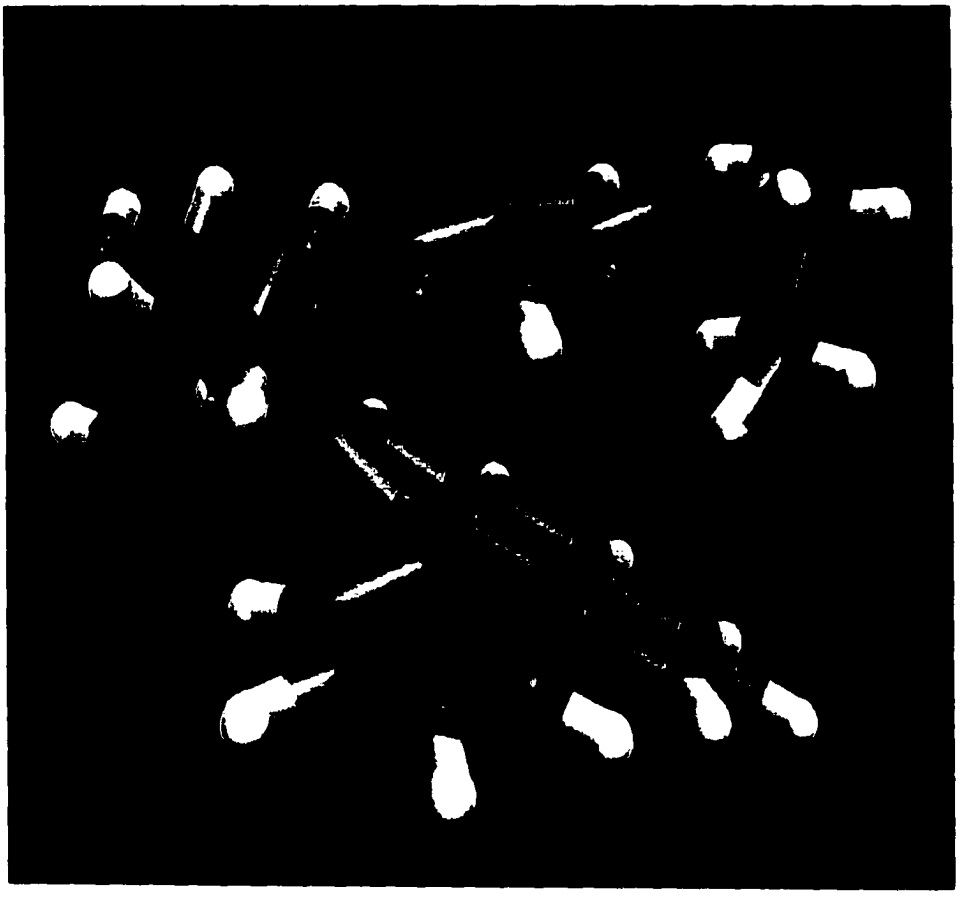

Figure A-7. Optimized 0 K ground-state structure of the *trans-anti*-DB[*a,l*]PDE-N^6dA adduct (conformation II') obtained after simulated annealing and subsequent geometry optimization.

Another unique conformation of *trans-anti*-dA (with similar local energy minimum of ~34 kcal/mol) was also observed in the simulations. In this conformation, the (α, β) values are (28°, –63.7°) with the dA moiety in a pseudoaxial position, thus leading to the open-type structure with a large γ value of 158.4°. Consequently, no significant interaction between dA and the aromatic system is possible. We associate this structure with the experimentally observed minor conformer (I′) having its origin band at 383.0 nm. Although this conformer is hardly observed in ethanol (see Fig. A-4C), it is preferentially formed in a micellar CE buffer matrix.[3] The FLN spectra obtained for the *trans-anti-* dA-isomer are shown in Fig. A-8; frames A and B were obtained for two different excitation wavelengths, 374.0 nm and 378.0 nm, respectively. Comparison of spectra a,c (ethanol) with spectra b,d (glycerol/water) indicates that the major, red-shifted, conformer II′ is the same in both glasses. The weak modes at 422, 549, 627 cm^{-1} (spectrum a) correspond to the minor conformer I′ with its origin band at 383.0 nm.

The NLN spectra for the *cis-anti*-DB[*a,l*]PDE-dA adduct (Fig. A-4D), in contrast to *cis-anti*-DB[*a,l*]P-tetrol [26], imply that two conformers may exist in ethanol, while only one conformer is observed in the glycerol/water glass. The origin bands of these conformers are at 385.4 nm and 389.8 nm, respectively. Room temperature NMR data obtained in Me_2SO revealed the presence of only one conformation with $J_{11,12}$ = large, $J_{12,13}$ = small, and $J_{13,14}$ (not determined). These coupling constants, based on the calculations for *cis-anti*-DB[*a,l*]P-tetrol [26] and preliminary data for the *cis-anti*-DB[*a,l*]PDE-dA adduct (data not shown), are consistent with conformation II in which the cyclohexenyl ring adopts a half-chair structure with a positive value of the dihedral

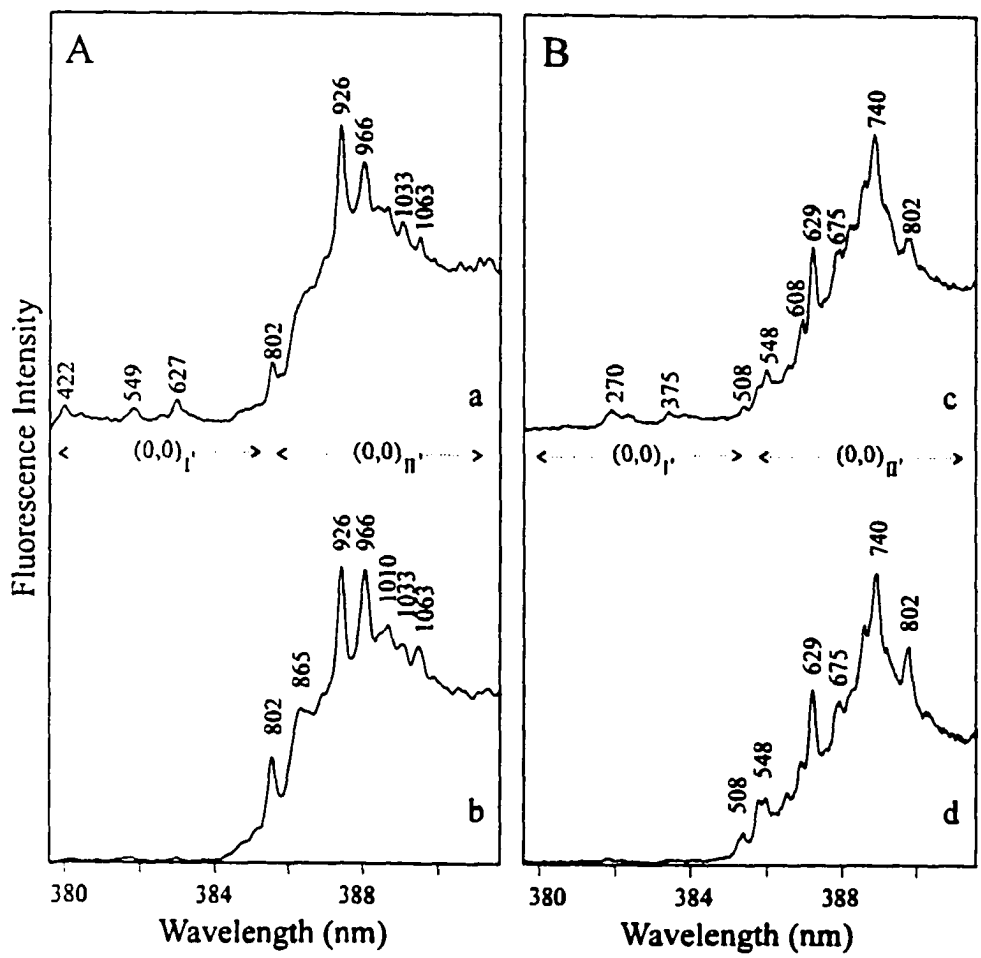

Figure A-8. FLN spectra for (−)-*trans-anti*-DB[*a,l*]PDE-N^{6}dA adducts in ethanol (spectra a and c) and 50/50 glycerol/water glass (spectra b and d) obtained for excitation wavelengths of 374.0 nm (Frame A) and 378.0 nm (Frame B), respectively. T = 4.2 K. The FLN peaks are labeled with their excited-state vibrational frequencies, in cm^{-1}. The spectral range shown covers the fluorescence origin bands of conformations I′ and II′. The peaks at 270, 375, 422, 549, and 627 cm^{-1} correspond to the minor conformation I′ (see text for details).

angle β. The blue-shifted conformation ((0,0) = 385.0 nm) most probably has a negative value of β with dA in an open-type configuration.

Time-resolved spectroscopy revealed the *cis-anti*-dA adducts in conformation I possess a different fluorescence lifetime compared to adducts in conformation II, so the fraction of adducts in conformation I can be resolved. The spectrum obtained as the difference between two delay times (60 and 20 ns) of the observation window is shown in Fig. A-9. This temporal difference spectrum reveals that the adducts in conformation I have a longer fluorescence lifetime. As a result, only the origin band at 385.0 nm and its corresponding vibronic progression is exposed. This is in contrast to spectrum g of Fig. A-4D, where both conformers and their vibronic modes are observed.

The FLN spectra in Fig. A-10 for the *cis-anti*-isomer also suggest the presence of two unique conformations, consistent with the data shown in Fig. A-4D. Comparison of the vibrational frequencies (~850-1100 cm^{-1}) in spectra b of Figs. A-8A and A-10 showed that the red-shifted conformers of the *trans-anti-* and *cis-anti*-dA adducts have different vibrational frequencies (e.g., 926 and 966 cm^{-1} versus 929 and 960 cm^{-1}, respectively). This supports our earlier assignment that conformer II′ of the *trans-anti-* and conformer II of *cis-anti*-DB[*a,l*]PDE-N^6dA isomers are clearly not the same.

A.4.3. Comparison of *trans-syn-* and *cis-syn-* vs *trans-anti-* and *cis-anti*-DB[*a,l*]PDE-N^6dA adducts.

Fig. A-11 shows four FLN spectra (in glycerol/water glass) obtained under identical conditions for *trans-syn-* (a), *cis-syn-* (b), *trans-anti-* (c), and *cis-anti-*DB[*a,l*]PDE-N^6dA (d) diastereomers, respectively. These data show that the *syn*-type adducts (frame A), with ZPL at 387, 407, 436, 463, and 498 cm^{-1} are indicative of *trans-*

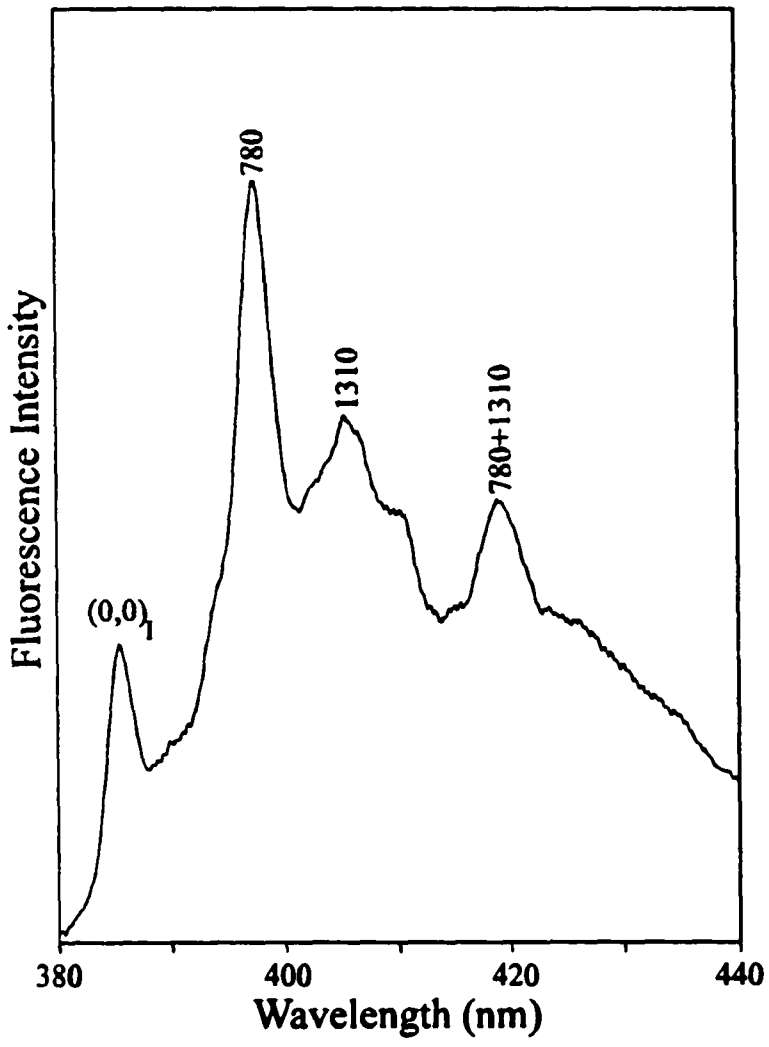

Figure A-9. NLN fluorescence spectrum revealing the pure contribution from conformer I of the (–)-*cis-anti*-DB[*a,l*]PDE-N^6dA adducts. The spectrum was obtained as a difference between 60 ns and 20 ns delay time of the observation window; λ_{ex} =308 nm, T=77 K (see text for details).

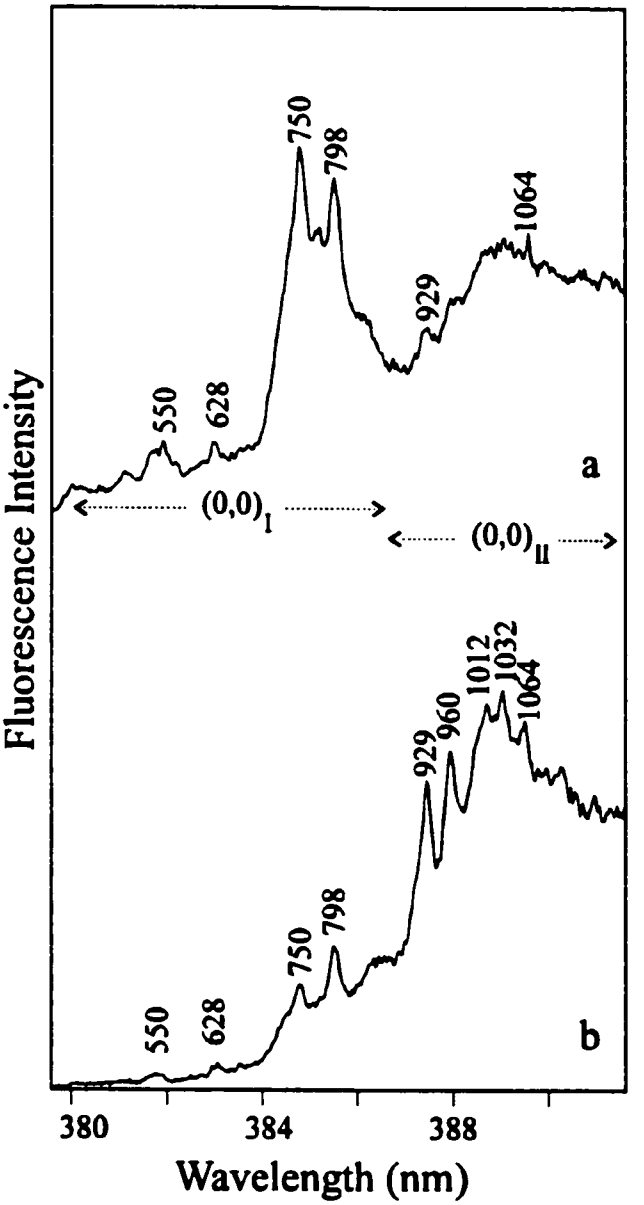

Figure A-10. FLN spectra for (−)-*cis-anti*-DB[*a,l*]PDE-N^6dA adducts in ethanol (spectrum a) and 50/50 glycerol/water glass (spectrum b) obtained at excitation wavelength of 374.0 nm. Delay time 40 ns, T = 4.2 K. In ethanol glass the major conformation is I, while in glycerol/water, conformation II predominates. The FLN peaks are labeled with their excited-state vibrational frequencies, in cm^{-1}.

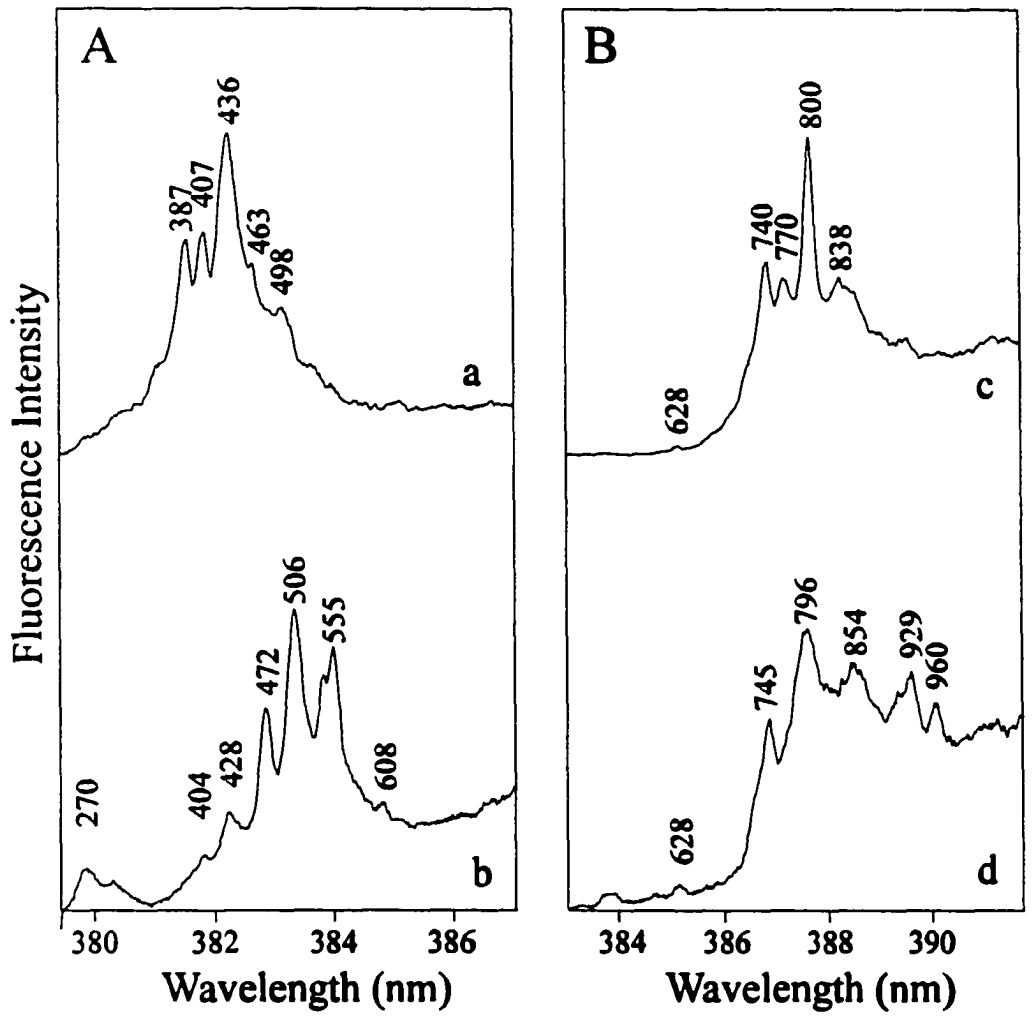

Figure A-11. FLN spectra of *trans-syn-* (curve a), *cis-syn-* (curve b), *trans-anti-* (curve c), and *cis-anti*-DB[*a,l*]PDE-N^6dA (curve d) adducts in a glycerol/water glass. T = 4.2 K. λ_{ex} = 376 nm. ZPL are labeled with their excited-state vibrational frequencies in cm^{-1}.

syn adducts, while strong lines at 428, 472, 506, and 555 cm^{-1} are characteristic for the *cis-syn*-dA isomers. A different pattern of zero-phonon lines is observed in frame B for *trans*- and *cis-anti*-dA adducts, spectra c and d, respectively. Here the characteristic modes are 740, 770, 800, and 838 cm^{-1} for *trans*- and 745, 796, 854, 929, and 960 cm^{-1} for *cis-anti*-dA. Differences were also observed in other frequency regions (data not shown). With an experimental uncertainty of ±3 cm^{-1}, the observed variations are considered to be significant. These results show that *trans*- and *cis*- isomers of the *syn*- and *anti*-DB[*a,l*]PDE derived dA adducts are readily distinguished by FLN spectroscopy.

A.5. Conclusions

We have demonstrated, using low-temperature fluorescence spectroscopy and computational chemistry, that not only the major but also the minor DB[*a,l*]PDE derived dA adduct conformations can be characterized. Conformational data, including the results from molecular modeling and solvent dependent studies performed for the diastereomeric DB[*a,l*]PDE-N^6dA adducts, provided insight on possible conformations of the cyclohexenyl ring and the orientation of the deoxyadenosine moiety. It was shown that both open-type (I/I′) and folded-type structures (II/II′) could be formed. Comparison of the fluorescence origin bands (Table A-2) reveals that in a glycerol/water glass *trans-syn*- and *cis-syn*- isomers adopt mostly conformation I, while *trans-anti*- and *cis-anti*- isomers exist mostly in conformation II′ and II, respectively. The major low-temperature conformations of *cis-syn*- (I), *trans-anti*- (II′) and *cis-anti*-dA (II) observed by fluorescence are compatible with the ^{1}H NMR data. However, for *trans-syn*-

DB[*a,l*]PDE-N^{6}dA the ^{1}H NMR data shows only conformer II, while the low-temperature fluorescence results shows a mixture of conformers I (major) and II (minor).

The major conformers observed for *trans-anti*-dA (II') and *cis-anti*-dA (II) are assigned as folded-type configurations with the same structure for the cyclohexenyl ring (positive β), opposite signs of α, and dA in pseudoequatorial position partially stacked over the distal ring (see Table A-2). The stacking leads to the experimentally observed red-shift of the fluorescence origin bands. In contrast, the minor conformations of the above two isomers (I'and I) are characterized by a different half-chair (negative β) with the dA moiety in a pseudoaxial position. Both minor conformers appear to have similar deviation from planarity in the fjord-region (positive α), as shown in Table A-2. In contrast to the *trans-anti-* and *cis-anti*-DB[*a,l*]PDE-N^{6}dA adducts, where the major conformations have a half-chair structure in the cyclohexenyl ring, conformers I and II of *trans-syn*-dA feature half-boat and half-chair structures, respectively, with different orientations of the dA moiety. The *cis-syn*-dA adduct with the half-chair cyclohexenyl ring in conformers I (open) and II (folded), and (α, β) being (positive, negative) and (negative, positive), respectively, are in agreement with the *cis-syn*-DB[*a,l*]P-tetrol calculations [26]. The different vibrational patterns in the FLN spectra can provide a means of distinguishing the *trans-* and *cis-* isomers for both *syn-* and *anti*-DB[*a,l*]PDE-14-N^{6}dA adducts. It is anticipated that these high resolution FLN spectra will prove

useful for future identification of DB[*a,l*]PDE-DNA adducts (at the dAMP level) formed in biological systems.[4]

These fluorescence results establish that *anti*-DB[*a,l*]PDE derived dA adducts, the major adducts formed in mouse skin and calf-thymus DNA [16], preferentially adopt conformation II (or II') with origin bands at ~388-390 nm. The large red-shift of the (0,0)-band is in agreement with modeling studies, which indicate that these conformers exist in a folded-type geometry with significant π-π interactions. This suggests that molecular conformations of -dA adducts may be important for understanding the preference of the bound metabolite towards external, base-stacked and intercalated conformations, which were recently observed in DNA [16,25]. Specifically, it was shown that in mouse skin the majority of *anti*-DB[*a,l*]PDE-derived DNA adducts adopt intercalated conformations, which in turn may influence their recognition by repair enzymes [25,33]. The analysis of mouse skin DNA exposed to DB[*a,l*]P, which showed that external adducts are repaired more efficiently than intercalated adducts [16], accentuates the importance of adduct conformation. The conformational data presented in this manuscript suggest the majority of *anti*-DB[*a,l*]PDE-14-N^{6}dA adducts, due to a folded-type configuration, may be easily accommodated by the double helix of DNA. Moreover, the fact that the *anti*- dA adducts assume a folded-type configuration is consistent with the significant red-shift of the fluorescence origin band of intercalated *anti*-DB[*a,l*]PDE-dA adducts observed for intact DNA [16]. Therefore, we conclude that the large shift (to ~ 398 nm) of the fluorescence origin bands of DNA adducts observed

[4] P. Devanesan, F. Ariese, R. Jankowiak, G. J. Small, E. G. Rogan and E. Cavalieri, A novel method for the isolation and identification of stable DNA adducts formed by dibenzo[*a,l*]pyrene and dibenzo[*a,l*]pyrene 11,12-dihydrodiol-13,14,-epoxides *in vitro*. *Chem. Res. Toxicol.*, accompanying paper.

in Ref. 16 are caused by type II (or II') conformers, which allow intercalation and, as a result, strong π-π interactions between the adduct and the DNA bases. In addition, it was shown here that the *cis-anti*-DB[*a,l*]PDE-14-N^6dA adduct forms an open-type structure (I), implying that this adduct adopts an external conformation with intact DNA, consistent with our earlier findings [16]. Hence, it is entirely possible that the diverse structural conformations formed by DB[*a,l*]PDE-derived DNA adducts are responsible for the high carcinogenic potency of DB[*a,l*]P.

A.6. Acknowledgments

Ames Laboratory is operated for the U.S. Department of Energy by Iowa State University under contract no. W-7405-Eng-82. This research was supported by the National Institutes of Health, grant # POI CA49210-0. Partial support to RJ and GJS was provided by the Office of Health and Environmental Research, Office of Energy Research. The authors thank Dr. A. Seidel for providing the optically pure *syn*- and *anti*-DB[*a,l*]P diol epoxides, Dr. E.L. Cavalieri for providing adduct standards, and Dr. F. Ariese for experimental help at the initial stage of this project.

References

1. Cavalieri, E.L., Higginbotham, S., RamaKrishna, N.V.S., Devanesan, P.D., Todorovic, R., Rogan, E.G., and Salmasi, S. (1991) Comparative dose-response tumorigenicity studies of dibenzo[*a,l*]pyrene versus 7,12-dimethylbenz[*a*]anthracene, benzo[*a*]pyrene, and two dibenzo[*a,l*]pyrene dihydrodiols in mouse skin and rat mammary gland. *Carcinogenesis* **12**, 1939-1944.

2. Higginbotham, S., RamaKrishna, N.V.S., Johansson, S.L., Rogan, E.G., and Cavalieri, E.L., (1993) Tumor-initiating activity and carcinogenicity of

dibenzo[*a,l*]pyrene versus 7,12-dimethylbenz[*a*]anthracene and benzo[*a*]pyrene at low dose in mouse skin. *Carcinogenesis* **14**, 875-878.

3. Kozin, I.S., Gooijer, C., and Velthorst, N.H. (1995) Direct determination of dibenzo[*a,l*]pyrene in crude extracts of environmental samples by laser-excited Shpol'skii spectroscopy. *Anal. Chem.* **67**, 1623-1626.

4. Mumford, J.L., Li, X., Hu, F., Lu, X.B., and Chuang, J.C. (1995) Human exposure and dosimetry of polycyclic aromatic hydrocarbons in urine from Xuan Wei, China with high lung cancer mortality associated with exposure to unvented coal smoke. *Carcinogenesis* **16**, 3031-3036.

5. de Ratt, W.K., Kooijman, S.A.L.M., and Gielen, J.W.J. (1987) Concentrations of polycyclic hydrocarbons in airborne particles in the Netherlands and their correlation with mutagenicity. *Sci. Total Environ.* **66**, 95-114.

6. Li, K.-M., Todorovic, R., Rogan, E.G., Cavalieri, E.L., Ariese, F., Suh, M., Jankowiak, R., and Small, G.J. (1995) Identification and quantitation of dibenzo[*a,l*]pyrene-DNA adducts formed by rat liver microsomes *in vitro*: preponderance of depurinating adducts. *Biochemistry* **34**, 8043-8049.

7. Cavalieri, E. and Rogan, E. Mechanism of Tumor Initiation by Polycyclic Aromatic Hydrocarbons in Mammals. In *The Handbook of Environmental Chemistry*, Vol. 3, Part I, *PAHs and Related Compounds* (ed. by A. H. Neilson), Springer-Verlag, Berlin Heidelberg 1998.

8. Jankowiak, R. and Small, G.J. (1998) Analysis of PAH-DNA Adducts-Fluorescence Line-Narrowing Spectroscopy. In *The Handbook of Environmental Chemistry*, Vol. 3, Part I, *PAHs and Related Compounds* (ed. by A. H. Neilson), Springer-Verlag, Berlin Heidelberg 1998.

9. Cavalieri, E.L. and Rogan, E.G. (1992) The approach to understanding aromatic hydrocarbon carcinogenesis. The central role of radical cations in metabolic activation. *Pharmac. Ther.* **55**, 183-199.

10. Ralston, S.L., Seidel, A., Luch, A., Platt, K.L., and Baird, W.M. (1995) Stereoselective activation of dibenzo[*a,l*]pyrene to (-)-*anti*(11*R*,12*S*,13*S*,14*R*)- and (+)-*syn*(11*S*,12*R*,13*S*,14*R*)-11,12-diol-13,14-epoxides which bind extensively to deoxyadenosine residues of DNA in the human mammary carcinoma cell line MCF-7. *Carcinogenesis* **16**, 2899-2907.

11. Conney, A.H. (1982) Induction of microsomal enzymes by foreign chemicals and carcinogenesis by polycyclic aromatic compounds. *Cancer Res.* **42**, 4875-491.

12. Luch, A., Glatt, H., Platt, K.L., Oesch, F., and Seidel, A., (1994) Synthesis and mutagenicity of the diastereomeric fjord-region 11,12-dihydrodiol 13,14-epoxides of dibenzo[*a,l*]pyrene. *Carcinogenesis* **15**, 2507-2516.

13. Harvey, R.G. (1991) *Polycyclic Aromatic Hydrocarbons: Chemistry and Carcinogenicity*. Cambridge University Press, Cambridge.

14. Ralston, S.L., Lau, H.H.S., Seidel, A., Luch, A., Platt, K.L., and Baird, W.M. (1994) The potent carcinogen dibenzo[*a,l*]pyrene is metabolically activated to fjord-region 11,12-diol 13,14-epoxides in human mammary carcinoma MCF-7 cell cultures. *Cancer Res.* **54**, 887-890.

15. Li, K.-M., RamaKrishna, N.V.S., Padmavathi, N.S., Rogan, E.G., and Cavalieri, E.L. (1994) Synthesis and structure determination of the adducts of dibenzo[*a,l*]pyrene diol epoxides and deoxyadenosine and deoxyguanosine. *Polycyclic Aromat. Compd.* **6**, 207-213.

16. Jankowiak, R., Ariese, F., Hewer, A., Luch, A., Zamzow, D., Hughes, N.C., Phillips, D., Seidel, A., Platt, K-L., Oesch, F., and Small, G.J. (1998) Structure, Conformations, and Repair of DNA Adducts from Dibenzo[*a,l*]pyrene: ^{32}P-Postlabeling and Fluorescence Studies *Chem. Res. Toxicol.* **11**, 674-685.

17. Jankowiak, R. and Small, G.J. (1991) Fluorescence line narrowing: a high-resolution window on DNA and protein damage from chemical carcinogens. *Chem. Res. Toxicol.* **4**, 256-269.

18. Rogan, E.G., Devanesan, P.D., RamaKrishna, N.V.S., Higginbotham, S., Padmavathi, N.S., Chapman, K., Cavalieri, E.L., Jeong, H., Jankowiak, R., and Small, G.J. (1993) Identification and quantitation of benzo[*a*]pyrene-DNA adducts formed in mouse skin. *Chem. Res. Toxicol.* **6**, 356-363.

19. Devanesan, P.D., RamaKrishna, N.V.S., Padmavathi, N.S., Higginbotham, S., Rogan, E.G., Cavalieri, E.L., Marsh, G.A., Jankowiak, R., and Small, G.J. (1993) Identification and quantitation of 7,12-dimethylbenz[*a*]anthracene-DNA adducts formed in mouse skin. *Chem. Res. Toxicol.* **6**, 364-371.

20. Kok, S.J., Posthumus, R., Bakker, I., Gooijer, C., Brinkman, U.A.Th., and Velthorst, N.H. (1995) Identification of benzo[*a*]pyrene tetrols by reversed-phase liquid chromatography coupled semi-on-line to fluorescence line-narrowing spectroscopy. *Anal. Chim. Acta* **303** 3-10.

21. Marsh, G.A., Jankowiak, R., Suh, M., and Small, G.J. (1994) Sequence dependence of benzo[*a*]pyrene diol epoxide-DNA adduct conformer distribution: a study by laser-induced fluorescence/polyacrylamide gel electrophoresis. *Chem. Res. Toxicol.* **7**, 98-109.

22. Suh, M., Jankowiak, R., Ariese, F., Mao, B., Geacintov, N.E., and Small, G.J. (1994) Flanking base effects on the structural conformation of the (+)-*trans-anti*-benzo[*a*]pyrene diolepoxide adduct to N^2-dG in sequence-defined oligonucleotides. *Carcinogenesis* **15**, 2891-2898.

23. Suh, M., Ariese, F., Small, G.J., Jankowiak, R., Liu, T.-M., and Geacintov, N.E. (1995) Conformational studies of the (+)-*trans*-, (-)-*trans*-, (+)-*cis*-, and (-)-*cis* adducts of *anti*-benzo[*a*]pyrene diolepoxide to N^2-dG in duplex oligonucleotides using polyacrylamide gel electrophoresis and low-temperature fluorescence spectroscopy. *Biophys. Chem.* **56**, 281-296.

24. Ariese, F., Small, G.J., and Jankowiak, R. (1996) Conformational studies of depurinating DNA adducts from syn-dibenzo[a,l]pyrene diolepoxide. *Carcinogenesis* **17**, 829-837.

25. Suh, M., Ariese, F., Small, G.J., Jankowiak, R., Hewer, A., and Phillips, D.H. (1995) Formation and persistence of benzo[*a*]pyrene-DNA adducts in mouse epidermis *in vivo*: importance of adduct conformation. *Carcinogenesis* **16**, 2561-2569.

26. Jankowiak, R., Ariese, F., Zamzow, D., Luch, A., Kroth, H., Seidel, A., and Small, G.J. (1997) Conformational Studies of Stereoisomeric Tetrols Derived from *syn*- and *anti*-Dibenzo[*a,l*]pyrene Diol Epoxides. *Chem. Res. Toxicol.* **10**, 677-686.

27. Burkert, U. and Allinger, N.L. (1982) Molecular mechanics. ACS Monograph Vol. 177.

28. Allinger, N.L. (1977) Conformational analysis 130. MM2: a hydrocarbon force field utilizing V1 and V2 torsional terms. *J. Am. Chem. Soc.* **99**, 8127-8134.

29. Brown, J.C. (1982) Ph.D. Thesis, Iowa State University, pp. 131.

30. Brown, J.C., Duncanson, J.A., and Small, G.J. (1980) Fluorescence line narrowing spectrometry in glasses for direct determination of polycyclic aromatic hydrocarbons in solvent-refined coal. *Anal. Chem.* **52**, 1711-1715.

31. Herzberg, G. (1966) Molecular Spectra and Molecular Structure, III. Electronic Spectra and Electronic Structure of Polyatomic Molecules; van Nostrand and Reinhold Co., New York, Chapter II.

32. Geacintov, N.E., Cosman, M., Hingerty, B.E., Amin, S., Broyde, S., and Patel, D.J. (1997) NMR Solution Structures of Stereoisomeric Covalent Polycyclic

Aromatic Carcinogen-DNA Adducts: Principles, Patterns, and Diversity. *Chem. Res. Toxicol.* **10**, 112-146.

33. Wei, D., Maher, V. and McCormick, J.J. (1995) Site-specific rates of excision repair of benzo[*a*]pyrene diol epoxide adducts in the hypoxanthine phosphoribosyl transferase gene of human fibroblasts: correlation with mutation spectra. *Proc. Natl Acad. Sci. USA*, **92**, 2204-2208.

APPENDIX B. PRELIMINARY INVESTIGATION OF 4-HDROXYTAMOXIFEN AND α-ACETOXYTAMOXIFEN DNA ADDUCTS WITH LOW-TEMPERATURE FLUORESCENCE SPECTROSCOPY

B.1. Introduction

The anti-estrogen drug tamoxifen (TAM) is being used in the treatment of women with breast cancer and has demonstrated potential as a chemopreventive agent to breast cancer [1,2]. However, its use as a chemopreventive agent has shown an increase in endometrial cancers, and studies with rats showed that TAM is a genotoxic liver carcinogen [2]. Metabolic activation and the subsequent DNA damage from TAM are not clearly understood. This is primarily because characterization of DNA damage at the real-world level has mainly been accomplished with the highly sensitive technique of ^{32}P-postlabeling [1,2], which can provide inconclusive results due to the amount of time needed to perform the analysis, leading to post-digestion degradation of TAM-DNA adducts. Therefore, to better elucidate the genotoxic mechanism of TAM, we will utilize low-temperature laser-induced fluorescence and fluorescence line-narrowing spectroscopy (FLNS) to identify/characterize intact DNA adducts produced with various activated forms of tamoxifen. Following the analysis of intact TAM-DNA adducts, DNA will be digested to the nucleoside level for analysis by capillary electrophoresis (CE) combined with on-line FLNS to identity the individual adducts and determine their relative abundance. In this preliminary report, two metabolic forms of TAM (4-hydroxytamoxifen [3] and α-acetoxytamoxifen [4]) are reacted with DNA to determine the nature of their DNA adduction.

TAM on its own produces very weak and broad fluorescence at room temperature. However, by photocyclizing TAM with UV light [5], as shown in Figure B-1, a rigid phenanthrene structure is formed which provides highly characteristic spectra at 77 K (308 nm excitation wavelength). By this method various TAM-DNA adduct isomers can be spectroscopically characterized and identified in intact DNA and, after digestion, at the nucleoside level. Below are the preliminary results of such analyses, beginning with DNA adducts formed with 4-hydroxytamoxifen using various activation systems.

B.2. Results and Discussion

B.2.1. 4-Hydroxytamoxifen

Shown in Figure B-2A are the fluorescence results (T = 77 K, λ_{ex} = 308 nm) of activating the reaction of calf-thymus DNA and 4-hydroxytamoxifen with MnO_2 as a chemical oxidizing agent, before (spectrum a) and after photocyclization (spectrum b) with a 15 watt Hg-lamp for 15 minutes at a distance of 5 cm. The DNA samples were dissolved (1mg/mL) in SSC buffer. As can be clearly seen, before cyclization the spectrum is broad and featureless, centered at ~ 413 nm. However, after 15 minutes of cyclization a highly characteristic spectrum can be obtained (b) with an origin band at 361.5 nm. Similarly, shown in Figure B-2B are the before and after photocyclization results of activating the reaction of calf-thymus (CT) DNA and 4-hydroxytamoxifen with horseradish peroxidase (HRP) and H_2O_2. Again, before cyclization the 77 K fluorescence spectrum is broad, featureless, and centered, in this case, at 419 nm. In contrast, after

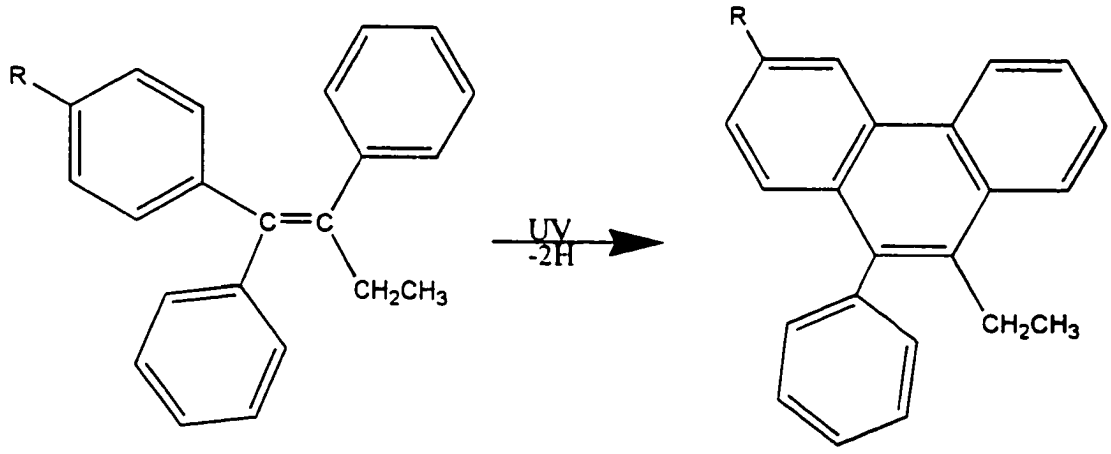

$R = OCH_2CH_2N(CH_3)_2$

B-1. Photocyclization mechanism of tamoxifen with UV light.

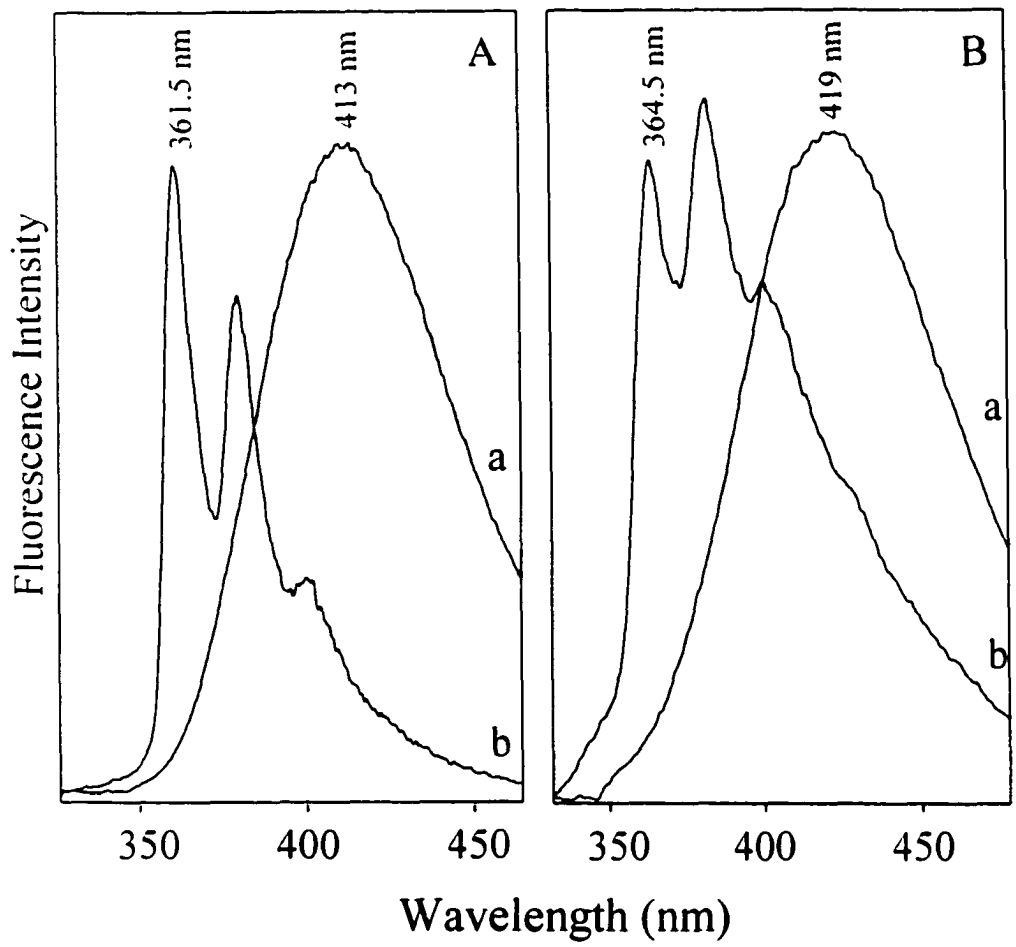

Figure B-2. Fluorescence spectra for DNA reacted with 4-hydroxytamoxifen using MnO_2 (Frame A) and HRP/H_2O_2 (Frame B) activation systems before photocyclization (spectrum a in each frame) and after cyclization (spectrum b in each frame). T = 77 K, λ_{ex} = 308 nm.

photocyclization a more characteristic spectrum is revealed, with its origin band at 364.5 nm.

It has been suggested by ^{32}P-postlabeling that rat liver and human liver microsomes (with various cofactors) produce similar adducts with CT-DNA [3]. The first test of this assertion by low-temperature fluorescence detection of intact DNA is shown in Figure B-3A. Using the procedure described above, spectrum a is before photocyclization and spectrum b is after photocyclization of 4-hydroxytamoxifen activated with human liver microsomes and cumene hydroperoxide as a cofactor. Similar to the two activation systems described above, the spectrum before cyclization is broad and featureless, with a maximum near 415 nm. However, in contrast to the systems described above, after photocyclization (spectrum b) the blue-shifted spectrum remains broad, centered at ~ 374 nm. This suggests strong interaction/coupling of the activated tamoxifen with DNA, possibly an internal type adduct.

Frame B of Fig. B-3 shows the fluorescence results from activation of 4-hydroxytamoxifen with human liver microsomes and NADPH as a cofactor. Oddly, before photocyclization (spectrum a), after 15 minutes of photocyclization (spectrum b), and after 35 minutes of photocyclization (spectrum c), results in very similar spectra (centered at ~ 415 nm), where no blue-shift of the spectra occurs after exposure to the UV lamp. This could possibly be the result of a cross-linked type of adduct, where the TAM moiety is bound to both strands of the DNA.

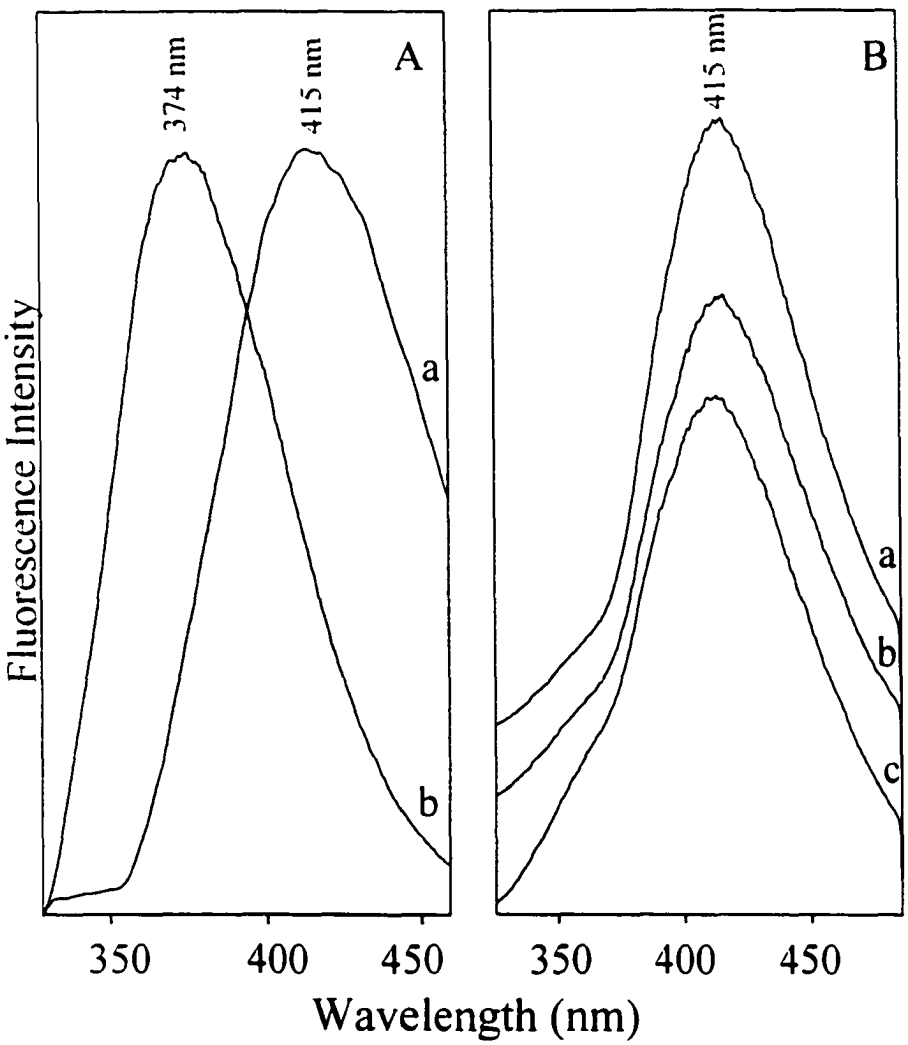

Figure B-3. Fluorescence spectra for DNA reacted with 4-hydroxytamoxifen using human liver microsomes/cumene hydroperoxide (Frame A) and human liver microsomes/ NADPH (Frame B) activation systems before photocyclization (spectrum a in each frame) and after cyclization (spectrum b in each frame). T = 77 K, λ_{ex} = 308 nm.

These results indicate that in all four activation systems, at least four different types of products are formed. Activation of 4-hydroxytamoxifen with MnO_2 shows sharp, structured spectra, indicating that in this case, the adduct if of the external type, where electron-phonon coupling is weak. Similarly, activation of 4-hydroxytamoxifen with human liver microsomes and NADPH indicate that adducts are also of the external type, yet different from those formed with MnO_2, due to the shift in the fluorescence origin band. The possibility of more than one type of adduct being formed can also be considered, which would explain spectra being more broad than that of MnO_2 activation, but could also be due to adducts with larger electron-phonon coupling with DNA. Moreover, there could also be residual, unreacted 4-hydroxytamoxifen that is intercalated (physically bound) in the DNA and not completely removed during washing procedures, or the formation of internal type adducts, i.e., adducts covalently bound within the DNA helix. Lastly, the shift in the fluorescence origin band indicates that the adduct is not identical to that formed with MnO_2. In the case of activating 4-hydroxytamoxifen with human liver microsomes and cumene hydroperoxide (Figure B-3A) the results indicate that an internal type of adduct may be formed, or simple intercalation. However, in the latter case, the signal was much stronger than that observed for the control, where intercalation was observed (data not shown). In regard to activation of 4-hydroxytamoxifen with human liver microsomes and NADPH (Figure B-3B), the adduction appears to be of an internal type, yet different than that for the system previous system of human liver microsomes and NADPH. Similar results were previously shown by Bodell et al. [3], where it was reported by ^{32}P-postlabelling that some adducts formed with NADPH are different from those formed with cumeme hydroperoxide.

These results also indicate that low-temperature fluorescence spectroscopy can be useful in characterizing different types of adducts formed with 4-hydroxytamoxifen. However, studies that are more conclusive should include higher resolution spectroscopy (i.e., FLNS) on the intact DNA samples, followed by digestion of the DNA to the nucleoside level. Once digested, FLNS can be used on-line with capillary electrophoresis and HPLC to separate the adducts, determining not only their identity (when compared to synthetic standards) but also their relative abundance.

B.2.2. α-Acetoxytamoxifen

Osborne *et al.*, [4] have also reported the detection of covalent DNA-TAM adducts in the liver of rats treated with tamoxifen [4]. It was suggested that tamoxifen is most likely metabolized to α-acetoxytamoxifen, which binds to DNA. The major adducts found in rat liver tissue were isolated and purified by and characterized by HPLC, MS, and NMR. They are the E and Z form of 4-{-[2-(dimethylamino)ethoxy]phenyl}-3,4-diphenyl-2-(9β-deoxyribofuranosyl-6-oxopurin-2-ylamino)-3-butene, also known as TG1 and TG2, respectively [4]. In what follows, all samples were photocyclized as described above, and fluorescence spectra were taken at 77 K with an excitation wavelength of 308 nm and in an ethanol solvent. The fluorescence spectra of TG1 had its before cyclization maximum at ~ 413 nm, and TG2 at ~ 410 nm (data not shown). After cyclization, the fluorescence origin band of TG1 and TG2 were both at ~ 357.5 nm, as shown in Figure B-4. Since these two adducts are E/Z isomers, it is possible that they photocyclize to the same species. Moreover, the spectrum of TG2 after cyclization appears to have contributions from more than one species, with a

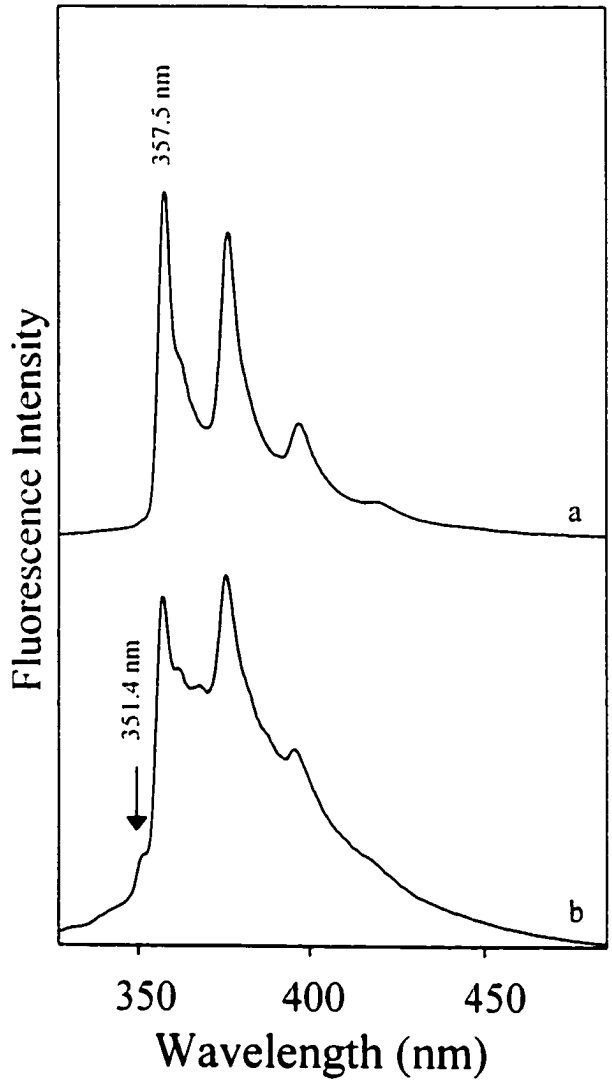

Figure B-4. Fluorescence spectra for TG1 and TG2 after 15 minutes of photocyclization; T = 77 K, λ_{ex} = 308 nm, in ethanol (see text for details).

shoulder at 351.4 nm. This could possibly be the cyclized Z form of the adduct, however, off-line FLNS and on-line HPLC-/CE-FLNS should be used to confirm or deny this, so that a pure reference spectrum can be generated for these standards to determine if α-acetoxytamoxifen adducts are formed with calf-thymus DNA.

Shown in Figure B-5 are the 77 K fluorescence results of photocyclization (as described above) of intact calf-thymus DNA with different adduction level of α-acetoxytamoxifen (as established by ^{32}P-postlabeling), λ_{ex} = 308 nm. As can be seen, in going from high to low adduction levels (spectra a-e), the resultant spectra become broader and shift to the red (see figure caption). Spectrum a is the result of the highest adduction level in this study, 1 adduct in 400 base-pairs. This spectrum shows a characteristic phenanthrene type spectrum with a fluorescence origin band at 361.5 nm. The sharp fluorescence from the phenanthrene moiety becomes lost by spectrum d, which is an adduction level of 200 adducts in 10^6 base pairs. This suggests that at high adduction at least two types of adducts may be formed, one external and the other internal, whereas, at low levels, only one internal adduct is formed. To better characterize the types of adducts formed from α-acetoxytamoxifen with DNA, the DNA was digested to the nucleoside level for further low-temperature analysis.

Shown in Figure B-6 are the results of photocyclized DNA digests that were purified by HPLC. Spectra a and b correspond to the HPLC fraction for TG1 and TG2, (as established from rat liver DNA digests described above), digested from DNA with 1200 adducts per 10^6 base pairs. Spectrum c corresponds to digest that should contain both TG1 and TG2, from DNA adducted at a level of 5 adducts in 10^6 base-pairs. As

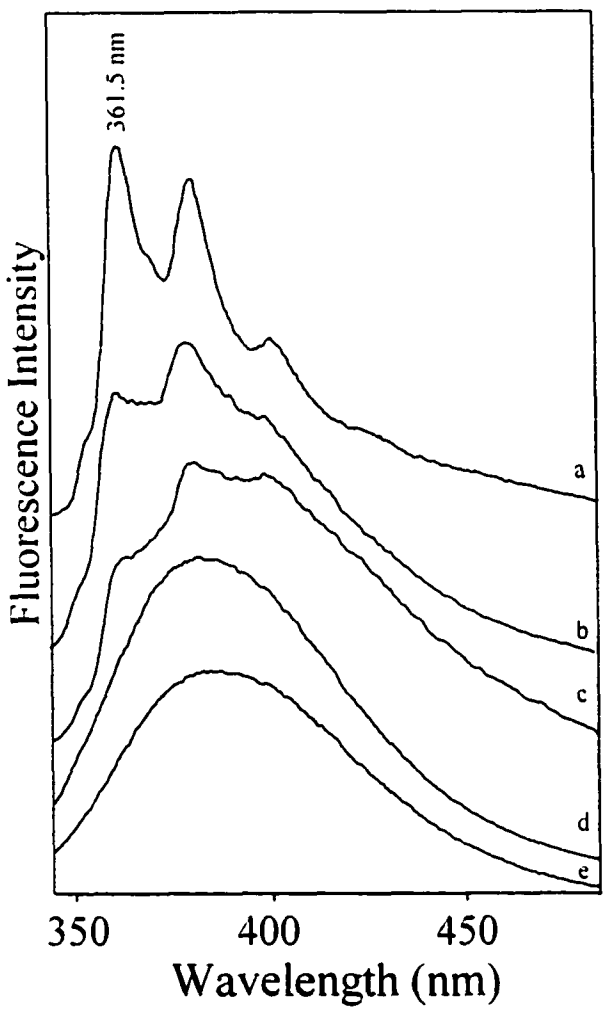

Figure B-5. Fluorescence spectra for various adduction levels of α-acetoxytamoxifen with DNA: (a) 1 adduct in 400 base-pairs, i.e., 1:400, (b) $1200:10^6$, (c) $200:10^6$, (d) $19:10^6$, (e) no adducts—physical intercalation only. Each was photocyclized for 15 minutes with a Hg lamp. T = 77 K, λ_{ex} = 308 nm, in 66% glycerol 33% water.

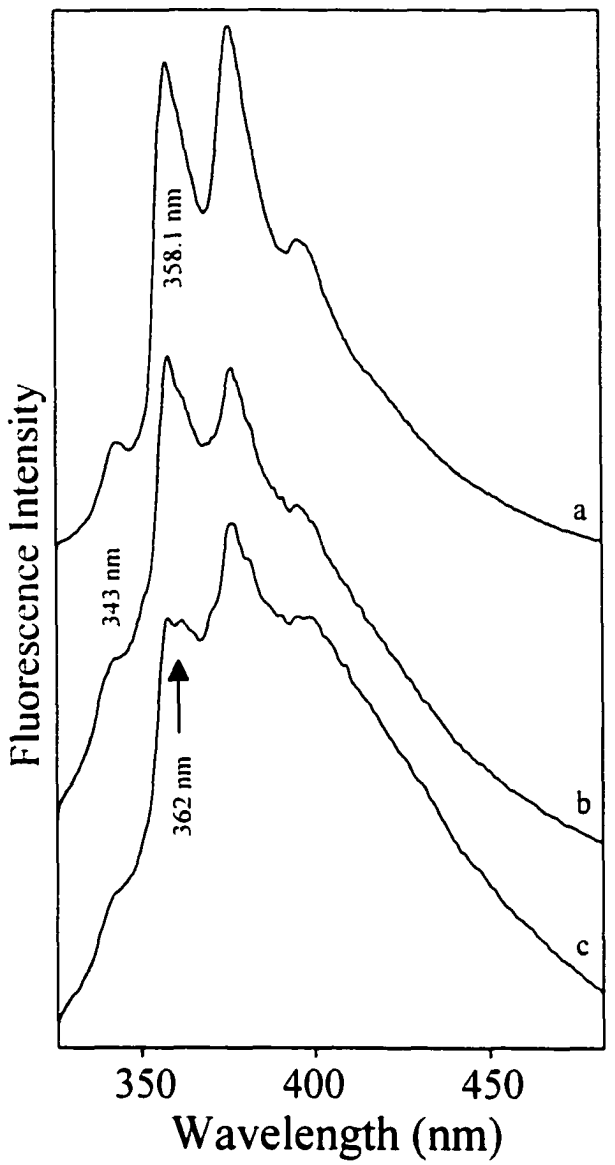

Figure B-6. Fluorescence spectra of photocyclized DNA digests that were purified by HPLC and photocyclized for 15 minutes. Spectra a and b correspond to fraction that contain TG1 and TG2, respectively. Spectrum c corresponds to a fraction containing both TG1 and TG2: T = 77 K, λ_{ex} = 308 nm, in ethanol.

shown in the spectra a and b, the fluorescence origin band is at 358.1 nm, with an unknown contaminant peak at 343 nm. On the other hand, spectrum c shows a more complex fluorescence spectrum with an origin band at ~ 362 nm. These results indicate that to be certain if the adducts formed in rats treated with tamoxifen are the same as those formed when reacting calf-thymus DNA with α-acetoxytamoxifen, that samples will require on-line FLNS detection. This is due to the large amount of impurities from incomplete fractionation by HPLC and the inherent low-resolution of 77 K, 308 nm excitation.

B.3. Conclusion and Future Prospects

By combining, results from off-line low-temperature fluorescence spectroscopy of intact TAM-DNA adducts with results from ^{32}P-postlabeling and HPLC-/CE-FLNS of DNA digested to the nucleoside level, more definitive identification/characterization and quantification of these adducts can be accomplished. Fluorescence results from intact DNA adducts may offer insight into the recognition and repair of these types of adducts. On the other hand, analysis at the nucleoside level will not only allow for more thorough identification and characterization, but will also provide the ability to determine the relative abundance of the various TAM-DNA adducts formed. It is anticipated that by utilizing these techniques in a complementary fashion to study the products formed by the two common activated forms of the anti-estrogen drug tamoxifen described above, a further understanding of the genotoxic nature of this drug and its viability as a chemopreventive agent to breast cancer can be realized.

References

1. Nease, R.J, Ross, J.M., *Am. J. Med.*, 1995, *99*, 180.
2. Jordan, V.C., J. *Natl. Cancer Inst.*, 1992, *84*, 231.
3. Bodell, W.J., Pathak, D.N., *Carcinogenesis*,1994, *15*, 529.
4. Osborne, M.R., Hardcastle, I.R., Phillips, D.H., *Carcinogenesis*, 1997, *18*, 539.
5. Wilson, S., Ruenitz, P.C., *J. Phar. Sciences*, 1993, *82*, 571.

APPENDIX C. PRELIMINARY INVESTIGATION OF AN INTACT NON-COVALENT PHOTOSYNTHETIC MEMBRANE PROTEIN (CP43) COMPLEX BY CAPILLARY ELECTROPHOREIS AND NON-LINE NARROWING FLUORESCENCE SPECTROSCOPY

C.1. Introduction

Photosystem II (PSII) is a large membrane protein complex found in green plants, algae, and cyanobacteria, and is made up of at least 25 smaller protein subunits [1]. CP43 (M.W. 43 kDa) is one such subunit containing non-covalently bound chlorophyll and serves as an antenna for funneling solar energy captured by peripheral antenna subunits to the reaction center, where the photochemical reactions take place [2]. To study these mechanistic processes, as they would occur in nature, the 3-dimensional structure of the protein needs to remain in its native state. A common procedure for studying these processes is to fractionate the particular subunits of PSII via chromatography and/or electrophoresis, followed by off-line spectroscopic characterization [3-5]. However, these proteins often denature (to varying degrees) under even the most careful experimental conditions, which can lead to the release of chlorophyll molecules and/or reorientation of the chlorophyll's local environment. This, along with possible aggregation of the monomeric subunit, can alter the spectral (absorbance/fluorescence) properties of CP43, leading to many contributing factors (additional spectral bands) in the off-line spectral analyses. Consequently, interpretation of the relative contributions is the subject of much debate due to the subjective nature of deconvolving spectroscopic data [4,5]. In what follows, a fractionated CP43 sample is analyzed by capillary electrophoresis (CE) with on-line low temperature laser-induced

fluorescence spectroscopy, under non-line-narrowing (NLN) conditions, i.e., 4.2 K, λ_{ex} = 351.1 nm. Any denaturation that occurs during sample handling or contamination of other subunits from incomplete fractionation can be electrophoretically displaced from the native, intact CP43 zone, which can then be frozen to 4.2 K in mid-separation for spectroscopic characterization. The CE-buffer (see below) was chosen to keep the proteins in their native state and minimize aggregation [4]. Although these results are preliminary, and more studies of on-line fluorescence line-narrowing detection should be done, this is a promising approach of studying subunits of PSII in their most native form.

C.2. Experimental

The same experimental setup for room- and low-temperature CE-LIF as that described in Chapter 4 was used. The difference being that in this case there was no FLNS, only NLN spectra were obtained to determine if there is denaturation. The sample buffer was 20 mM BisTris, 20 mM NaCl, 0.1% (w/v) n-dodecyl-β,D-maltoside, 10% glycerol (w/v), pH 8.0. This buffer, excluding the percentage of glycerol (used for glass formation), has been reported to be suitable for CP43 [4]. The excitation wavelength was 351.1 nm. The operating voltage for the CE was 20 kV, which resulted in a ~ 20 μA current; 75 μm i.d. x 365 μm o.d., UV-transparent capillary (Polymicro Tech., Phoenix, AZ). Low-temperature experiments were obtained at 4.2 K, with a resolution of 0.8 nm.

C.3. Results and Discussion

Shown in Figure C-1a is the CE-separation of a HPLC-fractionated CP43 sample. A variety of peaks is separable under these conditions with the two most pronounced at

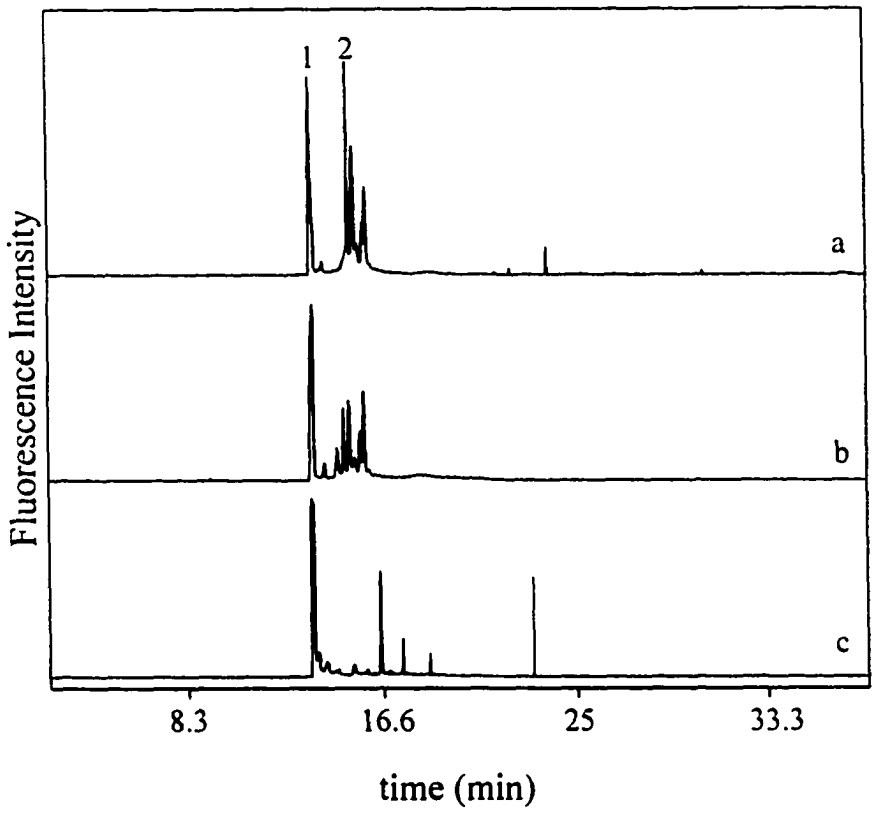

Figure C-1. CE electropherograms of (a) CP43 after immediately thawing from -70°C, (b) after 4 hours at room-temperature in the dark, (c) after refreezing for 1-month at -70°C. CE conditions: 20 mM BisTris, 20 mM NaCl, 0.1% (w/v) n-dodecyl-β,D-maltoside, 10% glycerol (w/v), pH 8.0; 20 kV (~ 20 μA); 75 μm i.d. x 365 μm o.d.

~ 13 minutes (peak 1) and ~ 14.5 minutes (peak 2). By monitoring room temperature fluorescence at an excitation wavelength of 351.1 nm, peak 1 revealed fluorescence near ~ 675 nm, while that for peak 2 was ~ 681 nm (data not shown). This indicated that peak 1 could possibly be denaturation of peak 2. Moreover, it was shown in a previous study of a similar core antenna subunit system (CP47) that denaturation can be revealed with the aid of ion-exchange chromatography [5]. The other peaks are possibly aggregated dimers or other multimers since there fluorescence at room temperature was red-shifted beyond what has been reported for monomeric CP43 [6].

To further characterize and identify peaks 1 and 2 in electropherogram a of Fig. C-1, the separation was repeated and this time the first two peaks were frozen in mid-separation to 4.2 K. The resulting non-line-narrowed fluorescence (λ_{ex} = 351.1 nm) for each is shown in Figure C-2. The spectrum corresponding to peak 1 revealed a broad fluorescence (fwhm ~ 20 nm) centered at 674 nm (spectrum a), possibly denatured CP43, while the spectrum corresponding to peak 2 in the electropherogram was only ~ 6 nm at fwhm, centered at 683.3 nm. The latter is indicative of intact CP43 at 4.2 K [4,5].

Further evidence that the first peak in the electropherogram was the result of protein denaturation was accomplished by leaving the sample at room temperature in the dark for ~ 4 hours. The result of the CE separation is for this sample is shown in Figure C-1b. As shown, the large peak with CP43-type fluorescence (peak 2 in the electropherogram) has significantly decreased, while peak 1 in the electropherogram has increased. This suggests that peak 1, with its broad 4.2 K fluorescence centered at 674 nm, could be the partial denaturation product of peak 2.

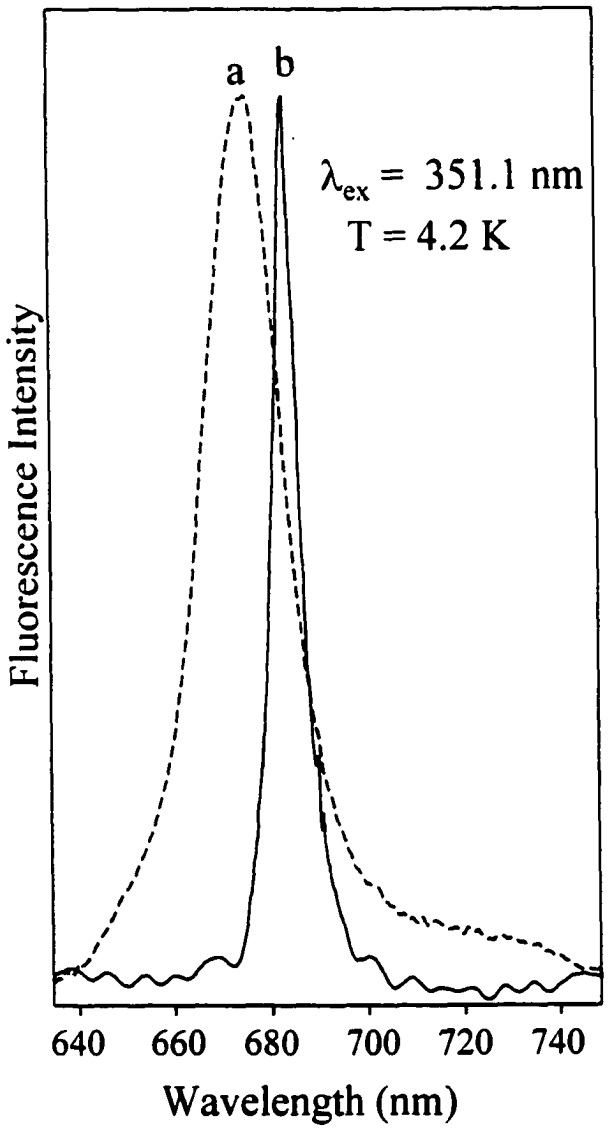

Figure C-2. On-line NLN fluorescence spectra of peaks 1 (spectrum a) and 2 (spectrum b) in the electropherogram of Figure C-1. T = 4.2 K, λ_{ex} = 351.1 nm. The fluorescence maximum of spectra a and b are 674 and 683.3 nm, respectively.

After leaving the sample in a freezer at -70°C for one month and then re-thawing, another CE-separation was performed, shown in Figure C-1c. In this figure, it is clear that the majority of all peaks have disappeared, likely denaturing into peak 2 under ambient conditions and from thawing and refreezing.

C.4. Conclusion and Future Prospects

Although the above buffer is likely better than previous buffer systems (e.g., Triton X) to maintain CP43 in its native state, the results indicate that CP43 can readily denatured under these conditions, with possible aggregation. However, with CE coupled on-line to high-resolution fluorescence detection (FLNS), future studies can be performed on the on-line purified analyte zone corresponding to native CP43. Furthermore, studies NLN and FLN studies should also be conducted on the remaining peaks in the electropherogram to assess their exact nature, i.e., dimer, trimer, etc.

References

1. Hankamer, B., Barber, J., Boekema, E.J., *Annu. Rev. Plant Phys. Plant Mol. Biol.* 1997, *48*, 641.

2. Eijckelhoff, C., Dekker, J.P., Boekema, E.J. *Photosynthesis: from Light to Biosphere,* P.Mathis, ed., Kluwer Academic Publishers, Dordrecht, Vol.1, pp. 499-502.

3. Zhevleva, D., Hankamer, B., Barber, J., *Biochemistry*, 1996, *35*, 15074.

4. Jankowiak, R., Zazubovich, V., Rätsep, M., Matsuzaki, S., Alfonso, M., Picorel, R., Siebert, M., Small, G.J., *J. Phys. Chem. B*, 2000, *104*, 11805.

5. Groot, M.-L., Frese, R.N., de Weerd, F.L., Bromek, K., Pettersson, Å, Peterman, E.J.G., van Stokkum I.H.M, van Grondelle, R., Dekker, J.P. *Biophysical Journal*, 1999, *77*, 3328.

6. den Hartog, F.T.H., Vacha, F., Lock, A.J., Barber, J., Dekker, J.P., Völker, S., J. Phys. Chem. B 1998, 102, 9174.